THE
PHYSICAL REVIEW
A Journal of Experimental and Theoretical Physics
VOL. 45, NO. 8 APRIL 15, 1934 SECOND SERIES

Gamma-Ray Ionization in Several Gases as a Function of Pressure and Collecting Field

EVERETT F. COX,* *California Institute of Technology*
(Received February 21, 1934)

Ionization by low intensity γ-radiation in N_2, CO_2, A and He has been measured with pressures of from 0.98 to 93 atm. of N_2, 61 atm. of CO_2, 25 atm. of A, and 98 atm. of He and with uniform collecting fields from 1.57 to 1065 volts/cm, direct comparison being made with the results of Bowen for air. The marked increase in current with increased collecting gradient and independence of the shape of the current-field curves on intensity of radiation up to the intensity used demands rejection of the wall emission theory of Broxon and adaption of some recombination theory. Junction of Kaye and Laby's results to those of Bowen shows a gradient of 4×10^3 volts/cm as saturation value for air at 10 atm. pressure. A field of only 100 volts/cm is saturation value for argon up to 25 atm., and with this field the current from the inert gases examined is a linear function of the pressure up to 25 atm.

INTRODUCTION

DURING the last thirty years many observers[1, 2, 3, 4, 5, 6, 7, 8, 9] have studied γ-ray ionization in various gases as a function of pressure and collecting field; but excepting Bowen's[7] recent measurements on air and the present investigation of other gases, all observers have employed (1) either cylindrical or spherical ionization chambers, or (2) they have used a very high rate of ionization. In the first case the field is non-uniform and cannot be increased to large values because of the small central collecting electrode ordinarily used. Indeed the field amounts to only a few volts per cm in the regions of greatest volume even when several hundred volts are applied. Ordinary volume recombination complicates case (2) and makes theoretical interpretations very difficult. For example the very complete and careful study by Erikson[1] was made on ionization produced by 6 mg of Ra Br placed in the center of the ionization chamber, and hence the average ionization became thousands of times that now determined in cosmic-ray work.

APPARATUS AND PROCEDURE

To avoid objection (1) given above, the ions were collected between parallel plates 1 cm apart; to avoid objection (2) the ionization was always kept less than 20 times the residual ionization. The number of ions per cc per sec.

* Now at Colgate University.

[1] H. A. Erikson, Phys. Rev. **27**, 473 (1908).
[2] T. H. Laby and G. W. C. Kaye, Phil. Mag. **16**, 879 (1908).
[3] W. Wilson, Phil. Mag. **17**, 216 (1909).
[4] K. M. Downey, Phys. Rev. **16**, 420 (1920); **20**, 186 (1922).
[5] H. F. Fruth, Phys. Rev. **22**, 109 (1923).
[6] J. W. Broxon, Phys. Rev. **27**, 542 (1926); **28**, 1071 (1926); **38**, 1704 (1931); **40**, 1022 (1932).
[7] I. S. Bowen, Phys. Rev. **41**, 24 (1932).
[8] J. J. Hopfield, Phys. Rev. **43**, 675 (1933).
[9] S. Chylinski, Phys. Rev. **45**, 309 (1934).

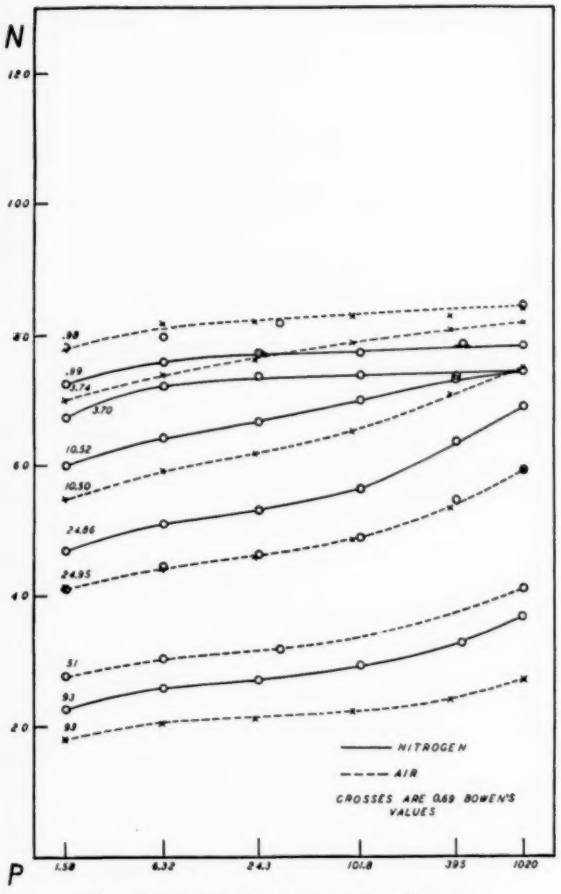

FIG. 1. Ionization observed in nitrogen.

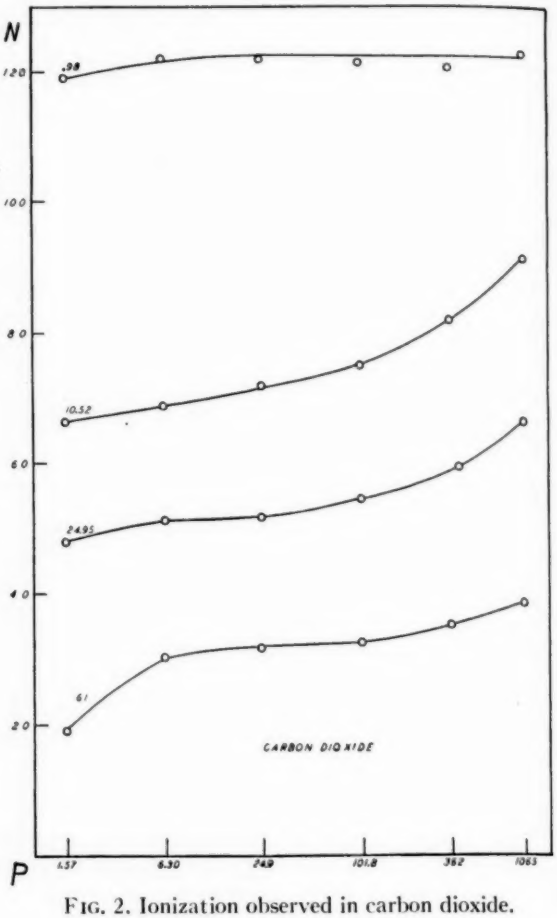

FIG. 2. Ionization observed in carbon dioxide.

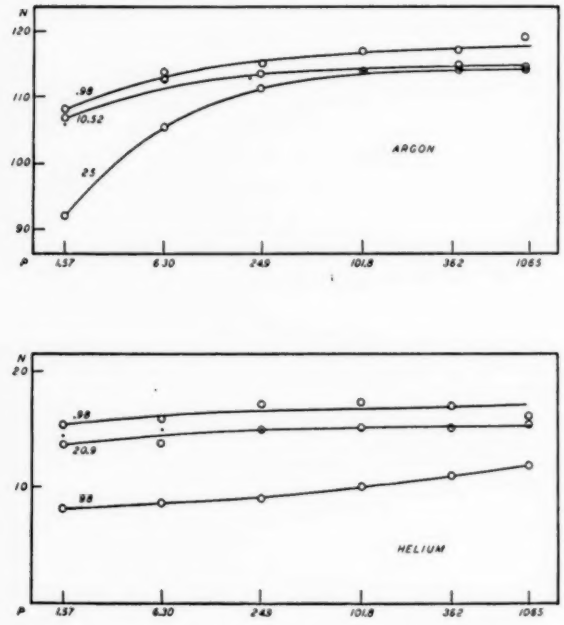

FIG. 3. Ionization observed in argon and helium.

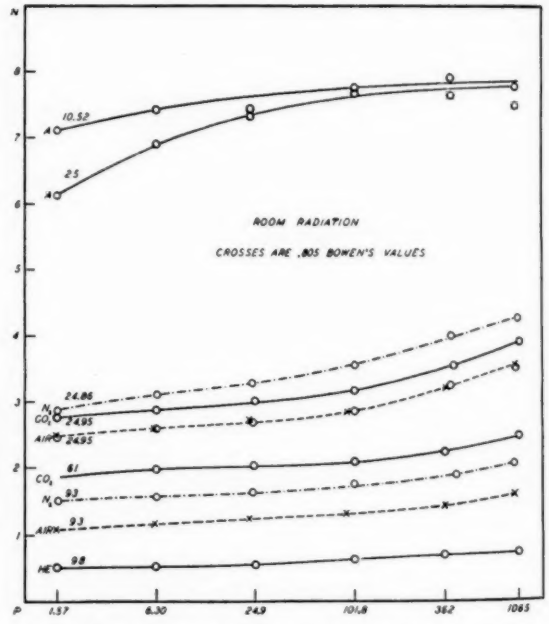

FIG. 4. Observed residual ionization in various gases.

per atm. was determined with the same apparatus and procedure described by Bowen[7] except that a small correction for the pressure change of dielectric constant of the gases, neglected by Bowen, was introduced.

Pressures near 1 atm. were read to about 2 percent with a manometer, while those from 2 to 50 atm. were registered by a periodically calibrated new 6-inch U. S. Test Gauge and should not be more than 0.1 atm. in error. For higher pressures it was necessary to use uncalibrated gauges whose errors may have been as large as 10 percent, probably too high if the new gauges of the California Institute cryogenic laboratory are assumed correct.

In order to fix the curves obtained by Bowen for air with those of the writer for other gases, data were taken for air at pressures of 0.98, 24.95, and 51 atm. Multiplication of Bowen's values by a factor of 0.69 gave nearly perfect agreement; and a factor 0.805 multiplying Bowen's values for room radiation did likewise. These transposed values with those of the writer for air appear in Figs. 1 and 4.

Similar measurements were next made in nitrogen, carbon dioxide, argon and helium. The nitrogen which was obtained from the Linde Air Products Co. was tested by Mr. W. M. Zaikowsky and found to contain no traces of CO_2 and 0.93 ± 0.025 percent of O_2. Commercial CO_2 was purchased from the Pure Carbonic Company but was not tested for purity. Dr. C. E. Hablutzel analyzed the argon obtained from the General Electric Co. and found it to contain 0.2 percent of O_2 but no trace of CO_2; an insensitive weight determination gave no evidence of nitrogen. The helium used was kindly furnished by Dr. A. Goetz from the supply of the cryogenic laboratory.

The general process of introducing the gases into the chamber was first to evacuate the chamber to less than 3 mm pressure. In the case of the cheaper gases the chamber was then filled with the gas to atmospheric pressure and re-evacuated several times before observations were begun. The chamber was flushed out with argon only once, but the evacuation was carried to a considerably lower pressure.

Results

The ionizations observed in N_2, CO_2, A and He at various pressures and collecting fields are displayed in Tables I–IV, and Figs. 1, 2, 3, respectively. Table V and Fig. 4 give the observed

Table I. *Number of ions/cc/sec./atm. from N_2.*

Field in volts/cm	Pressure in atm.				
	0.99	3.70	10.52	24.86	93
1.58	72.3	67.1	60.0	46.7	22.7
6.32	76.3	71.9	64.0	51.1	26.0
24.3	76.9	73.4	66.4	53.1	27.1
101.8	77.2	73.4	69.7	56.2	29.3
395	78.2	73.1	72.7	63.2	32.6
1020	78.0	74.0	73.9	68.6	36.7

Table II. *No. of ions/cc/sec./atm. from CO_2.*

Field in volts/cm	Pressure in atm.			
	0.98	10.52	24.95	61
1.57	118.8	66.2	47.8	18.8
6.30	121.7	68.5	51.1	30.2
24.9	121.4	71.5	51.5	31.5
101.8	120.9	74.6	54.3	32.4
362	120.1	81.6	59.1	35.1
1065	122.3	91.1	66.0	38.4

Table III. *No. of ions/cc/sec./atm. from argon.*

Field in volts/cm	Pressure in atm.			I_1	4.55 I_2
	0.98	3.72	10.52	25	
1.57	108.2	105.9	106.9	92.1	95.1
6.30	113.8	112.3	112.7	105.5	105.5
24.9	115.1	112.8	113.5	111.2	111.2
101.8	117.0	114.0	114.0	114.0	112.6
362	117.2	114.1	114.9	114.1	113.8
1065	119.2	114.2	114.6	114.2	111.9

Table IV. *No. of ions/cc/sec./atm. from helium.*

Field in volts/cm	Pressure in atm.			
	0.98	10.52	20.9	98
1.57	15.4	14.4	13.7	8.20
6.30	15.9	14.9	13.8	8.77
24.9	17.2	14.9	15.0	9.12
101.8	17.3	14.9	15.1	10.0
362	17.0	15.2	15.1	11.0
1065	16.1	15.2	15.4	11.8

TABLE V. *No. of ions/cc/sec./atm. by room radiation.*

Gas	Pressure in atm.	Field in volts/cm					
		1.57	6.30	24.9	101.8	362	1065
Air	24.95	2.45	2.60	2.70	2.87	3.26	3.53
	93	1.08	1.17	1.25	1.32	1.42	1.60
N_2	24.86	2.86	3.10	3.28	3.56	4.00	4.26
	93	1.51	1.57	1.65	1.76	1.89	2.05
CO_2	24.95	2.76	2.88	3.01	3.19	3.56	3.92
	61	(2.76)	1.98	2.05	2.10	2.24	2.49
A	10.52	7.10	7.41	7.43	7.74	7.90	7.48
	25.0	6.12	6.91	7.32	7.66	7.64	7.77
He	98	.502	.530	.565	.635	.702	.742

residual ionization. In general each value listed represents the average of from 10 to 20 separate determinations. Due to the lower ionization and therefore longer observation time in helium only 7 observations were made for each point. N_2 and CO_2 evidently behave very similar to air, and the reader is again referred to Bowen's paper[7] for the interpretation. In the noble gases the ionization approaches much more nearly to proportionality with the pressure, indicating that *preferential* recombination with the parent ion plays a much smaller rôle in the case of these gases. This is in agreement with Hopfield's[8] observations on argon.

In the case of argon at its highest pressure the presence of volume recombination was further tested by measuring the ionization when the γ-ray intensity was cut to 1/4.55 of its normal value. The last column of Table III headed 4.55 I_2 gives the observed ionization times 4.55. A comparison of this column with the preceding one, giving the ionization with the normal intensity of γ-radiation, indicates that no volume recombination occurred except at the lowest collecting field.

The results here presented are useful in attempting a theory which will explain the decreasing ionization per atmosphere as the pressure is increased. Of the theories that have been advanced,[10, 11, 12, 13] only two allow quantitative comparison with the writer's results; and Gross[12] candidly concedes that his *initial* recombination theory cannot account for the high ionization in argon.

The writer wishes to thank Mr. W. M. Zaikowsky and Dr. C. E. Hablutzel for determining the purity of the gases used; Mr. B. E. Merkel for technical assistance with the high pressure gas system; Professor A. Goetz for the use of the helium gas from the supply of the cryogenic laboratory; and especially Professor I. S. Bowen for his patience, aid, and obliging advice throughout the course of experiment.

---

[10] A. H. Compton, R. D. Bennett and J. C. Stearns, Phys. Rev. **39**, 873 (1932).

[11] W. R. Harper, Proc. Camb. Phil. Soc. **28**, 219 (1932); **29**, 149 (1933).

[12] B. Gross, Zeits. f. Physik **78**, 271 (1932); **80**, 125 (1933).

[13] D. O. North, *Ph.D. Thesis*, California Institute of Technology, 1933, soon to be published.

Artificial Production of Neutrons

H. R. CRANE, C. C. LAURITSEN AND A. SOLTAN,* *Kellogg Radiation Laboratory, California Institute of Technology*

(Received January 26, 1934)

A porcelain vacuum tube capable of producing currents of positive ions up to 30 microamperes and with energies up to 10^6 electron-volts has been constructed and used for artificial disintegration experiments. Neutrons have been produced by bombarding beryllium with helium ions, and by bombarding lithium and beryllium with the ions of the heavy isotope of hydrogen. The curve obtained for the efficiency of production of neutrons by helium ions as a function of voltage is in agreement with the curve obtained by a downward extrapolation of curves known from work with polonium α-particles. The present paper is mainly a discussion of the apparatus and methods of measurement, since brief reports of the results have already been presented.

INTRODUCTION

DURING the short time neutrons have been known, the relative yields of neutrons from beryllium and from boron as a function of the energy of the bombarding α-particles has been investigated in some detail. With the exception of one, or possibly more than one, resonance level, the excitation curve has been found to be in good agreement with that predicted on the basis of the Gamow theory. The curve is of exponential form, given approximately by $Ae^{-b/\sqrt{V}}$ where A and b are constants and V is the energy of the α-particles. It has been possible, however, by the use of radioactive sources of α-particles, to investigate the excitation curve only down as far as about 1.3×10^6 electron-volts,[1] because of the very rapidly decreasing efficiency, and the limited number of α-particles obtainable from existing radioactive sources. If we take the experimental curve in the region of energy in which it is accurately known and extrapolate it downward according to the exponential formula, we obtain the curve shown in Fig. 1. From this can be determined the relative intensities of α-particle sources necessary to produce a given effect at various voltages. It is evident that if artificial α-particles, or helium ions, are to be used at voltages in the region of 10^6 and below, their extremely low efficiency must be compensated by great numbers. In order to produce an effect in the disintegration of beryllium equal to that produced by the α-particles from 100 millicuries of polonium, it would be necessary to have the following currents of helium ions at the following voltages.

Voltage (10^6 volts)	0.50	0.65	0.75	0.90	1.00
Current (μa)	5000	450	90	20	5

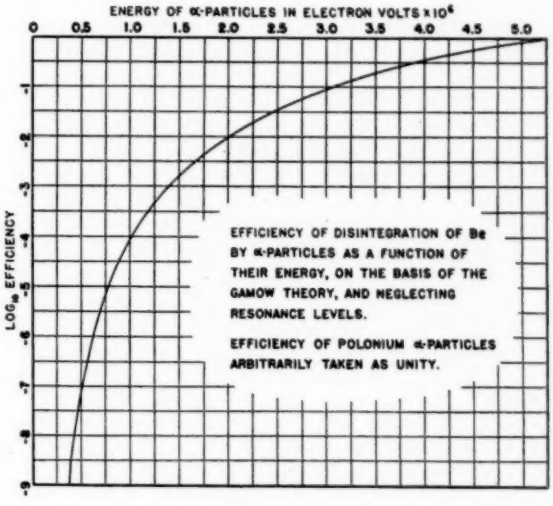

FIG. 1.

The problem undertaken by the authors has been the production of helium ions of energy up to 10^6 electron-volts, in sufficient quantity to give a strong artificial source of neutrons, and to make possible an investigation of the excitation curve in that region of voltage.

*International Research Fellow of the Rockefeller Foundation.

[1] Curie and Joliot, Comptes Rendus **196**, 397 (1933).

Description of Apparatus

The first apparatus used to accelerate helium ions was a modification of a porcelain x-ray tube[2] which had recently been constructed in this laboratory, and which was capable of running on alternating current at 650,000 volts, peak value. With this apparatus, ion currents of the order of 100 microamperes were obtained, and small intensities of neutrons were detected. As can be seen from the above table, only a small effect, at best, should be expected at that voltage and current. In order to reach higher voltages, a tube for accelerating the ions in two stages was then constructed, with two of the same type of porcelain bushings. A sectional view of this tube is shown in Fig. 2. The million-volt (root-mean-square value) cascade transformer set in the High Voltage Laboratory is used as the source of high potential. The top of the upper tube is connected, through a suitable protective resistance, to the high potential end of the transformer set, and the midpoint between the two tubes is connected to the half potential point of the transformer set. The apparatus therefore operates as two separate tubes, each giving the ions half their total acceleration.

The source of the ions is located in the end of the inner electrode of the upper tube. A metal ring in the shape of a doughnut, 3 in. (7.5 cm) in diameter and having a 1 in. (2.5 cm) hole is supported from the bottom plate of the upper tube, about 5 in. (12.5 cm) from the end of the electrode. This modifies the field in a way that is favorable to concentration of the ion beam. From here the ions pass down the hollow central electrode, and receive the second half of their acceleration in the gap of the lower tube. An enlarged view of the ion pipe at the bottom of the tube and the target is shown in Fig. 3. The target consists of a 2 in. (5 cm) brass disk mounted on a shaft, so that either side can be exposed to the ion beam. One side of the disk is covered with the material to be disintegrated, and the other side is covered with some material which gives no effect, such as brass or aluminum, for the purpose of comparison. A paraffin lined electroscope, for detecting neutrons, is located in a lead cylinder of 5 cm wall thickness, in the position indicated in the figure. A magnetic field is applied to the ion beam above the target to bend out any electrons which may arrive during the reverse half cycle of the alternating potential. Some additional lead is placed on top of the cylinder containing the electroscope, so as to

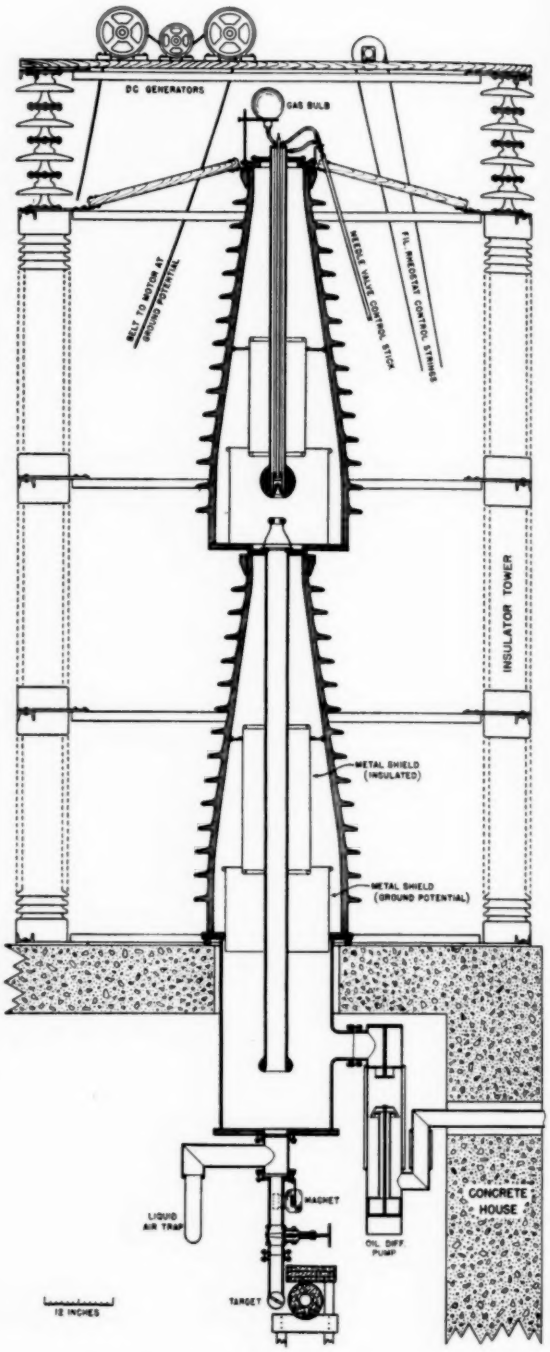

Fig. 2. Sectional view of the entire tube.

[2] Crane and Lauritsen, Rev. Sci. Inst. **4**, 118 (1933).

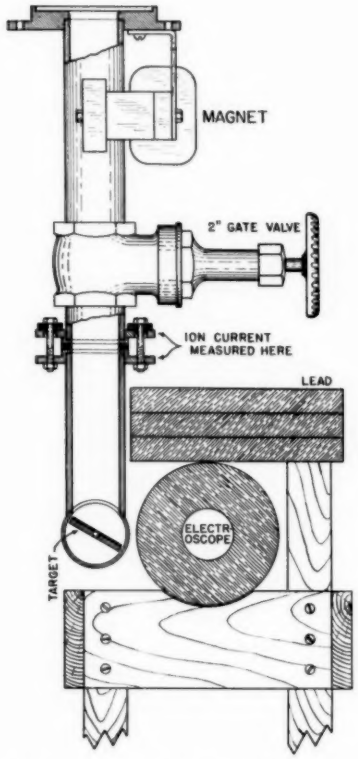

FIG. 3. Part-sectional view of the lower end of the tube, showing the lead shielding and the position of the electroscope with respect to the target.

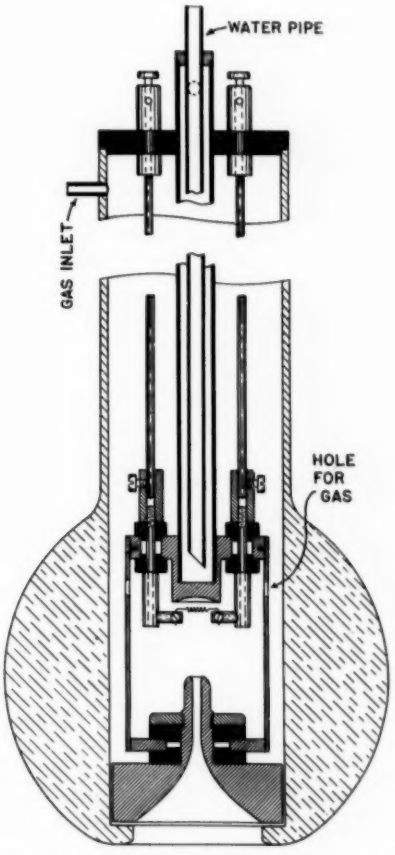

FIG. 4. End of the upper electrode with the ion source in place.

reduce further the effect of x-rays produced by the electrons that are deflected to the wall of the pipe by the magnetic field. The electroscope is placed at the side of the target, rather than below it, so that, a greater thickness of lead can be put in the path of the x-rays, which come principally from above, than in the path of the neutrons. The intensity of neutrons is presumably not quite as great in a direction perpendicular to the ion beam as in the downward direction, but the decrease in the background radiation in the present arrangement probably more than compensates for this difference in neutron intensity.

A 2 in. (5 cm) gate valve is placed in the pipe just above the target. When it is closed, the target chamber can be opened to the atmosphere, and the pressure in the tube does not rise to more than 10^{-1} mm during the operation.

Ion source

A cross section of the end of the upper electrode with the positive ion source in place is shown in Fig. 4. A potential of about 1000 volts d.c. is applied between the filament and the water-cooled anode. The helium or hydrogen from which the ions are made is admitted continuously through a needle valve into the space around the filament, and escapes, together with the ions, through a 1/8 in. canal directly below the filament. By adjusting the needle valve a pressure of between 10^{-2} and 10^{-3} mm is maintained inside the electrode, and this results in a pressure of from 10^{-4} to 5×10^{-4} in the main tube. Because of the very small cross section for ionization of helium and of hydrogen, the tube will operate satisfactorily with pressures of helium up to 10^{-3} and with hydrogen up to 5×10^{-4} mm. With an electron current in the ion source of 0.5 ampere, the current of positive ions escaping through the canal is about 200 microamperes. Of this, about 30 microamperes arrive at the target, which is 11 feet from the source.

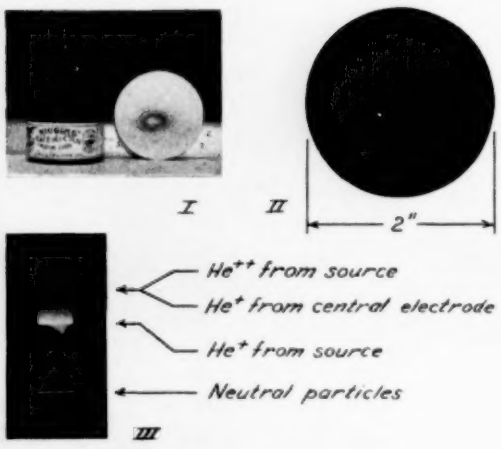

FIG. 5. I, Photograph of a target after many hours exposure to the ion beam. II, Spot produced on a photographic film during a fraction of a second exposure to the ion beam. III, Magnetic spectrum of the ion beam.

The horn shaped opening at the bottom of the canal causes the ions to be in a converging field at the time they are leaving the canal, and consequently when they are moving slowly and are easily influenced by the field. There is probably very little additional concentration of the beam in the gap of the lower tube, because the ions are by that time moving too fast to be much influenced by the field. A photograph of the spot produced on one of the targets after many hours of running is shown in Fig. 5. The spot appears elongated, because the target was inclined at 45° to the incident beam, but it is evident that most of the ions strike within a circle about 1/2 in. in diameter. A photographic film was placed over the target and an exposure of a fraction of a second was made. The ions completely destroyed the emulsion in a spot about 1/16 in. in diameter without producing appreciable photographic blackening over the rest of the film. This shows that while there is some intensity of ions over a spot about 1/2 in. in diameter, a large part of the intensity is confined to a very small area at the center of the spot.

Composition of the ion beam

Since alternating current was used, it was desirable to determine the approximate distribution in velocity of the ion beam. The beam was allowed to fall on a slit and then bent in a magnetic field. A photograph of the resulting spectrum is shown in Fig. 5. It can be seen from this that a very large part of the total intensity is at, or near, the high voltage limit. Such a distribution is to be expected, assuming that the ion current is constant, and knowing that the time spent near the top of the sine wave is much greater than the time spent at any lower voltage. Actually the distribution is even more favorable because the ion current measured at the target is roughly proportional to the voltage, because of better focussing at the higher voltages. If we then multiply the current at each instant by the efficiency of the ions in the disintegration of beryllium at that particular voltage, it is apparent that almost all of the disintegration can be attributed to ions having very nearly the full voltage. Thus the inaccuracy introduced into the experiment by using alternating, rather than constant, potential is very small compared to other sources of error, such as the inaccuracy with which the factor between neutrons and recoil H-particles, and the absorption and scattering of the neutrons in the lead cylinder, are known.

With the present apparatus, no quantitative determination of the amount of doubly ionized helium present in the beam can be made, although some idea of the composition of the beam can be gained from the magnetic spectrum shown in Fig. 5. The ions that originate singly charged at the source and remain singly charged during the whole of their journey are seen in the spectrum as a bright line with a sharp high velocity limit, and it is estimated that this comprises roughly 90 percent of the total ion current. In a position corresponding to $\sqrt{2}$ times the deflection of the above line can be seen a diffuse line representing principally the He^+ which originate as secondaries in the central electrode, and receive acceleration only in the lower gap. These are readily identified, because they are poorly defined in direction, most of them going through the slit obliquely, and giving rise to a line considerably longer than the slit itself. If there were present in the beam any ions which had come through the entire tube in the doubly ionized state, they would fall in the same position as this diffuse line, except that, due to their uniformity of direction, their line would be sharp and only as long as the slit. No such line

can be detected in the photograph. The component of He^{++} is therefore assumed to be small enough to be neglected. In the region of 10^6 volts, He^{++} should be about 100 times as effective in disintegrating beryllium as a He^+, since it would acquire twice the energy during its travel through the tube, so He^{++} would have to be present to at least one percent to be as important as the He^+.

Electroscope

A sensitive electroscope, having a cylindrical chamber 5 cm in diameter and 8 cm long is employed as a means of detecting and measuring the intensity of the neutrons. The entire electroscope, including the eyepiece, is enclosed in a lead cylinder, shown in Fig. 3, to shield it from x-rays. A small lead plug in front of the eyepiece is removed when readings are made. The inside walls of the electroscope are coated with a layer of paraffin about 1 mm thick, with a wire gauze over it. The neutrons penetrate the 5 cm walls of the lead cylinder and eject recoil hydrogen particles from the paraffin on the walls of the chamber, the ionization due to these recoil particles giving a measure of the neutron intensity. The sensitivity of the electroscope and the intensity of the background radiation are such that about one recoil particle per minute can be detected with certainty in a one hour measurement.

Results

The yields of neutrons obtained by bombarding various targets with helium ions,[3] and also with deutons[4] and protons,[5] have already been presented in letters to the *Physical Review*, so only a brief resumé of the method of measurement and results will be given here. In plotting the curve of the efficiency of production of neutrons from beryllium by helium ions (Fig. 6, curve III), a

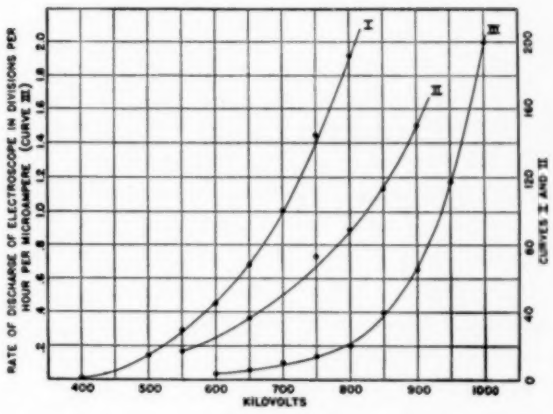

FIG. 6. Relative efficiency of production of neutrons as a function of voltage. Curve I, beryllium bombarded with deutons; curve II, lithium chloride bombarded with deutons; curve III, beryllium bombarded with helium ions.

series of one hour runs was made at a number of voltages between 6×10^5 and 10^6, with an ion current of 10 microamperes. Two curves were first obtained, one giving the rate of discharge of the electroscope when the beryllium was exposed to the ion beam, and the other giving the rate of discharge when the brass target was exposed to the beam, all other conditions being kept the same. The latter curve is taken to be the background, and is composed of the natural leak of the electroscope plus the rate of discharge due to stray x-rays from the tube. At 6×10^5 volts the total background is not measurably different from the natural leak when the tube is not running, namely, about 4 divisions per hour, and at 10^6 volts it becomes about twice the natural leak. Each of the three curves in Fig. 6 is the observed effect, per microampere, after subtracting the background, and should therefore represent just the effect due to neutrons and possibly also to some γ-rays produced in the disintegration. In order to gain some idea of the intensity of the γ-rays present, measurements were made with the paraffin removed from the electroscope. In each case the effect observed without paraffin was less than half the effect with paraffin. Although this result does not exclude the possibility of the presence of some γ-rays, it indicates that at least the greater part of the effect observed with the paraffin chamber was due to neutrons. It is clear that a quantitative separation of the effects of neutrons and γ-rays

[3] Crane, Lauritsen and Soltan, Phys. Rev. **44**, 514 (1933).
[4] Crane, Lauritsen and Soltan, Phys. Rev. **44**, 692 (1933).
[5] Crane and Lauritsen, Phys. Rev. **44**, 783 (1933); Lauritsen and Crane, Phys. Rev. **45**, 63 (1934). A rather strong radiation was observed when lithium was bombarded with protons, and was at first interpreted to be neutrons. Later absorption measurements with paraffin and lead showed that at least the greater part of it was γ-radiation of about 1.5×10^6 e.v. energy.

cannot be made simply by comparing the observations with and without paraffin in the chamber, since in either case the chamber is somewhat sensitive to both neutrons and γ-rays. In the disintegration of beryllium by α-particles, Becker and Bothe[6] found that photons of high energy accompany the neutrons, in approximately equal number.

An estimate of the absolute efficiency of the disintegration of beryllium by helium ions can be made by considering the following constants of the experimental set-up.

Sensitivity of the electroscope, as determined with a radium γ-ray source of known intensity: 1 division $= 2.5\times10^{6}$ ion pairs $= 70$ recoil H-particles.

Solid angle subtended by the electroscope is 0.127π or $1/30$ the total sphere.

Absorption in 5 cm of lead, taking into account scattering, can be assumed to be not more than 20 percent.

Rate of discharge of the electroscope at 10^{6} volts with 10 microamperes ion current (from Fig. 6) is 5.5×10^{-3} div./sec., corresponding to 0.4 recoil H-particles/sec.

Assumed factor between the number of neutrons and the number of recoil H-particles is 5×10^{3}.

10 microamperes is 6×10^{13} ions/sec.

The efficiency, from the above data, is 1 neutron per 10^{9} helium ions at 10^{6} volts. By comparing the three curves in Fig. 6, an estimate can also be made of the efficiency of production of neutrons from lithium and beryllium by deuton bombardment. At 8×10^{5} volts this is, for lithium chloride, 1 neutron per 2×10^{7} deutons, and for beryllium, 1 neutron per 10^{7} deutons.

The shape of the excitation curve in Fig. 6 for helium ions is in good agreement with that predicted by theory, although there are several disturbing factors which could cause the experimental curve to depart considerably from the theoretical. Thin layers of oxides and deposited material on the target, which are not important in dealing with very fast ions, become increasingly important as the lower limit of the curve is approached. Also a curve of much less intensity but of quite different slope, due to a small component of He^{++} in the ion beam, is superimposed on the true curve. The exponential formula, with the exponent determined from the experimental curve between 750 and 950 kv is $I = Ae^{-640/\sqrt{V}}$ where I is the relative yield of neutrons and V the voltage in kv. The two deuton curves are not so much subject to the above sources of error. The deutons penetrate to a greater depth in the target than the helium ions, making surface conditions less important, and the whole effect can be attributed to one kind of ion, namely $(H^{2})^{+}$, since it is not only predominant in number, but is from 10 to 100 times as effective in disintegration as $(H^{1}H^{2})^{+}$ or $(H^{2}H^{2})^{+}$ of the same energy.

As a source of neutrons, it is apparent that the method of production with deutons is orders of magnitude better than the method of production with helium ions. However, by using helium ions, we have been able to plot the curve for the efficiency of excitation, beginning at about the lowest point reached with radioactive α-particle sources, and extending down to 6×10^{5} volts, where the efficiency is not more than 10^{-11} neutrons per α-particle.

The work we have described has been supported entirely by the Seeley W. Mudd Fund. We wish to express our gratitude for this aid, and also to Professor G. N. Lewis of the University of California, who furnished the heavy hydrogen used in these experiments.

[6] Becker and Bothe, Zeits. f. Physik **76**, 421 (1932).

Magnetic Refocussing of Electron Paths*

W. E. STEPHENS, *Washington University, St. Louis*

(Received January 31, 1934)

A general method of magnetic direction refocussing, i.e., the refocussing of slightly divergent electron paths in a uniform magnetic field, has been found, of which the familiar 180° refocussing is a particular case. If we use a wedge-shaped magnetic field, whose lines of force are perpendicular to the plane of motion of an electron beam, the field being produced by a solenoid or magnet pole pieces of such a shape that the effective boundaries of the field projected on the plane of motion of the electrons is V shaped; and if the electron beam enters the magnetic field perpendicular to one edge, with the strength of the field set so that the electron beam will leave perpendicular to the other edge; then the refocussing of slightly divergent electron paths will occur. The position of best refocussing is on a line through the point of divergence of the electron beam and the apex of the wedge field. A magnetic field approximating the desired field has been obtained and the theoretical results have been checked for a particular case in which the angle at the apex of the wedge field was 90°. The particular value of this general refocussing property is that, with it, velocities of electrons can be analyzed without the deflecting magnetic field straying over into the region from which the electrons originate.

INTRODUCTION

IN analyzing the velocity distribution of beams of charged particles by deviation methods, it is usually desirable to increase the intensity of the collected beam by refocussing paths of particles which diverge from a given point by a small, but finite angle. This is called direction refocussing and has been found to occur at 180° deflection in a magnetic field,[1, 2, 3] at 127° 17′ deflection in a radial electrostatic field,[4] and at 360° deflection in a magnetic field superimposed on a parallel electrostatic field.[5] The disadvantage of the regular magnetic refocussing in experiments on electron scattering is the difficulty of keeping the field in the magnetic analyzer from straying over into the region from which the electrons originate.[6] Electrostatic refocussing apparatus has the disadvantages that surface charges, contact potentials, and secondary electrons from the plates may affect the results. Therefore, it was desired to find a magnetic deflection method of analyzing electron velocities in which the deflecting field could be kept from straying over into the scattering space from which the electrons come.

It was soon realized that the 180° magnetic refocussing is a particular case of a general refocussing property of wedge-shaped magnetic fields, in which the electrons are refocussed at a deflection angle equal to the angle of the wedge bounding the field. Furthermore, the entrance slit can be some distance from the field, leaving the scattering space or collision area field free.

GENERAL CASE

The general case is illustrated in Fig. 1. If we have a homogeneous magnetic field, H, perpendicular to the paper, and bounded by planes which are perpendicular to the paper and intersect it in lines OPQ and OWV, which lines make arbitrary angles θ and γ, respectively, with the normal to the line AO, then inside the region $QPOWV$ electron paths will be arcs of circles which are tangent at the edges of the field to the direction of entrance and exit. Outside this wedge-shaped field, it is assumed, there is no field and electron paths are straight lines. A homogeneous electron beam of velocity v, which passes through an entrance slit at A making an angle θ with the base line will enter the field at

* Presented at the Cincinnati Meeting of the American Physical Society, December 1, 1933.

[1] J. Danysz, Le Radium **10**, 4 (1913).

[2] A. J. Dempster, Phys. Rev. **11**, 316 (1918).

[3] C. D. Bock, Rev. Sci. Inst. **4**, 575 (1933).

[4] A. L. Hughes, V. Rojansky and J. H. McMillen, Phys. Rev. **34**, 284 (1929).

[5] H. Busch, Phys. Zeits. **23**, 438 (1922).

[6] Gagge avoided this difficulty by having the field homogeneous throughout the scattering and analyzing regions. A. P. Gagge, Phys. Rev. **44**, 808 (1933).

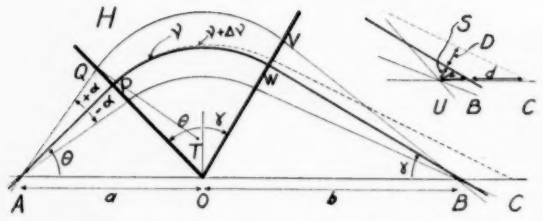

FIG. 1. Refocussing of electron paths. Offset shows region near B enlarged.

P perpendicular to OPQ. If the field H is set to turn the electron beam in an arc of radius of curvature $R=a\sin\theta=OP=OW$, where H is determined by the equation,

$$RH(e/m)=v, \tag{1}$$

then, the center of curvature of the arc PW will be O and the electron beam will leave the field at W perpendicular to the edge OVW and enter the collecting chamber at B. All other beams, such as AQV, of velocity v and passing through A, but making a small but finite angle $\pm\alpha$ with the original beam will be refocussed so that they will cross very close to B. Hence, for a given point of divergence A of an electron beam entering a wedge-shaped field perpendicular to one edge and leaving perpendicular to the other edge, best refocussing will occur at a point B at a distance b from the apex O of the field and on a line through A and O, where $b=a\sin\theta/\sin\gamma$.

The departure from perfect refocussing will be called the spread and will be defined as the distance S in the offset of Fig. 1. This is the separation, at the position of best refocussing B, between the original or normal electron path $APWB$ and paths such as AQV making a small angle $\pm\alpha$ with the normal path at A. UB or s is the "spread along the base line" and when multiplied by $\sin\gamma$ gives S, the spread.

If now a beam of slightly greater velocity $v+\Delta v$ starts out along AP, its radius of curvature in the magnetic field will be larger, it will follow the dotted line APC, and intersect the base line at C. The dispersion of the apparatus is defined as the distance D, on the offset of Fig. 1. This dispersion is the ability of the apparatus to separate beams of slightly different velocities. The dispersion along the base line is d or BC and when multiplied by $\sin\gamma$ gives D. The spread and dispersion are defined as perpendicular to the electron path, since in practic plane of the collector slit is usually placed perpendicular to the path. The function of practical importance is, of course, the ratio of D to S which gives a measure of the theoretic resolving power of the apparatus.

To find the spread, S, in terms of α, θ, γ and a, we proceed as follows:

In Fig. 1, let AOB be the X axis and let the Y axis be perpendicular at A. Considering the path $AQVU$ of the beam of velocity v making an angle $+\alpha$ with the normal beam, we proceed by standard methods of analytic geometry to obtain the coordinates (x_1, y_1), (x_2, y_2), (x_3, y_3), and (x_4, y_4) of the points Q, T, V and U, knowing that $QT=R=a\sin\theta$, and QT is perpendicular to AQ.

$$\begin{aligned} x_1&=a\cos\theta\cos(\theta+\alpha)/\cos\alpha,\\ y_1&=a\cos\theta\sin(\theta+\alpha)/\cos\alpha, \end{aligned} \tag{2}$$

$$\begin{aligned} x_2=a[&(1/\cos\alpha)\cos\theta\cos(\theta+\alpha)\\ &+\sin\theta\sin(\theta+\alpha)], \end{aligned} \tag{3}$$

$$\begin{aligned} y_2=a[&(1/\cos\alpha)\cos\theta\sin(\theta+\alpha)\\ &-\sin\theta\cos(\theta+\alpha)], \end{aligned}$$

$$\begin{aligned} x_3&=[-n+(n^2-4mc)^{\frac{1}{2}}]/2m,\\ y_3&=(x_3-a)\cot\gamma, \end{aligned} \tag{4}$$

where $m=\csc^2\gamma$

$$n=-2(x_2+y_2\cot\gamma+a\cot^2\gamma),$$

$$c=(x_2^2+y_2^2+2ay_2\cot\gamma+a^2\cot^2\gamma-a^2\sin^2\theta),$$

$$\begin{aligned} y_4&=0,\\ x_4&=x_3+y_3(y_3-y_2)/(x_3-x_2). \end{aligned} \tag{5}$$

Then

$$s=(a+b)-x_4 \tag{6}$$

or

$$\begin{aligned} S=&a(\sin\gamma+\sin\theta)\\ &-\{\sin\gamma[x_3(x_3-x_2)+y_3(y_3-y_2)]/(x_3-x_2)\}. \end{aligned} \tag{7}$$

Now by expanding functions of α and approximating by dropping powers of α greater than two, we get

$$S=(a\alpha^2/2)[(\sin^2\theta/\sin\gamma)+(\sin^2\gamma/\sin\theta)]. \tag{8}$$

When $\theta=\gamma$, this reduces further to $S=a\alpha^2\sin\theta$, and for $\theta=\gamma=90°$, the familiar 180° case, we get $S=a\alpha^2$, a result already known.

To find D, the dispersion, we know that the increase in velocity Δv causes an increase in the radius of curvature ΔR such that $\Delta R/R=\Delta v/v$, if the field H is kept constant. If we draw in the new radius as $R+\Delta R$ and determine the new position and the new angle with which the beam leaves the field, we can find its intercept on AOB. We get this distance in terms of a, θ, γ, and ΔR, dropping all powers of ΔR greater than one, and substituting for ΔR, we find,

$$D=a(\sin\theta/\sin\gamma)(\Delta v/v)(\sin\theta+\sin\gamma). \quad (9)$$

When $\theta=\gamma$, this reduces to $D=2a\sin\theta(\Delta v/v)$, and for the 180° case, $D=2a(\Delta v/v)$, which is the known value, where a is then the radius of curvature. To get an idea of the values of θ and γ which will give the best combination of D and S, we plot the ratio of D to S in Fig. 2 in units of $(2/\alpha^2)(\Delta v/v)$, as a function of θ and γ. The greater the ratio of D to S, the better the theoretical resolving power. The graph indicates that the maximum value of D/S occurs for values of θ and γ determined by $2\sin\gamma=\sin\theta$, giving a value of D/S one and a third times that for either the 180° case or the ($\theta=45°$, $\gamma=45°$) case. The value given by the graph for $\gamma=0$, or $\theta=0$, is meaningless, since refocussing does not occur under those conditions. To satisfy the requirements of our original problem, that of keeping the deflecting field from straying past the entrance slit, we choose $\theta=45°$, so that the entrance slit will be distant from the edge of the field by an amount equal to the radius of curvature in the field. Then we choose $\gamma=45°$, so that the edges of the field are 90° apart, so that we may secure the desired field with a square solenoid. For this case then, $S=a\alpha^2/2$, $D=2a(\Delta v/v)$, and $D/S=(2/\alpha^2)(\Delta v/v)$, (from Eqs. (8) and (9)). Now, since $H\propto I$, where I is the current through the solenoid producing the field H, and since $RH\propto v$ (Eq. (1)), then we get $\Delta H/H=\Delta I/I$, and $\Delta R/R=\Delta v/v=-\Delta H/H$. Now, if we let $S=D$, we get,

$$\Delta I/I=-\alpha^2/2, \quad (10)$$

where ΔI is the change in current through the solenoid necessary to compensate for a change α in original direction of the beam. Also, since $V\propto v^2$, we find,

$$\Delta V/V=2(\Delta v/v)=2(\Delta I/I), \quad (11)$$

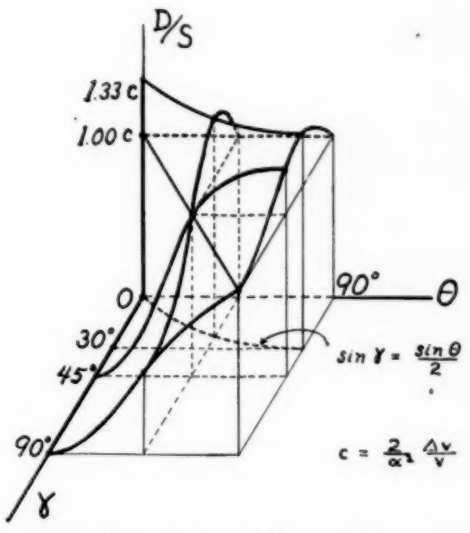

FIG. 2. Theoretical values of D/S (resolving power) as a function of θ and γ.

where ΔI is the change in current necessary to compensate for a change ΔV in accelerating voltage. These Eqs. (9) and (10), can be checked experimentally.

APPARATUS AND RESULTS

A diagrammatic sketch of the apparatus is shown in Fig. 3a. The cross-hatched square marked H represents the projection on the plane of cross section of the apparatus of the square solenoids which produced the 90° wedge-shaped field. These two solenoids (8×8×10 cm, 10 turns per cm) were placed end to end and separated about two centimeters to permit insertion of the apparatus as shown in Fig. 3b. The intensity of the field produced in this manner as measured along the perpendicular bisector of the edge of the solenoids in the plane of cross section of the apparatus is given in Fig. 5b by the dashed curve. Although this field does not accurately correspond to the theoretical field, since it does not cut off sharply at the edge of the solenoids, nevertheless, it was considered satisfactory for the present experiment since it did give good refocussing.

An oxide-coated filament f, Fig. 3a, supplies an electron current of one milliamp. which is accelerated through a 150 mesh grid g by a potential of 100.0 volts. This produces a fan-shaped beam of electrons which sprays the walls of the cylinder G_0. Those electrons which pass

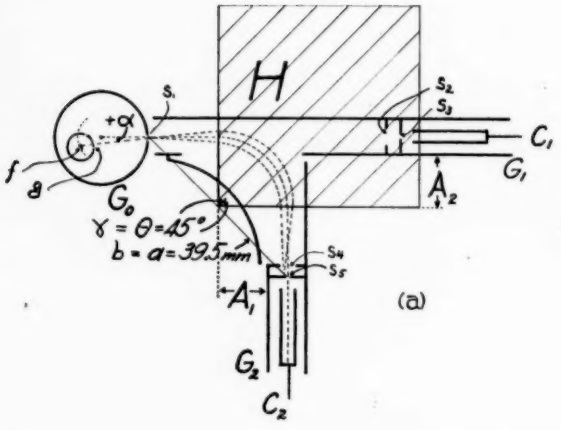

FIG. 3a. Diagrammatic cross section of apparatus for securing refocussing at $\theta = 45°$, $\gamma = 45°$.

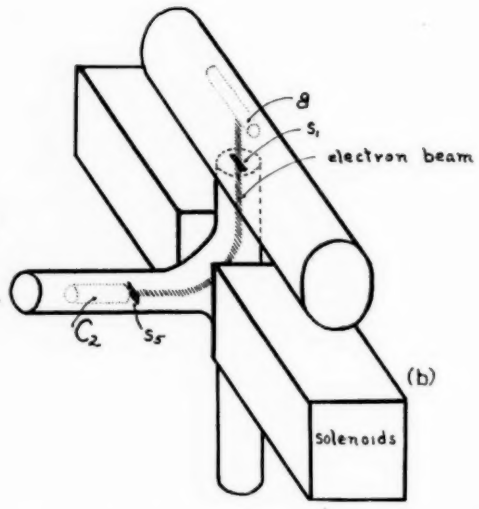

FIG. 3b. Perspective view of apparatus, showing arrangement of the solenoids.

through the slit S_1 (1×5 mm) form a narrow beam with an entrance angle α, which can be varied by rotating a ground glass joint to which the gun is attached. With no magnetic field on, this beam travelled straight down the tube through a guard slit S_2 (3×7 mm), and a collecting slit S_3 (1×5 mm) to the collector C_1 giving a current called C_1. Zero angle was assumed for α for the position which gave a maximum current C_1. When the field H was applied, the electron beam was bent as shown by the dotted lines on Fig. 3. It then passed through a similar set of slits S_4 and S_5 to collector C_2. Its path length from S_1 was 100 mm in both cases. The radius of curvature of the beam was calculated to be 28 mm. The currents C_1 and C_2 were always expressed as C_1/G_0 and C_2/G_0 where G_0 is the gun emission. The metal parts, shield, slits and collectors, indicated by heavy lines in Fig. 3a, were made of copper or brass and those parts subjected to electron bombardment were sooted to reduce secondaries. This was all enclosed in a glass tube and evacuated to a pressure below 10^{-5} mm Hg.

For different angle settings α of the gun, the magnetizing current I necessary to give a maximum current C_2 was determined. I in amperes was plotted against α in degrees in Fig. 4 for different positions of the solenoids relative to the apparatus as indicated by the distances A_1 and A_2 in mm (see Fig. 3a). The dotted curve in Fig. 4 is the theoretical curve $\Delta I/I = -\alpha^2/2$, (Eq. (10)), plotted arbitrarily from $\alpha = 0$, $I = 1.6$ amp. The shape of the curve is important rather than the relative positions. The flatter the curve the better the refocussing. The position of the coils is not critical as it can be seen that changes of a few millimeters in A_1 or A_2 does not affect the refocussing appreciably.

To find the dispersion of the apparatus, I was found for maximum current to C_2 for different accelerating voltages V of the electrons. If I in amperes is plotted against V in volts, the experimentally determined points in Fig. 5a are obtained. The straight line is the theoretical curve, Eq. (11), drawn arbitrarily from the point $V = 100$ and $I = 1.47$.

DISCUSSION

The graphs in Fig. 4 indicate the excellent refocussing obtained. Comparing the shape of the curves for positions of A_1 and A_2 near the calculated position, curves Fig. 4b, c, and d, with the shape of the theoretical dotted curve e, we see that refocussing is better than calculated. This is probably due to the finite size of the collector slit. Furthermore, due to the fact that the solenoids are small and square the field bulges out more at the center of the edge than at the corners, so the effective edge of the field in the plane of the electron beam is not parallel to the edge of the solenoids, but slightly rounded.

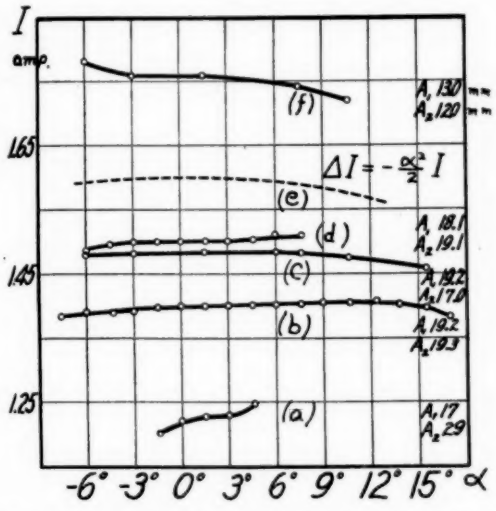

FIG. 4. Experimental test of spread. *Dotted line*, theoretical; *solid lines*, experimental (I, α) curves for different positions of solenoids.

This would have the effect of improving the refocussing since if the two diverging rays leave the field sooner than they would with a straight edge to the field, they will not be deflected so much and will come nearer perfect refocussing. Another contributing factor to the good refocussing may be the fact that the field is not perfectly homogeneous, but falls off towards the apex of the solenoids, fulfilling to some degree the conditions for the third order refocussing described by Bock.[3] The "$-\alpha$"-ray will then be deflected in a circle of greater radius and will, therefore, come closer to perfect refocussing. The interpretation of the curves in Fig. 4 can be carried further. It will be noticed (see Fig. 1) that at the position of best refocussing, the $+\alpha$-divergent ray ($AQVU$) and $-\alpha$-divergent ray both fall on the near side of the normal ray. Thus the field has to be decreased to bring both the $+$ and $-\alpha$-rays back to the collector, giving a maximum in the (I, α) curves as shown in Fig. 4b, c, d, and e. If, however, we move the collector towards the solenoid along the electron path, or equivalently, move the solenoid closer to the collector, i.e., increase A_1 and A_2, the $+\alpha$-ray will now fall on the opposite side of the normal ray from the $-\alpha$-ray. For this position, the field has to be increased for $+\alpha$ and decreased for $-\alpha$ to give the maximum C_2. This is what the curve Fig. 4a indicates, and we see from the large A_1 and A_2 (see Fig. 3) that the solenoids are closer to the collector than best position.

If the collector is moved away from the edge of the solenoids along the electron path or equivalently, the solenoids moved away, or A_1 and A_2 decreased, then the rays start to diverge again and the $+$ and $-\alpha$-rays are on different sides of the normal ray in such a manner that for $+\alpha$ the field has to be decreased, while for $-\alpha$ it has to be increased as indicated by curve Fig. 4f. Thus these (I, α) curves give criteria for determining the best position of the solenoids for best refocussing on a given apparatus: the curve must decrease for $+$ and $-\alpha$ and the maximum should be as flat as possible for best

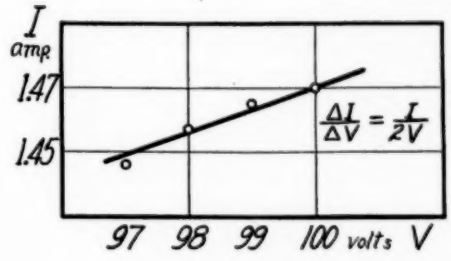

FIG. 5a. Experimental test of dispersion. *Solid line*, theoretical; *points*, experimental.

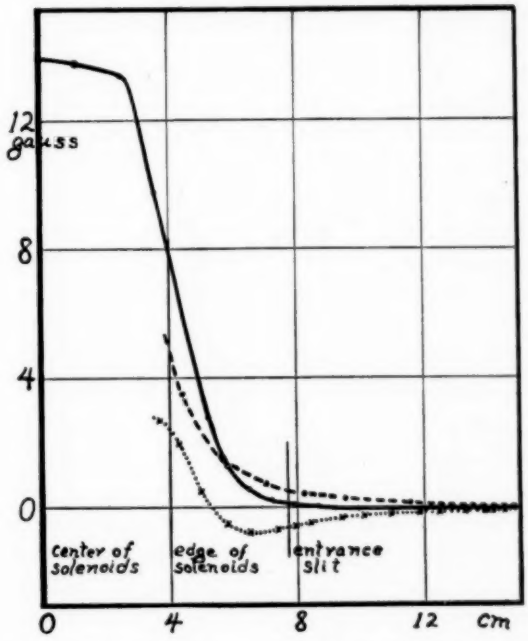

FIG. 5b. Straying of magnetic field due to separation of solenoids. *Dashed line*, field without compensating coils; *dotted line*, field due to compensating coils; *solid line*, field due to solenoids and compensating coils together.

refocussing. This best position is approximately that calculated. The apex of the solenoids should be placed on a line connecting the entrance and collecting slits, with the distances a and b determined from $b=a \sin\theta/\sin\gamma$. In the experimental case for $\theta=\gamma=45°$, and $a=b$, the calculated values were (A_1, 18.2, A_2, 18.2 mm).

It has been found possible to get a magnetic field which more exactly satisfies the theoretical conditions desired, i.e., homogeneity and a sharp cut-off. The most practical method is to add two small narrow square coils which fit over the ends of the large solenoids at each side of the gap.[7] These produce a field shown in Fig. 5b by the dotted line. The number of turns and the position and dimensions of these coils can be so fixed that the stray field outside the entrance slit will be approximately compensated and the field will be of the form of the solid line. This also makes the field inside the solenoids more homogeneous. In an analyzer, designed and built by Dr. Hergenrother of this laboratory for analyzing scattered electrons, two small coils ($10.2\times10.2\times0.7$ cm) carrying the same number of ampere turns per cm as the solenoids are added on each side of the gap of the solenoids which are similar to the ones used in this experiment. This combination gives a field whose value is shown in the solid line of Fig. 5b. A more direct, but less practical method of reducing the stray field is by reducing the effective gap of the solenoids. This effective decrease in gap can be secured either by reducing the thickness of the apparatus and putting the solenoids closer together or by increasing the cross-sectional area of the solenoids. If the cross-sectional area is increased, care must be taken that the solenoids are long enough to avoid stray fields from the outer ends.

A further application of this general refocussing property would result theoretically in perfect refocussing. Suppose for a convenient θ, say 50°, we let $\gamma=180°+\theta$. Then $\sin\theta=-\sin\gamma$, $\cos\theta=-\cos\gamma$, $S=0$, and $D=0$. With this arrangement the boundaries of the magnetic field would have an angle of $180°+2\theta$ and the beam would refocus at A, the point of entrance. There would be perfect direction and velocity refocussing to the accuracy of our approximations. For $\alpha=\pm3°$, the direction refocussing would be accurate to 1 part in 10,000. For $\Delta V=1$ volt for 100 volt electrons, the velocity refocussing would also be accurate to 1 part in 10,000. To use this arrangement for e/m or mass analysis the plane of the initial beam would have to be tilted slightly so that the refocussing point would be separated from the entrance point. For velocity analysis, two charged deflecting plates would have to be inserted where the beam leaves the magnetic field to give a vertical separation between beams of different velocities.

Another way of securing more perfect refocussing is to so shape the right-hand boundary of the magnetic field, see Fig. 1, that the diverging rays will refocus perfectly at B. The shape of the edge for this third order refocussing can be most easily obtained by graphical methods. Lines from B are drawn tangent to the circles of curvature in the magnetic field for different values of α. The loci of the points of tangency of such lines will be the desired edge of the field. This can be secured approximately by so shaping one side of the solenoids. This third order refocussing method is an alternative to the variation in intensity of the magnetic field method described by Bock.[3]

The refocussing described here occurs only in the plane of the electron beam. If the set-up shown in Fig. 1 were duplicated for every plane through AOB in the figure of revolution obtained by turning the figure about AOB as axis, then all rays leaving A making an angle $\theta\pm\alpha$ with AOB would be refocussed at B. The desired field could be obtained by a ring solenoid of proper shape in which the wires with which the solenoid is wound are far enough apart to permit the electrons to pass through without unduly distorting the field. This arrangement would constitute an electron "lens" if the rays that had angles of entrance other than $\theta\pm\alpha$ were cut off by proper diaphragms. The magnifying properties of the lens would depend on the ratio of θ to γ and focussing would be accomplished by variation of the magnetizing current.

In conclusion, I wish to thank Professor A. L. Hughes, under whose direction this work was carried out.

[7] Similar coils on the end to increase homogeneity inside solenoids were used by A. Buhl and F. Coeterier, Phys. Zeits. **33**, 773 (1932).

A New Method of Investigating Thermionic Cathodes

CLIFTON G. FOUND, *Research Laboratory, General Electric Company*
(Received February 16, 1934)

Under certain conditions, the electron current from a thermionic cathode is determined by the positive ion current reaching it. Two methods of using this relation to measure the thermionic emission of a cathode in a gaseous discharge are described. The constants, $b_0=30{,}000$, $A=10$ for a thoriated tungsten filament, and $b_0=22{,}700$, $A=88$ for an oxide-coated cathode, were obtained by use of these methods. The zero-field emission of an oxide-coated cathode was found to be only about 10 percent of the current at which the cathode was normally operated in practical discharge tubes. The increased current is due to the influence at the cathode of an external field which is established by an increase in the rate of generation of positive ions. The emission increases linearly with field up to fields of 150 volts/cm. Use is made of an auxiliary discharge to determine the relative ionizing power of electrons of different velocities. With cumulative ionization predominating, the total ionizing power increases linearly with the accelerating potential of the electron for voltages above the resonance potential and up to about two or three times this value.

INTRODUCTION

AS the voltage between a thermionic cathode and an anode of a high vacuum tube is increased, the current rises until finally it reaches a saturation value which corresponds to the thermionic emission of the cathode. A determination of this saturation value for different cathode temperatures furnishes an emission-temperature curve for the cathode. For cathodes having high electron emissivity, such as oxide-coated and thoriated-tungsten cathodes, the high voltage necessary to overcome electron space charge develops sufficient power to cause overheating of the tube. For this reason, it has been customary to measure the emission of such cathodes at temperatures below the operating temperature and to calculate the emission for higher temperatures by means of Richardson's or Dushman's equation.

When the tube contains gas and the applied voltage exceeds the ionization potential of the gas, ions are produced which neutralize the electron space charge and permit the large currents to flow at low voltages. However, energy from the discharge raises the temperature of the cathode, increasing its emission and the current tends to run away unless limited by some external means, such as a ballasting resistance. Under these conditions, it is impossible to obtain any definite saturation and therefore impossible to determine any definite emission value for a cathode operating in a gaseous discharge.

In the following paper there will be described a method of measuring the emission from a hot cathode in a gaseous discharge under operating conditions.

CONDITIONS FOR A DOUBLE CATHODE SHEATH

A few years ago, Langmuir[1] showed that a thermionic electrode, when placed in the plasma of a gas discharge and maintained at a negative potential of such low magnitude that electrons leaving it could not produce additional ions in the plasma, emitted an electron current of only a few milliamperes, although it was capable of emitting amperes. The electron current from the inserted thermionic electrode increased with the arc current, which produced the plasma, and it was shown that the number of electrons leaving the hot electrode was directly proportional to the number of positive ions reaching it. In the same paper, it was deduced from theoretical considerations that the sheath surrounding a thermionic electrode having a surplus of electron emission is actually a double sheath with an electron space charge close to the cathode followed by a positive ion space charge at the

[1] I. Langmuir, Phys. Rev. **33**, 954 (1929). See especially exp. 560, p. 983.

plasma edge. The relation between electron and positive ion current densities at the thermionic electrode was derived and found to be given by

$$I_e/I_p=(m_p/m_e)^{\frac{1}{2}}, \qquad (1)$$

where I_e and I_p are respectively the electron and positive ion current densities and m_e and m_p the corresponding masses.

Application of this fundamental relation furnishes a new method of measuring the thermionic emission of cathodes, as well as the variation of electron emission with electric field, the disintegrating effect of positive ion bombardment and the relative ionizing power of electrons of different velocities.

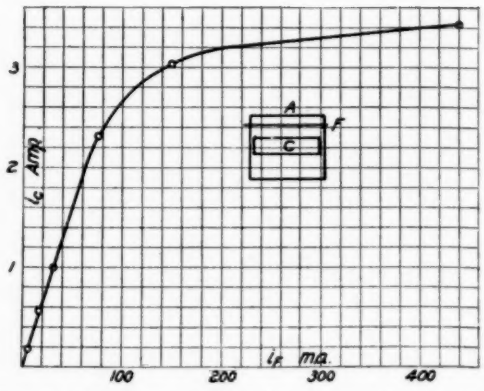

FIG. 1. Electron emission from C as function of arc current. C is 4 volts negative with respect to A. Arc volts $=E_{AF}=30$. Neon at 2 mm pressure.

MEASUREMENT OF ZERO-FIELD EMISSION

A typical tube used for measuring the electron emission of a cathode was a bulb 10 cm diameter in the center of which was a cylindrical anode, A, 3 cm long and 2.5 cm in diameter; concentric with this anode was a cylindrical oxide cathode, C, 6 mm in diameter and 2.5 cm long, which was heated by an internal tungsten coil. At a distance of 6 mm from C and parallel to its long axis was a tungsten filament, F, 0.18 mm diameter and 2.5 cm long. After the usual high vacuum exhaust, the tube was filled with neon to a pressure of 2 mm mercury. A potential of 30 volts was applied between F and A and the current limited by the temperature of F. C was made 4 volts negative to A. The positive ion current to it was found to increase linearly with increase of arc current between F and A. The cathode, C, was then heated by passing 10 amperes through the tungsten heater and the current from C measured as a function of the arc current, i_F. The results are shown in Fig. 1.

As long as C has a surplus electron emission, there is a double sheath with zero voltage gradient at C and the electron current, i_e, from it is limited by the ion current from the plasma so that i_e is directly proportional to i_F. This holds true up to $i_F=75$ m.a. Beyond this point, i_e does not increase as rapidly as i_F and the current is then limited by the electron emission of C. Thus the *value of i_e at the point of departure from linearity is a measure of the zero-field thermionic emission of the cathode C.* It should be noted in this connection that with an ionizing current of only one hundred milliamperes, sufficient ions are produced to permit an electron current from C of 2.5 amperes with an applied potential of only 2 volts. This is due in part to locating C close to F in a region of dense ionization and also to the fact that since the arc current is limited by the temperature of F, a high accelerating voltage could be used to obtain greater ionizing power of the electrons. The subsequent discussion will explain these arguments more fully.

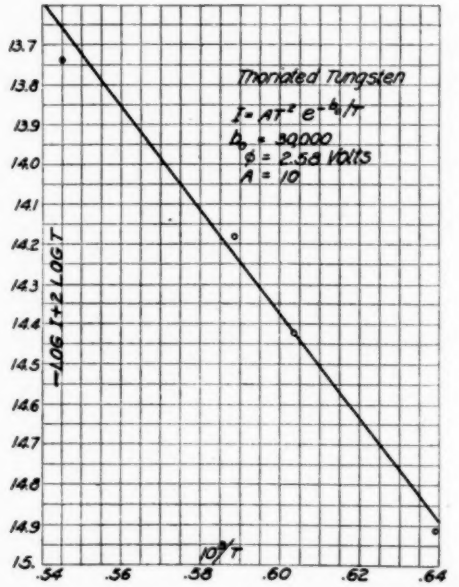

FIG. 2. Emission from thoriated tungsten filament in neon at 2 mm pressure measured by use of auxiliary discharge.

The emission from a thoriated tungsten filament as measured by Dr. L. R. Koller, of this laboratory, using this method, is reproduced in Fig. 2. It will be observed from the curve that the values of the emission constants are in good agreement with those obtained by other methods.

Field Emission

When the current from C becomes limited by its electron emission, it does not reach a flat saturation value but continues to increase slowly as the arc current (i.e., the positive ion current density) is increased. The slow approach to a saturation value is due, undoubtedly, partly to the nonhomogeneous nature of the surface and partly to unequal temperature distribution. However, the electric field established at the cathode when the ion current exceeds that required for the formation of a double sheath must have a decided influence on the electron current from C.

It is well known that the electron emission increases with field. At fields above 10,000 volts per cm, the increase can be accounted for by the Schottky effect.[2] However, at low fields the observed currents have been found to be much less than those expected from an extrapolation according to Schottky's equation, indicating that the zero-field emission is much less than that obtained from measurements made in the presence of a field. The effect of small fields is much more pronounced for composite cathodes, such as the thoriated tungsten, caesium on tungsten,[3] and oxide-coated cathodes. The results obtained in the present investigation also show that the zero-field emission from oxide-coated cathodes is actually only about ten percent of that at which the same cathodes are operated, without disintegration, in practical discharge tubes. The higher currents obtained in practice are the result of the effects of the external electric fields established in the cathode sheath by the creation of a positive ion space charge.

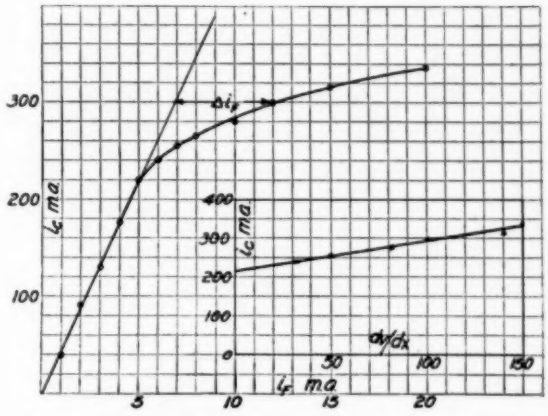

Fig. 3. Emission from unipotential oxide-coated cathode in mercury vapor. *Insert:* Emission *vs.* field at the cathode. $\Delta i_P = \Delta I_P \times$area of electrode.

The field, E, at a plane electrode to which positive ions are flowing is given by[4]

$$E^2 = 7.57 \times 10^5 I_p V^{\frac{1}{2}} (m_p/m_e)^{\frac{1}{2}} \text{ volts/cm}, \quad (2)$$

where I_p is the positive ion current density in amperes per cm^2, V the voltage drop at the electrode in volts, and m_p/m_e the ratio of the mass of an ion to the mass of an electron.

If the electrode also emits electrons, the following similar expression can be derived easily

$$E^2 = 7.57 \times 10^5 \Delta I_p V^{\frac{1}{2}} (m_p/m_e)^{\frac{1}{2}}, \quad (3)$$

where ΔI_p is the positive ion current density in excess of that necessary to establish a double sheath.

The curve of Fig. 3 is the emission curve for an oxide-coated cathode, similar to the cathode, C, described above, taken in the presence of mercury vapor at room temperature. The zero-field emission is about 225 m.a. or about 35 m.a./cm^2. The curve in the inset is the emission as a function of field at the cathode. The field was determined by considering the cathode as a plane and applying Eq. (3). This procedure is not seriously in error as the cathode sheath is less than 0.2 mm thick.

The value of ΔI_p was obtained in the following manner. For the linear portion of the curve, Eq. (1) gives $I_e/I_p = (m_p/m_e)^{\frac{1}{2}} = 605$, but from

[2] For a summary of the effect of field on electron emission see K. T. Compton and I. Langmuir, Rev. Mod. Phys. **2**, 147 (1930).

[3] For an illustration of this see recent paper by J. B. Taylor and I. Langmuir, Phys. Rev. **44**, 436 (1933) in which they find that the zero-field emission may be much lower than that obtained by extrapolating, according to the Schottky slope, to zero fields the values obtained with higher fields.

[4] S. S. Mackeown, Phys. Rev. **34**, 612 (1929).

the curve, $I_e = 43 I_F$. Hence

$$I_p = 43 I_F / 605. \tag{4}$$

The value of ΔI_p is then obtained from (4) by reading the value ΔI_F (see Fig. 3) corresponding to a given value I_e, where ΔI_F and I_e are the current densities corresponding to Δi_F and i_e, respectively.

The results show that the emission increases linearly with field strength up to fields of 150 volts per cm. For higher fields, the relation between emission and field strength must merge into that given by Schottky's equation.

Production of External Fields at Cathodes

The electron current, in excess of the zero-field current, which is obtained from a thermionic cathode in a practical discharge device, is due to the action of the external electric field at the cathode. This external field is created by an increase in cathode drop and also by an increase in positive ion current density at the cathode. The latter is much more effective in producing a field than the increased voltage drop *per se*.

As has already been shown, the electron current from a thermionic cathode is determined by the positive ion current to it as long as the cathode has a surplus electron emission. The number of positive ions, n_p, generated per second by an electron current, i_e, assuming single impact ionization, has been shown to be given by the relation[5]

$$n_p / i_e = K(V_c - V_i), \tag{5}$$

where V_c is the cathode drop and V_i the voltage necessary to cause ionization and K is a constant for low values of V_c, such as exist in thermionic discharges. If f is the fraction of the ions which reach the cathode, the positive ion current at the cathode is

$$i_p = i_e \cdot f \cdot K(V_c - V_i). \tag{6}$$

Although this equation has been shown to hold only for single impact ionization, it will be shown later that, while cumulative ionization existed in the tubes studied, an expression similar to (6) is valid for this case also.

[5] K. T. Compton and I. Langmuir, Rev. Mod. Phys. **2**, 125 (1930).

When the zero-field emission exceeds the arc current, both (1) and (6) must apply, and, hence, a simultaneous solution gives the conditions for the existence of a double sheath, which is

$$V_c - V_i = (m_e/m_p)^{\frac{1}{2}} / f \cdot K. \tag{7}$$

Since in this expression the only variable quantity is V_c, the latter must adjust itself to a definite value at which the electrons leaving the cathode generate a sufficient number of positive ions so that the number reaching the cathode will permit the electron current to leave it. As an illustration, let us calculate the voltage drop at the cathode of a hot cathode discharge in neon at 2 mm pressure. It will be shown later in this paper that, at this pressure, ions are formed by cumulative ionization and the value of V_i is about 16.5 volts, corresponding to the resonance potential. Moreover, since the free paths of the electrons are small compared to the tube dimensions, a value of K should be taken corresponding to the total ionizing power of the electrons. An estimated value of $K = 0.02$ can be obtained from the results of Langmuir and Jones.[6] If we further assume that fifty percent[7] of the ions generated return to the cathode, we find by substituting these values in (7) that $V_c - V_i = 0.5$ volt or $V_c = 17.0$. A similar calculation for mercury for the case of ionization by single impact gives $K = 0.06$ and $V_c - V_i = 0.05$ volt. Although the values of the constants for mercury are less accurately known than for neon, it is certain that $V_c - V_i$ is much less in the case of mercury. This is due to the fact that the probability of ionization is greater for mercury and also to the fact that due to the larger mass of the mercury ion fewer ions are needed to neutralize a given electron space charge.

When the arc current exceeds the zero-field emission of the cathode, the cathode drop increases in order to establish the field necessary to obtain the excess current. In order to illustrate the relative influence of ion current and cathode drop in establishing a field at the cathode, let

[6] I. Langmuir and H. A. Jones, Phys. Rev. **31**, 402 (1928).

[7] Since there is practically no recombination of positive ions and electrons in the space, all of the ions which are generated must disappear either at the electrodes or the tube walls. By the use of a collecting electrode at the wall, the total positive ion current to the walls was found to be the same order of magnitude as that to the cathode.

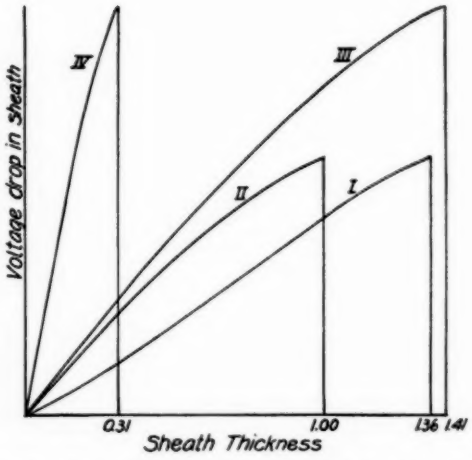

FIG. 4. Potential distribution in sheath. I, double sheath; II, non-emitting collector at 17 volts; III, non-emitting collector at 27 volts; IV, emitting electrode at 27 volts.

us consider the distribution of potential in a sheath under different conditions. Such a series of curves are plotted in Fig. 4.

Curve I shows the potential distribution in the double sheath at a plane cathode of a neon discharge at 2 mm pressure when the arc current is less than the zero-field emission of the cathode. Under these conditions, the voltage drop is 17 volts and the gradient is zero at both the cathode and plasma. The relation between positive ion and electron currents is that given by Eq. (1). As long as the conditions for a double sheath exist, both the voltage drop and potential distribution remain constant. The only change is a decrease in the thickness of the sheath as the current increases. A plane non-emitting electrode, at the same potential as the cathode, is surrounded by a positive ion sheath in which the voltage distribution is that shown in curve II. Under these conditions there is an electric field, the magnitude of which is given by Eq. (2). Also, the thickness of the sheath is reduced to 66.5 percent of that for the double sheath. If in the case of a non-emitting electrode the potential drop in the sheath is increased to 27 volts, corresponding to the value of the disintegration voltage of neon ions as determined by Hull,[8] the distribution of potential is that given in curve III. The thickness of the sheath is increased by about forty-one percent, but the field at the electrode is only twelve percent greater than for curve II.

If the arc current exceeds the field emission to such an extent that a cathode drop of 27 volts is required to create the necessary external field (as mentioned previously), then the positive ion current in the plasma is increased twenty-fold according to Eq. (5). In this case, the thickness of the sheath is reduced to 31 percent and the potential distribution, which is plotted in curve IV, shows a gradient at the cathode 4.7 times that in curve II.

These curves show that the primary cause of the field at the cathode in an arc discharge is an increase in the ion current density at the cathode rather than voltage drop as is evident from consideration of the significance of Eqs. (3) and (6). Thus, in attempting to interpret phenomena at the cathode of a gaseous discharge, it is helpful to consider the ion current density as governing the magnitude of the external field at the electrode.

From the above considerations it is seen that the operation of a cathode in a gaseous discharge may be divided into two phases based on the magnitude of the current in the arc. At currents less than the zero-field emission of the cathode, the primary electrons create ions necessary for the neutralization of electron space charge only and the cathode drop is independent of discharge current. At currents exceeding the zero-field emission, an extra supply of ions must be produced in order to create a positive ion space charge at the cathode. For the first phase, the ratio of i_p/i_e remains constant, while in the second the ratio increases with increase in arc current and thus necessitates an increased cathode drop.

CURRENT RATING OF CATHODES

From a consideration of the results obtained by Hull, it follows that a cathode may be operated without injury as long as the cathode drop is less than the critical disintegration voltage. Thus the maximum current at which a cathode may be safely operated is equal to the zero-field emission plus the field emission that can be obtained by the maximum field which can be created at the cathode without causing the cathode drop to exceed the disintegration voltage.

[8] A. W. Hull, Trans. A. I. E. E. **47**, 753 (1928).

As has been pointed out earlier, the value of the field at the cathode depends not only on the cathode drop, but also on the positive ion current density. The following calculations illustrate the influence of the kind of gas on the production of a field. Let us compare the fields at a cathode operating in a neon discharge with those when it is operating in mercury. In both cases let us assume that 50 percent of the ions generated reach the cathode. It has previously been shown that under conditions for a double sheath, $V_c - V_i$ is 0.5 volt for neon and 0.05 volt for mercury.

No information is available for the voltages at which an oxide-coated cathode is disintegrated, but Hull[7] has found that neon ions with a velocity corresponding to 27 volts disintegrate thorium on tungsten and that the corresponding value for mercury is 17 volts. For a thoriated tungsten cathode, these values represent the maximum permissible cathode drop and when substituted for V_c in Eq. (6) give the maximum positive ion current at the cathode. For neon, this is found to be twenty times that required for a double sheath and one hundred and thirty times for mercury. If y represents this ratio, we can write $\Delta I_p = yI_p$ and, combining with Eq. (6) we obtain

$$\Delta I_p = y \cdot f \cdot I_e (m_e/m_p)^{\frac{1}{2}}. \tag{8}$$

Substitution of this expression for ΔI_p reduces Eq. (3) to

$$E^2 = 7.57 \times 10^5 y \cdot f \cdot I_e \cdot V^{\frac{1}{2}}. \tag{9}$$

Using the values of the constants given above, we find that at the upper limit of safe operation for a thoriated tungsten cathode the field at a cathode in a mercury discharge is more than ten times that in neon. Since the available emission is a function of the field, a cathode may be operated, without disintegration, at a much higher current in mercury than in neon. *Thus the safe current rating of a cathode in a gaseous discharge is not a characteristic of the cathode alone but is also dependent on the gas in which the discharge takes place.*

From Eq. (9) it is seen that any change in tube design which lowers the value of f will also lower the maximum field and therefore the current rating of the cathode. As the gas pressure is decreased, the positive ions are generated farther from the cathode and a smaller fraction of those generated reach it. This reduction in f decreases the maximum field and lowers the current rating of the cathode at the reduced pressure.

Probe Method of Measuring Zero-Field Emission

As has been pointed out, the ratio of i_p/i_e at the cathode is constant for arc currents less than the zero-field emission of the cathode. As the arc current is increased beyond the value corresponding to zero-field emission, i_p increases more rapidly than i_e so that the value of i_e at which an i_e *vs.* i_p curve departs from linearity is to be regarded as a measure of the zero-field emission. As has been shown above, this critical value of i_e may be determined by the use of an auxiliary arc. However, it is often much more practicable to use another method of determining this value of the zero-field emission. The random positive ion current, i_g, as measured by a probe in the plasma of the arc maintained by the cathode under investigation may be used as a measure of the positive ion current, i_p, actually reaching the cathode. The ratio i_p/i_g remains constant if the distribution of ion generation in the discharge is constant. Thus, under these conditions, the zero-field emission of the cathode will be indicated by the value of i_e at which the plot of i_e *vs.* i_g departs from a straight line. Since the cathode drop is constant for discharge currents less than the zero-field emission, the distribution of ion generation will remain the same over this range of discharge currents. If, however, the method of ion formation changes, as, for example, from single impact to cumulative ionization, a redistribution in the region of generation will take place and the interpretation of the results becomes more difficult.

The probe method is especially applicable to three electrode tubes, such as Thyratrons. Mr. C. H. Peck, of this laboratory, has used this method to measure the emission from the cathode of a FG 17 Thyratron tube. His measurements are given in Fig. 5. The ion current to the grid, which was made 12 volts negative to the anode, was measured as a function of arc current. The zero-field emission is seen to be about 250 m.a. Fig. 6 gives a zero-field emission *vs.* temperature

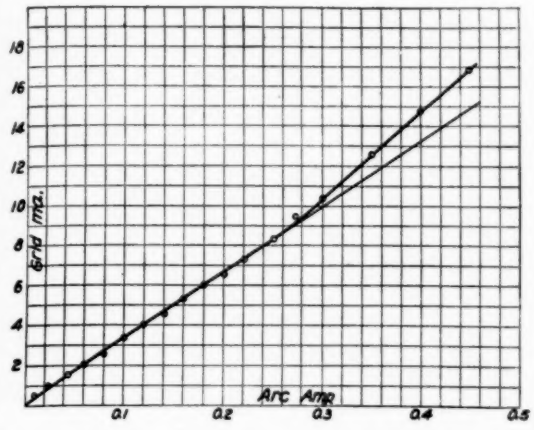

FIG. 5. Ion current to grid *vs.* arc current for FG 17 Thyratron. Grid 12 volts negative to anode.

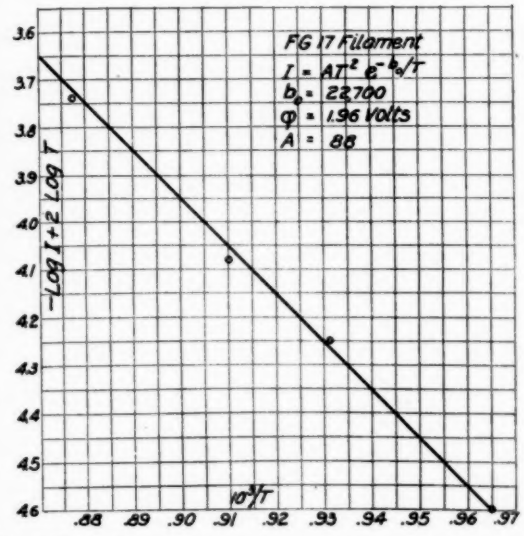

FIG. 6. Emission *vs.* temperature curve for cathode of FG 17 Thyratron.

curve for this cathode. The thermionic constants obtained from this curve are in good agreement with values obtained from measurements on oxide-coated cathodes in vacuum.

The probe method is not adapted for measuring the effect of external field on the emission, since at currents greater than the zero-field emission the cathode drop increases and causes a change in the distribution of ion generation.

IONIZING POWER OF ELECTRONS

Since the electron current from a thermionic electrode with or without field is determined primarily by the positive ion current to it, it follows that an electrode emitting a given number of electrons receives the same positive ion current regardless of the method by which the ions are formed. Consequently, this fact can be utilized to determine the relative ionizing power of electrons as a function of velocity. In a tube with an ionizing discharge and an electrode arrangement similar to the one described in the first part of this paper, the electron emission from the cathode, *C*, was measured as a function of the ionizing current from *F* for different ionizing voltages. The results of such a series of measurements are shown in Fig. 7. The tube contained neon at a pressure of 1 mm and *C* was 2 volts negative to the anode. The ionizing current necessary to liberate a given electron current from *C* is about three times greater for electrons having a velocity equivalent to 19.2 volts than for those at 23 volts. Thus 23 volt electrons are three times as effective in producing ions as those of 19.2 volts. In a similar manner, a comparison of the curves for the other voltages permits the relative ionizing power of the electrons to be plotted as a function of the

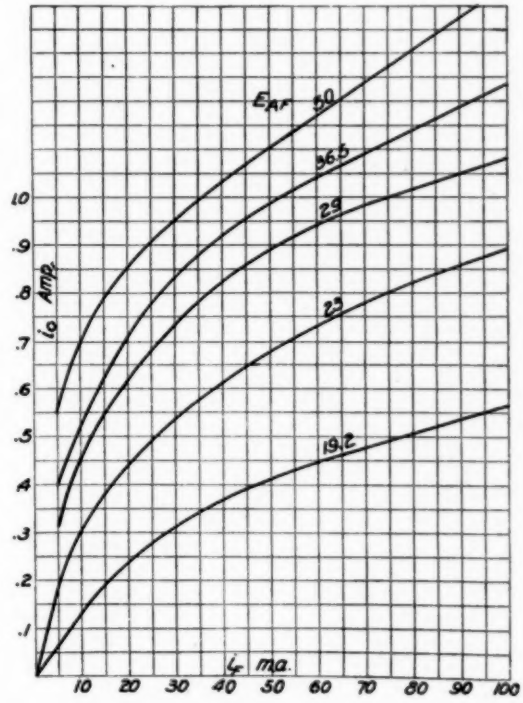

FIG. 7. Electron emission from *C* as function of auxiliary arc current and voltage. *C* is 2 volts negative to *A*. Neon at 1 mm pressure.

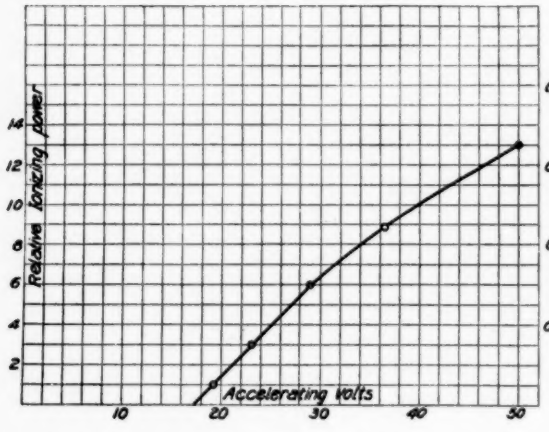

FIG. 8. Relative ionizing power of electrons in neon.

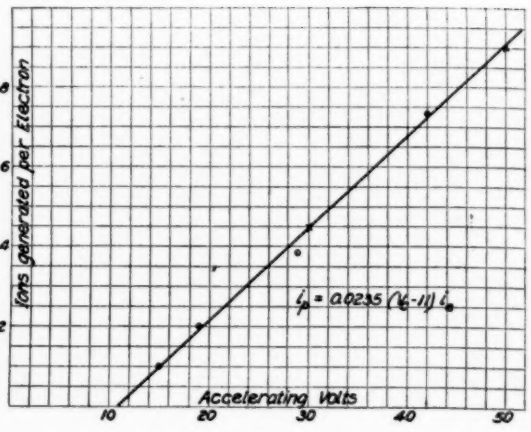

FIG. 9. Total ionizing power of electrons of different velocities in argon.

electron energy. This curve for neon is given in Fig. 8. Since other measurements with probes show that the energy of the primary electrons from F is decreased to a value less than V_i within a distance small compared to the tube dimensions, the relative ionizing power measured corresponds to the total number of positive ions formed or to β maximum as determined by Jones and Langmuir.[6] In the case of neon, the values obtained in the present investigation cannot be compared with the electron velocities used by them which were very much higher. However, it is possible to make such a comparison in the case of argon since the voltages used overlap those for which data are given by Jones and Langmuir. By adjusting the relative values of β maximum obtained in this investigation with those obtained by Jones and Langmuir, the two sets of measurements are found to agree. The results for argon at a pressure of 1 mm are shown in Fig. 9 and the crosses on the curve indicate results from the paper by Langmuir and Jones.

Since the voltage axis of curves in Figs. 8 and 9 are less than the values of V_i for neon and argon, respectively, it follows that ionization in these experiments must have been of the cumulative type. Although the relation given in Eq. (6) is based on the assumption that ionization occurs by single impact, it is interesting to find that the same relation is valid if V_i is replaced by a new constant of the order of the minimum excitation potential of the gas, which, as is shown by Figs. 8 and 9, is 11 volts for argon and 17 volts for neon.

DISINTEGRATION OF CATHODES BY ION BOMBARDMENT

Although only qualitative results have been obtained, the use of a double cathode tube offers an excellent method of studying the effect of positive ion bombardment of a cathode surface. For example, cathode C can be bombarded by ions of any velocity produced by the discharge between F and A. The influence of this bombardment on the electron emission can then be determined by measuring the emission of C at a voltage sufficiently low to assume the absence of disintegration.

In conclusion, the writer would like to point out that in the above discussion emphasis has been placed on the methods, and only such experimental data have been given as were necessary to illustrate the application of these methods. Furthermore, no attempt has been made to include the modifications that would be necessary in order to take into account the effect of initial velocities. However, the manner in which this factor would modify the relations given in this paper is evident from the consideration of the equations derived by Langmuir.[9]

The writer wishes to thank Dr. I. Langmuir for many helpful discussions and Dr. S. Dushman for his assistance in the way of advice and criticism.

[9] I. Langmuir, Phys. Rev. **33**, 975 (1929).

Hyperfine Structure of Fluorine

F. W. BROWN AND J. H. BARTLETT, JR., *Department of Physics, University of Illinois*

(Received January 29, 1934)

The theory of Breit and Doermann has been extended and applied to the case of fluorine. The wave functions for the $2p^4 3s$ and $2p^4 3p$ configurations were found by the Hartree method. Hyperfine structure separation formulae have been derived for the $2p^4(^3P)3s$ and $2p^4(^3P)3p$ states, both for the case of pure (LS) coupling, and for the case in which the perturbations between levels of the same configuration (and same state of the core) are considered. With the above $2p$ and $3p$ radial functions, the ordinary multiplet structure has been calculated, and found to agree well with experiment, indicating that these functions are quite accurate. By using the experimental results of Campbell, the magnetic moment of the fluorine nucleus has been calculated. Fairly consistent results are obtained, the mean value of the nuclear magnetic moment being about three nuclear magnetons.

I. INTRODUCTION

ACCORDING to present theory, the hyperfine structure of an element may be explained on the assumption of a magnetic field produced by the nucleus. As a first approximation, one supposes the nucleus to be representable by a magnetic dipole, and that higher magnetic moments may be neglected.[1] If now, accurate[2] wave functions for various states of the atom are known, it is possible to calculate the hyperfine structure splittings for each of these states as a (linear) function of μ, the nuclear magnetic moment. Comparison with the experimental values should give independent determinations of the value of μ (one for each state). If these values of μ agree with one another, then one has an indication that the theory is correct.

Unfortunately, most of the elements for which hyperfine structure is known are of rather high atomic number. For such elements, the wave functions have not as yet been calculated to a high degree of accuracy, so that the nuclear magnetic moments[3] must be regarded as uncertain to the same degree.

Of the lighter elements, hfs patterns have been found for Li II,[4] F I,[5] Na I,[6] and Al II.[7] For some time, there was doubt as to the value of the nuclear angular momentum of Li 7, due probably to the experimental difficulties. Now that the structure in F I has been measured, it would seem that this might offer a better opportunity for testing the existing theory.

For a many-electron system, no relativistic theory is as yet available. Accordingly, one does not know, really, how to proceed with hfs calculations for such a system. Breit and Doermann[8] have, however, advanced a tentative theory which assumes the perturbative part of the Hamiltonian function to be a sum of contributions, each of which represents the interaction of one electron with the nucleus. That is, each contribution is of the form $w=e(\boldsymbol{\alpha}\cdot\mathbf{A})$, where $\mathbf{A}=[\boldsymbol{\mu}\times\mathbf{r}]/r^3$ and $\boldsymbol{\alpha}$ is Dirac's vector matrix. The calculations which follow are based on the above theory.

In this work the hyperfine structures of the $2p^4(^3P)3s$ and $2p^4(^3P)3p$ states of fluorine are

[1] The sufficiency of this approximation must, of course, be decided by experiment. It may be that, for complicated nuclei, one will have to consider effects due to higher moments. To our knowledge, no theory of these has been given.

[2] The accuracy may be tested by determining the splittings of the gross structure (ordinary multiplets).

[3] Attempts to obtain consistent values of μ have been made by S. Goudsmit (Phys. Rev. **43**, 636 (1933)), and by E. Fermi and E. Segrè (Zeits. f. Physik **82**, 729 (1933)). See also G. Breit and L. A. Wills (Phys. Rev. **44**, 470 (1933)) for corrections involving relativity and intermediate coupling.

[4] See L. P. Granath, Phys. Rev. **42**, 44 (1932) for references.

[5] J. S. Campbell, Zeits. f. Physik **84**, 393 (1933).

[6] H. Schüler, Naturwiss. **16**, 512 (1928); H. Schüler u. H. Brück, Zeits. f. Physik **58**, 735 (1929).

[7] F. Paschen, Berl. Ber. p. 502 (1932).

[8] G. Breit and F. W. Doermann, Phys. Rev. **36**, 1732 (1930).

calculated. The magnetic moment of the nucleus is determined from our hfs formulae and the experimental data of Campbell.[5] The calculations have been made via (LS) coupling, using the Hartree radial functions. The results of the calculations for pure (LS) coupling are given in Section III, and those for intermediate coupling in Section V. The radial functions obtained by the self-consistent field method are tabulated in Section IV. A check on the accuracy of the $2p$ and $3p$ functions was obtained by calculating the multiplet structure and comparing with experiment.

Wave functions

As usual, we shall assume the wave function to be expansible as a linear combination of product functions, only a few terms of the expansion being considered as important. Thus, an atomic wave function is to be written as a linear combination of products, each of which is formed by multiplying a nuclear function (where I and M_I are specified) by an electronic function associated with a particular J and M_J. The electronic function is to be written as a linear combination of determinants, each determinant being generated by permutations on a product of single-electron wave functions. For extreme coupling, the "zeroth" approximation for the electronic function can be found by group theoretical methods.[9] For intermediate coupling, the perturbation between levels in the same configuration with the same J must be taken into account.

II. Single Electron Matrix Elements

As already stated, it is necessary to find the matrix elements of the operator $w=e\{\mathfrak{a}\cdot[\mathfrak{y}\times\mathfrak{r}]\}/r^3 = -e\{\mathfrak{y}\cdot[\mathfrak{a}\times\mathfrak{r}]\}/r^3=\mathfrak{y}\cdot\mathbf{V}$, where $\mathbf{V}$ is the vector $-e[\mathfrak{a}\times\mathfrak{r}]/r^3$. That is, we must determine matrix elements of operators of the type $(\mathbf{X}+i\mathbf{Y})$, $(\mathbf{X}-i\mathbf{Y})$, and $\mathbf{Z}$, where $\mathbf{X}$, $\mathbf{Y}$, $\mathbf{Z}$ are to refer to the x, y and z components of $\mathfrak{y}$ (or $\mathbf{V}$). General expressions for such matrix elements are known.[10] The formulae involve multiplicative factors (depending on the radial integrals), which must be determined directly.

The expression for the z-component of $\mathbf{V}$ has been given by Breit and Wills,[3] p. 474, Eq. (13). If we set $\mathfrak{y}_x+i\mathfrak{y}_y=\mu_p$, and $\mathfrak{y}_x-i\mathfrak{y}_y=\mathfrak{y}_q$, etc., then the interaction energy may be written $w=\frac{1}{2}(\mathfrak{y}_p\mathbf{V}_q+\mathfrak{y}_q\mathbf{V}_p)+\mathfrak{y}_z\mathbf{V}_z$.

The only nonvanishing matrix elements of w are associated with the transitions $M_I\rightarrow M_I$, $M_I\pm1$. We shall abbreviate as follows:

$$(M_I|\mu_p|M_I-1)=-(M_I-1|\mu_q|M_I)=(\mu/I)[(I-M_I+1)(I+M_I)]^{1/2}=\mu_p',$$
$$(M_I|\mu_z|M_I)=(\mu/I)M_I=\mu_z'.$$

The Bohr magneton will be denoted by μ_0. The matrix elements of w (for $l\rightarrow l$) are:

$j\rightarrow j-1$ (or $l+\frac{1}{2}\rightarrow l-\frac{1}{2}$)

$$(m_j-1|w|m_j)=-(\mu_p'/4j)[(j-m_j+1)(j-m_j)]^{1/2}C_l\mu_0,$$
$$(m_j|w|m_j-1)=(\mu_p'/4j)[(j+m_j-1)(j+m_j)]^{1/2}C_l\mu_0,$$
$$(m_j|w|m_j)=-(\mu_z'/2j)(j^2-m_j^2)^{1/2}C_l\mu_0,$$

$j\rightarrow j$

$$(m_j|w|m_j-1)=[\mu_p'/2j(j+1)][(j-m_j+1)(j+m_j)]^{1/2}A_l'\mu_0,$$
$$(m_j|w|m_j)=[\mu_z'/j(j+1)]A_l'm_j\mu_0.$$

[9] J. H. Bartlett, Jr., Phys. Rev. **38**, 1623 (1931).

[10] See, for example, E. Wigner, *Gruppentheorie*, p. 264. It is to be noted that the scheme used by Wigner is not the same as that of van der Waerden, to which Breit and Wills refer. We shall adhere to Wigner's formulae throughout.

Here $A_l'=A_l=(l+1)I_{l,\,l}$ for $j=l+\frac{1}{2}$; $A_l'=B_l=-lI_{-l-1,\,-l-1}$ for $j=l-\frac{1}{2}$; and $C_l=I_{l,\,-l-1}$, where $I_{k,\,l}$ is defined by

$$I_{k,\,l}=(2mc/\hbar)\int_0^\infty (F_kG_l+F_lG_k)dr.$$

(The F_k and G_k are the radial functions of Darwin.[11]) A comparison with formulas (12) and (14) of Breit and Wills[3] may be made by setting $A_l=j(j+1)\sigma_1$, $B_l=j(j+1)\sigma_2$, and $C_l=(2l+1)\rho$. This automatically establishes the connection with the a' and a'' of Goudsmit (see Breit and Wills, p. 478).

Now

$$F_kG_l+F_lG_k=\frac{\mu_0}{e}\left\{-\frac{d}{dr}(F_kF_l+G_kG_l)+\frac{k+l}{r}G_kG_l-\frac{k+l+4}{r}F_kF_l\right\}.$$

If we assume that $F^2\ll G^2$ and that $G_{-l-1}=G_l=$ the Schrödinger function, then the integral becomes

$$I_{k,\,l}=G_l^2(0)+(k+l)\overline{(r^{-3})}_l. \tag{1}$$

[The matrix elements[12] for $l\to l-2$ and $l-2\to l$ are the same as those given above except that C_l is replaced by $-I_{-l-1,\,l-2}$, and that there are, by definition, no matrix elements of this type corresponding to $j\to j$.]

For the case of (jj) coupling the above matrix elements can be used directly, but for (LS) coupling the strong field single electron functions must be used. The matrix elements of the strong field functions will be linear combinations of those given above. The strong field functions[13] can be written approximately as

$$\Psi_1=\left(\frac{l-m_j+\frac{1}{2}}{2l+1}\right)^{1/2}\psi_1-\left(\frac{l+m_j+\frac{1}{2}}{2l+1}\right)^{1/2}\psi_2,$$

$$\Psi_2=-\left(\frac{l+m_j+\frac{1}{2}}{2l+1}\right)^{1/2}\psi_1-\left(\frac{l-m_j+\frac{1}{2}}{2l+1}\right)^{1/2}\psi_2,$$

where Ψ_1, Ψ_2 refer to $m_s=\frac{1}{2}$, $-\frac{1}{2}$, respectively; ψ_1, ψ_2 are the Dirac functions for $j=l-(\frac{1}{2})$, $j=l+(\frac{1}{2})$, respectively, and $m_j=m_l+m_s$.

Let us write $D=[2A_l/(2l+3)]-[2B_l/(2l-1)]-C_l$. Then the matrix elements of the strong field functions are (remembering that $m_J\to m_J$ always):

$m_s\to m_s$:

(a): $$(m_l|w|m_l)=[2\mu_z'/(2l+1)^2]\{m_l(A+B-C)+2m_l^2m_sD+2m_s[\{A(l+1)/(2l+3)\}+\{Bl/(2l-1)\}+Cl(l+1)]_l,$$

(b): $$(m_l-1|w|m_l)=[\mu_p'/(2l+1)^2][(l-m_l+1)(l+m_l)]^{1/2}\{(A+B-C)+m_s(2m_l-1)D\}_l$$

$m_s\to m_s-1$:

(c): $$(m_l-1|w|m_l)=-[\mu_z'/(2l+1)^2](1-2m_l)[(l-m_l+1)(l+m_l)]^{1/2}D_l,$$

(d): $$(m_l|w|m_l)=[\mu_p'/(2l+1)^2]\{-Dm_l^2+[2A(l+1)^2/(2l+3)]-[2Bl^2/(2l-1)]+Cl(l+1)\}_l,$$

(e): $$(m_l-2|w|m_l)=[\mu_p'/(2l+1)^2][(l-m_l+1)(l-m_l+2)(l+m_l)(l+m_l-1)]^{1/2}D_l.$$

It is to be remembered that the matrix w is Hermitian.

---

[11] C. G. Darwin, Proc. Roy. Soc. **A118**, 673 (1928).

[12] Matrix elements of this type are neglected throughout the following calculation, since wave functions which differ in l value by two units do not overlap much.

[13] These were obtained from the secular equation given by P. A. M. Dirac, Proc. Roy. Soc. **A118**, 351 (1928).

Let us define the symbols h_s, h_l so that $h_s=G_l^2(0)$, and $h_l=\overline{(r^{-3})_l}$ for $l\neq 0$. Then, making the simplification (1), we have:

$$A+B-C=(2l+1)^2h_l,$$

$$D=[(2l+1)^2/(2l+3)(2l-1)][h_s-3h_l],$$

$$[A(l+1)/(2l+3)]+[Bl/(2l-1)]+Cl(l+1)=[(2l+1)^2/(2l+3)(2l-1)][(l^2+l-1)h_s+(l^2+l)h_l],$$

$$[2A(l+1)^2/(2l+3)]-[2Bl^2/(2l-1)]+Cl(l+1)=[(2l+1)^2/(2l+3)(2l-1)][(3l^2+3l-2)h_s-(l^2+l)h_l].$$

These expressions may be substituted in the formulae (a) to (e). If G_l is taken to be the Schrödinger function, then $h_s=0$ for all except s electrons. For s electrons, the coefficients of h_l vanish. The simplified matrix elements are the ones which are used in the subsequent work. [It is to be noted that $\psi^2(0)$, the square of the wave function at the origin, is equal to $(1/4\pi)G^2(0)$.]

III. Hyperfine Structure Formulae for (*LS*) Coupling

We shall assume that the hfs is so small in comparison to the ordinary multiplet structure that there are no appreciable perturbations between levels with the same hyperfine quantum number F but different J. In this case, the hyperfine splitting follows the interval rule

$$\Delta W=A(IJ)[F(F+1)-I(I+1)-J(J+1)]/2.$$

For pure (*LS*) coupling it is only necessary to calculate matrix elements of the type $(ILSJM_IM_J|W|ILSJM_IM_J)$, where M_J and M_I have their maximum values for the given J and I. Hence, we need only find the linear combination atomic functions corresponding to the maximum M_J for a given LSJ. These functions are given below.

Those weak field functions which are not the same as the strong field functions are given by:

$$^2P_{1/2}: \quad (1/3)^{1/2}\psi_{0,\,1/2}-(2/3)^{1/2}\psi_{1,\,-1/2},$$

$$^2D_{3/2}: \quad (4/5)^{1/2}\psi_{2,\,-1/2}-(1/5)^{1/2}\psi_{1,\,1/2},$$

$$^4D_{1/2}: \quad (2/5)^{1/2}\psi_{2,\,-3/2}-(3/10)^{1/2}\psi_{1,\,-1/2}+(1/5)^{1/2}\psi_{0,\,1/2}-(1/10)^{1/2}\psi_{-1,\,3/2},$$

$$^4D_{3/2}: \quad (2/5)^{1/2}\psi_{2,\,-1/2}-(2/5)^{1/2}\psi_{1,\,1/2}+(1/5)^{1/2}\psi_{0,\,3/2},$$

$$^4D_{5/2}: \quad (4/7)^{1/2}\psi_{2,\,1/2}-(3/7)^{1/2}\psi_{1,\,3/2},$$

$$^4P_{1/2}: \quad -(1/3)^{1/2}\psi_{0,\,1/2}+(1/2)^{1/2}\psi_{-1,\,3/2}+(1/6)^{1/2}\psi_{1,\,-1/2},$$

$$^4P_{3/2}: \quad (3/5)^{1/2}\psi_{0,\,3/2}-(2/5)^{1/2}\psi_{1,\,1/2}.$$

The subscripts on the strong field functions refer to M_L and M_S, respectively.

Since the matrix elements for a p^2 configuration have the same form as those of p^4 for hfs and the same except for a reversal of sign for the ordinary multiplet structure, we need list only the strong field functions for the p^2p configuration, leaving to the reader the relatively easy calculation of the p^2s functions. (We shall write a determinant function simply as $\alpha^1\alpha^{-1}\beta^1{}_p$, for instance, leaving off the vertical bars.) These follow:

$p^2(^3P)p$

$$^2P: \quad \psi_{1,\,1/2}=(1/72)^{1/2}\{-2\alpha^1\alpha^{-1}\beta_p{}^1+2\alpha^1\alpha^0\beta_p{}^0+\alpha^1\beta^{-1}\alpha_p{}^1+\beta^1\alpha^{-1}\alpha_p{}^1-\alpha^1\beta^0\alpha_p{}^0-\beta^1\alpha^0\alpha_p{}^0\},$$

$$\psi_{1,\,-1/2}=(1/72)^{1/2}\{2\beta^1\beta^{-1}\alpha_p{}^1-2\beta^1\beta^0\alpha_p{}^0-\alpha^1\beta^{-1}\beta_p{}^1-\beta^1\alpha^{-1}\beta_p{}^1+\alpha^1\beta^0\beta_p{}^0+\beta^1\alpha^0\beta_p{}^0\},$$

$$\psi_{0,\,1/2}=(1/72)^{1/2}\{2\alpha^1\alpha^0\beta_p{}^{-1}-2\alpha^0\alpha^{-1}\beta_p{}^1-\alpha^1\beta^0\alpha_p{}^{-1}-\beta^1\alpha_0\alpha_p{}^{-1}+\alpha^0\beta^{-1}\alpha_p{}^1+\beta^0\alpha^{-1}\alpha_p{}^1\},$$

$$^4S:\ \psi_{0,\,3/2}=(1/18)^{1/2}\{\alpha^1\alpha^0\alpha_p{}^{-1}+\alpha^0\alpha^{-1}\alpha_p{}^1+\alpha^1\alpha^{-1}\alpha_p{}^0\},$$

$$^2S:\ \psi_{0,\,1/2}=(1/108)^{1/2}\{2\alpha^1\alpha^0\beta_p{}^{-1}+2\alpha^0\alpha^{-1}\beta_p{}^1-2\alpha^1\alpha^{-1}\beta_p{}^0-\alpha^1\beta^0\alpha_p{}^{-1}-\beta^1\alpha^0\alpha_p{}^{-1}-\alpha^0\beta^{-1}\alpha_p{}^1$$
$$-\beta^0\alpha^{-1}\alpha_p{}^1+\alpha^1\beta^{-1}\alpha_p{}^0+\beta^1\alpha^{-1}\alpha_p{}^0\},$$

$$^2D:\ \psi_{2,\,1/2}=(1/6)\{2\alpha^1\alpha^0\beta_p{}^1-\alpha^1\beta^0\alpha_p{}^1-\beta^1\alpha^0\alpha_p{}^1\},$$

$$\psi_{2,\,-1/2}=(1/6)\{-2\beta^1\beta^0\alpha_p{}^1+\alpha^1\beta^0\beta_p{}^1+\beta^1\alpha^0\beta_p{}^1\},$$

$$\psi_{1,\,1/2}=(1/72)^{1/2}\{2\alpha^1\alpha^{-1}\beta_p{}^1+2\alpha^1\alpha^0\beta_p{}^0-\alpha^1\beta^{-1}\alpha_p{}^1-\beta^1\alpha^{-1}\alpha_p{}^1-\alpha^1\beta^0\alpha_p{}^0-\beta^1\alpha^0\alpha_p{}^0\},$$

$$^4D:\ \psi_{2,\,3/2}=(1/6)^{1/2}\alpha^1\alpha^0\alpha_p{}^1,$$

$$\psi_{2,\,1/2}=(1/18)^{1/2}\{\alpha^1\beta^0\alpha_p{}^1+\beta^1\alpha^0\alpha_p{}^1+\alpha^1\alpha^0\beta_p{}^1\},$$

$$\psi_{2,\,-1/2}=(1/18)^{1/2}\{\beta^1\beta^0\alpha_p{}^1+\alpha^1\beta^0\beta_p{}^1+\beta^1\alpha^0\beta_p{}^1\},$$

$$\psi_{2,\,-3/2}=(1/6)^{1/2}\beta^1\beta^0\beta_p{}^1,$$

$$\psi_{1,\,3/2}=(1/12)^{1/2}\{\alpha^1\alpha^{-1}\alpha_p{}^1+\alpha^1\alpha^0\alpha_p{}^0\},$$

$$\psi_{1,\,1/2}=(1/6)\{\alpha^1\alpha^{-1}\beta_p{}^1+\alpha^1\alpha^0\beta_p{}^0+\alpha^1\beta^{-1}\alpha_p{}^1+\beta^1\alpha^{-1}\alpha_p{}^1+\alpha^1\beta^0\alpha_p{}^0+\beta^1\alpha^0\alpha_p{}^0\},$$

$$\psi_{1,\,-1/2}=(1/6)\{\beta^1\beta^{-1}\alpha_p{}^1+\beta^1\beta^0\alpha_p{}^0+\alpha^1\beta^{-1}\beta_p{}^1+\beta^1\alpha^{-1}\beta_p{}^1+\alpha^1\beta^0\beta_p{}^0+\beta^1\alpha^0\beta_p{}^0\},$$

$$\psi_{0,\,3/2}=(1/6)\{\alpha^1\alpha^0\alpha_p{}^{-1}+\alpha^0\alpha^{-1}\alpha_p{}^1+2\alpha^1\alpha^{-1}\alpha_p{}^0\},$$

$$\psi_{-1,\,3/2}=(1/12)^{1/2}\{\alpha^1\alpha^{-1}\alpha_p{}^{-1}+\alpha^0\alpha^{-1}\alpha_p{}^0\},$$

$$\psi_{0,\,1/2}=(1/108)^{1/2}\{\alpha^1\alpha^0\beta_p{}^{-1}+\alpha^0\alpha^{-1}\beta_p{}^1+2\alpha^1\alpha^{-1}\beta_p{}^0+\alpha^1\beta^0\alpha_p{}^{-1}+\beta^1\alpha^0\alpha_p{}^{-1}+\alpha^0\beta^{-1}\alpha_p{}^1$$
$$+\beta^0\alpha^{-1}\alpha_p{}^1+2\alpha^1\beta^{-1}\alpha_p{}^0+2\beta^1\alpha^{-1}\alpha_p{}^0\},$$

$$^4P:\ \psi_{1,\,3/2}=(1/12)^{1/2}\{-\alpha^1\alpha^{-1}\alpha_p{}^1+\alpha^1\alpha^0\alpha_p{}^0\},$$

$$\psi_{1,\,1/2}=(1/6)\{-\alpha^1\alpha^{-1}\beta_p{}^1+\alpha^1\alpha^0\beta_p{}^0-\alpha^1\beta^{-1}\alpha_p{}^1-\beta^1\alpha^{-1}\alpha_p{}^1+\alpha^1\beta^0\alpha_p{}^0+\beta^1\alpha^0\alpha_p{}^0\},$$

$$\psi_{1,\,-1/2}=(1/6)\{-\beta^1\beta^{-1}\alpha_p{}^1+\beta^1\beta^0\alpha_p{}^0-\alpha^1\beta^{-1}\beta_p{}^1-\beta^1\alpha^{-1}\beta_p{}^1+\alpha^1\beta^0\beta_p{}^0+\beta^1\alpha^0\beta_p{}^0\},$$

$$\psi_{0,\,3/2}=(1/12)^{1/2}\{\alpha^1\alpha^0\alpha_p{}^{-1}-\alpha^0\alpha^{-1}\alpha_p{}^1\},$$

$$\psi_{0,\,1/2}=(1/6)\{\alpha^1\alpha^0\beta_p{}^{-1}-\alpha^0\alpha^{-1}\beta_p{}^1+\alpha^1\beta^0\alpha_p{}^{-1}+\beta^1\alpha^0\alpha_p{}^{-1}-\alpha^0\beta^{-1}\alpha_p{}^1-\beta^0\alpha^{-1}\alpha_p{}^1\},$$

$$\psi_{-1,\,3/2}=(1/12)^{1/2}\{\alpha^1\alpha^{-1}\alpha_p{}^{-1}-\alpha^0\alpha^{-1}\alpha_p{}^0\}.$$

In accordance with the theory of Breit and Doermann, we have assumed the magnetic interaction energy W between electrons and nucleus to be of the form $W=\sum_i w_i$. The general expression for the matrix elements of W with respect to the determinant functions is $(n|W|n')=(1/N!)\int|u(n_1/1)u(n_2/2)\cdots u(n_N/N)|^*W|u(n_1'/1)\cdots u(n_N'/N)|d\tau$. It is known[14] that $(n|W|n)=\sum_i I(n_i)$, where $I(n)=\int u^*(n_i)wu(n_i)d\tau$. In addition, if $n_1=n_1'$, $n_2=n_2'$, etc., with the sole exception of $n_i\neq n_i'$, the matrix element is $(n|W|n')=(-)^\sigma\int u^*(n_i)\bar{w}u(n_i')d\tau$, where σ is the number of permutations which must be made to bring the quantum numbers (n_i) and (n_i') into the same order. All other matrix elements of W vanish.

Using the above functions, one then obtains for the hfs displacements[15] (from the c.g.)

$$2p^4(^3P)3p$$

$$^2P_{1/2}:\ \{(10/9)h_{2p}+(8/9)h_{3p}\}[1,\,-3]\mu\mu_0,$$

$$^2P_{3/2}:\ \{(13/15)h_{2p}+(14/15)h_{3p}\}[1,\,(-5/3)]\mu\mu_0,$$

[14] J. C. Slater, Phys. Rev. **34**, 1404 (1929).

[15] We may note that $a(s)=(16\pi/3)g\mu_0{}^2\psi^2(0)=(4/3)g\mu_0{}^2h_s$.

$^4S_{3/2}$: 0; $^2S_{1/2}$: 0,

$^2D_{3/2}$: $\{(93/75)h_{2p}+(114/75)h_{3p}\}[1, (-5/3)]\mu\mu_0$,

$^2D_{5/2}$: $\{(34/15)h_{2p}+(32/15)h_{3p}\}[1, (-7/5)]\mu\mu_0$,

$^4D_{1/2}$: $\{(31/75)h_{2p}+(104/75)h_{3p}\}[1, -3]\mu\mu_0$,

$^4D_{3/2}$: $\{(48/75)h_{2p}+(132/75)h_{3p}\}[1, (-5/3)]\mu\mu_0$,

$^4D_{5/2}$: $\{(128/105)h_{2p}+(202/105)h_{3p}\}[1, (-7/5)]\mu\mu_0$,

$^4D_{7/2}$: $\{(12/5)h_{2p}+(8/5)h_{3p}\}[1, (-9/7)]\mu\mu_0$,

$^4P_{1/2}$: $\{(-4/9)h_{2p}+(-2/9)h_{3p}\}[1, -3]\mu\mu_0$,

$^4P_{3/2}$: $\{(64/75)h_{2p}+(-4/75)h_{3p}\}[1, (-5/3)]\mu\mu_0$,

$^4P_{5/2}$: $\{(4/5)h_{2p}+(6/5)h_{3p}\}[1, (-7/5)]\mu\mu_0$.

$2p^4(^3P)3s$

$^2P_{1/2}$: $\{(4/9)h_{2p}+(2/27)h_{3s}\}[1, -3]\mu\mu_0$,

$^2P_{3/2}$: $\{(34/15)h_{2p}+(-2/9)h_{3s}\}[1, (-5/3)]\mu\mu_0$,

$^4P_{1/2}$: $\{(-4/9)h_{2p}+(10/27)h_{3s}\}[1, -3]\mu\mu_0$,

$^4P_{3/2}$: $\{(-8/75)h_{2p}+(22/45)h_{3s}\}[1, (-5/3)]\mu\mu_0$,

$^4P_{5/2}$: $\{(12/5)h_{2p}+(2/3)h_{3s}\}[1, (-7/5)]\mu\mu_0$.

If the spin I were not 1/2, the only modification would be to substitute different numbers in the second bracket (by means of the interval rule).[16]

The values of the nuclear moment (in nuclear magnetons) calculated from the above formulae are recorded in Table II of Section V.

IV. Self-Consistent Wave Functions

The accuracy of the hfs calculations depends to a large extent on the accuracy of the radial functions used. The best nonrelativistic wave functions at present are those obtained by the self-consistent field method. A self-consistent field was obtained (by the Hartree method) for the $2p^43s$ configuration, and it was assumed that the functions of the inner electrons would not be changed appreciably when the $3s$ electron was excited to a $3p$ orbit.

The normalized Hartree functions as well as the values of $\eta=-(P'/P)$, $\xi=\eta+[(l+1)/r]$, and P' are given in Table I. The $1s$ function has been given elsewhere.[17]

These functions are not orthogonal. The orthogonalized functions are:

$$P_{\text{orth}}(1s)=P(1s),$$

$$P_{\text{orth}}(2s)=1.001\,P(2s)-0.0250\,P(1s),$$

$$P_{\text{orth}}(3s)=P(3s)-0.0296\,P(2s)-0.0047\,P(1s),$$

$$P_{\text{orth}}(2p)=P(2p),$$

$$P_{\text{orth}}(3p)=1.010\,P(3p)-0.144\,P(2p).$$

With the orthogonal functions, one obtains

$$P_{1s}^2(0)=2690,\quad \overline{(1/r^3)}_{2p}=8.05,\quad \overline{(Z/r^3)}_{2p}=58.3,$$

$$P_{2s}^2(0)=120,\quad \overline{(1/r^3)}_{3p}=0.028,\quad \overline{(Z/r^3)}_{3p}=0.181,$$

$$P_{3s}^2(0)=3.60,$$

where $Z(r)$ is an effective nuclear charge such that $[Z(r)/r^2]$ for a given electron represents the electric field acting on the electron.

[16] This remark is of no immediate interest. There exists the possibility, however, that other members of the same isoelectronic sequence might be investigated experimentally.

[17] F. W. Brown, Phys. Rev. **44**, 214 (1933).

TABLE I. *Hartree functions for the $2p^4 3s$ and $2p^4 3p$ configurations in fluorine.*

r	$P(2s)$	$\xi(2s)$	$P'(2s)$	$P(2p)$	$\xi(2p)$	$P(3s)$	$\xi(3s)$	$P'(3s)$	$P(3p)$	$\xi(3p)$	$P'(3p)$
0.	0.	9.000		0.	4.500	0.	9.000		0.	4.500	
.01	0.112	9.105		0.002	4.438	.023	9.110			4.436	
.02	.204	9.224		.008	4.377	.042	9.227		.001	4.373	
.03	.279	9.354		.017	4.316	.057	9.366		.003	4.312	
.04	.338	9.502		.028	4.256	.069	9.524		.005	4.251	
.05	.384	9.671		.042	4.198	.079	9.704		.008	4.191	
.06	.418	9.865		.058	4.142	.086	9.909		.011	4.133	
.07	.442	10.088		.076	4.088	.090	10.145		.015	4.078	
.08	.456	10.346		.095	4.037	.093	10.418		.018	4.025	
.09	.461	10.646		.116	3.989	.094	10.733		.022	3.975	
.10	.460	10.993		.138	3.942	.094	11.099		.027	3.929	
.11	.453	11.397		.160	3.898	.092	11.526		.031	3.884	
.12	.440	11.872		.183	3.857	.089	12.029		.035	3.841	
.13	.422	12.434		.207	3.818	.086	12.624		.040	3.801	
.14	.400	13.107		.231	3.782	.081	13.338		.045	3.763	
.15	.374	13.918		.256	3.748	.076	14.203		.049	3.727	
.16	.346		−2.997	.280	3.715	.070		−.613	.054	3.694	
.17	.316		−3.234	.305	3.684	.063		−.661	.059	3.661	
.18	.283		−3.432	.329	3.655	.056		−.701	.064	3.630	
.19	.247		−3.595	.354	3.628	.049		−.733	.069	3.601	
.20	.210		−3.726	.378	3.602	.041		−.759	.073	3.573	
.22	.135		−3.906	.426	3.552	.026		−.795	.083	3.522	
.24	.055		−3.993	.473	3.508	.010		−.811	.092	3.474	
.26	−.024		−4.005	.517	3.467	−.007		−.811	.100	3.430	
.28	−.104		−3.960	.560	3.429	−.023		−.799	.109	3.389	
.30	−.182		−3.868	.600	3.394	−.039		−.778	.117	3.351	
.32	−.258		−3.739	.639	3.360	−.054		−.748	.124	3.315	
.34	−.332		−3.584	.674	3.328	−.069		−.713	.131	3.280	
.36	−.401		−3.409	.707	3.297	−.083		−.674	.138	3.246	
.38	−.467		−3.218	.738	3.268	−.096		−.632	.144	3.215	
.40	−.530		−3.019	.766	3.240	−.108		−.586	.150	3.184	
.42	−.589		−2.814	.792	3.212	−.120		−.541	.155	3.153	
.44	−.642		−2.607	.815	3.184	−.130		−.494	.160	3.123	
.46	−.693		−2.401	.836	3.157	−.139		−.447	.164	3.094	
.48	−.738		−2.198	.855	3.131	−.148		−.401	.168	3.066	
.50	−.779		−2.001	.872	3.104	−.155		−.355	.171	3.038	
.52	−.817		−1.807	.887	3.078	−.162		−.311	.174	3.011	

r	$P(2s)$	$\eta(2s)$	$P'(2s)$	$P(2p)$	$\xi(2p)$	$\eta(2p)$	$P(3s)$	$\eta(3s)$	$P'(3s)$	$P(3p)$	$\xi(3p)$	$P'(3p)$
.54	−.852		−1.621	.899	3.052		−.168		−.268	.177	2.985	
.56	−.882		−1.444	.910	3.026		−.173		−.226	.180	2.960	
.58	−.909		−1.273	.919	3.002		−.177		−.186	.182	2.934	
.60	−.932		−1.111	.926	2.977		−.180		−.148	.183	2.910	
.62	−.953		−.957	.932	2.953		−.182		−.112	.185	2.886	
.64	−.970		−.811	.937	2.929		−.184		−.077	.186	2.863	
.66	−.985		−.675	.940	2.906		−.185		−.044	.187	2.841	
.68	−.997		−.547	.941	2.882		−.186		−.013	.187	2.819	
.70	−1.008		−.427	.942	2.859		−.186		+.016	.188	2.798	
.72	−1.016		−.314	.941	2.836		−.185		.043	.188	2.778	
.74	−1.020		−.210	.940	2.814		−.185		.069	.188	2.759	
.76	−1.024		−.114	.937	2.792		−.183		.094	.187	2.740	
.78	−1.025		−.024	.934	2.770		−.181		.117	.187	2.722	
.80	−1.025		+.060	.930	2.749		−.178		.138	.186	2.705	
.82	−1.023		.136	.924	2.728		−.175		.158	.185	2.689	
.84	−1.019		.207	.919	2.708		−.172		.177	.184	2.674	
.86	−1.014		.272	.912	2.687		−.168		.195	.183	2.660	
.88	−1.008		.330	.906	2.669		−.164		.211	.182	2.647	
.90	−1.000		.385	.898	2.649		−.160		.226	.181	2.635	−.075
.92	−.992	.438		.890		.456	−.155		.239	.179		−.081
.94	−.984	.487		.882		.484	−.150		.252	.177		−.086
.96	−.974	.533		.873		.510	−.145		.264	.176		−.091
.98	−.963	.577		.864		.535	−.140		.275	.174		−.096
1.0	−.951	.618		.855		.559	−.134		.285	.172		−.101
1.1	−.886	.790		.804		.659	−.104		.323	.161		−.121
1.2	−.814	.921		.750		.737	−.070		.346	.148		−.136
1.3	−.738	1.023		.694		.799	−.034		.357	.134		−.147
1.4	−.663	1.106		.639		.850	+.001		.360	.118		−.155
1.5	−.592	1.174		.586		.893	.037		.358	.103		−.162
1.6	−.525	1.230		.535		.929	.073		.350	.086		−.167
1.7	−.463	1.278		.487		.960	.107		.340	.069		−.171
1.8	−.406	1.319		.441		.988	.140		.327	.052		−.174
1.9	−.356	1.354		.400		1.012	.172		.312	.035		−.176
2.0	−.310	1.385		.361		1.034	.203		.297	.017		−.177
2.2	−.234	1.437		.292		1.072	.259		.264	−.018		−.177
2.4	−.175	1.478		.235		1.103	.308		.229	−.054		−.174
2.6	−.130	1.511		.188		1.129	.351		.195	−.088		− 170
2.8	−.095	1.539		.150		1.151	.386		.162	−.121		−.163
3.0	−.070	1.564		.119		1.170	.415		.130	−.153		−.156

TABLE I. (*Continued.*)

r	$P(2s)$	$\eta(2s)$	$P'(2s)$	$P(2p)$	$\eta(2p)$	$P(3s)$	$\eta(3s)$	$P'(3s)$	$P(3p)$	$\eta(3p)$	$P'(3p)$
3.5	−.032	1.608		.065	1.209	.463		.062	−.225		−.132
4.0	−.014	1.640		.035	1.236	.479		.008	−.285		−.106
4.5	−.006	1.663		.019	1.256	.473		−.031	−.331		−.078
5.0	−.003	1.680		.010	1.272	.450		−.057	−.364		−.052
5.5	−.001	1.692		.005	1.284	.418	.171		−.384		−.029
6.0		1.702		.003	1.293	.380	.209		−.394		−.009
6.5				.001	1.301	.340	.240		−.393		+.008
7.0					1.308	.299	.266		−.387		.021
7.5						.261	.288		−.373		.031
8.0						.225	.307		−.356		.039
8.5						.192	.323		−.336	.128	
9.0						.163	.337		−.313	.146	
10.0						.115	.361		−.266	.177	
11.						.079	.380		−.220	.203	
12.						.054	.396		−.178	.223	
13.						.036	.409		−.141	.240	
14.						.024	.420		−.110	.254	
15.						.015	.430		−.085	.267	
16.						.010	.438		−.065	.277	
17.						.006	.445		−.049	.286	
18.						.004	.452		−.036	.295	
19.						.003	.458		−.027	.302	
20.						.002	.463		−.020	.309	
22.						.001	.472		−.011	.320	
24.							.479		−.006	.329	
26.									−.003	.337	
28.									−.001	.344	
30.										.350	

V. PERTURBATION CALCULATIONS

The results are improved somewhat by taking into account perturbations between levels. The method used was to write the wave function for a particular set of values $(LSJM_J)$ as a linear combination of functions (for states in the same configuration with the same J) by calculating the matrix elements of

$$H=\sum_i \lambda_i+\sum_{i<j} e^2/r_{ij},$$

where $\lambda=\mu_0^2(\boldsymbol{l}\cdot\boldsymbol{\sigma})(Z/r^3)$, and $\boldsymbol{\sigma}$ is the Pauli spin vector. The electrostatic interaction has only diagonal elements, and these were determined from the experimental data. (This also gives a check on the accuracy of the radial functions, by comparing the calculated multiplet structure with the experimental values.)

Since fluorine has three sets of terms (based on the ^3P, ^1D, ^1S states of the core) the relative positions of which are not known, it is impossible to take into account perturbations between such sets of terms. It seems, from a consideration of the Ne II spectrum, that the effect of these perturbations will not be large because the terms of the ^1D and ^1S states of the core probably lie a considerable distance from those of the ^3P. The state $^2S_{1/2}$ of $2s2p^6$ probably lies fairly close to the states ^2P and ^4P of p^4s and will cause a large perturbation of the $J=1/2$ levels, but the calculations of magnetic moment based on those levels are not reliable anyway (because of the smallness of the hfs).

The secular equation and perturbed wave functions are given below. In every case the functions are listed in the order of decreasing energy of the states which they represent. For the p^4s configuration the center of gravity of ^2P is used as a reference and for p^4p the center of gravity of ^2D is used. All calculations are for the states based on the ^3P state of the core. We have abbreviated by setting

$$\overline{(Z/r^3)}_{2p}\mu_0^2=a=170\text{ cm}^{-1};\qquad \overline{(Z/r^3)}_{3p}\mu_0^2=b=0.53\text{ cm}^{-1}.$$

For the unperturbed multiplet structure, we have for the p^4s configuration

$$^2P:\ \Delta H=-(2/3)a(1,-2);\qquad ^4P:\ \Delta H=-a(1,-2/3,-5/3).$$

The secular equations for the $J=3/2$ and $J=1/2$ levels are given by

$$J=3/2:\begin{vmatrix}-(2a/3)-\epsilon & -(5/9)^{1/2}a\\ -(5/9)^{1/2}a & (2a/3)-2270-\epsilon\end{vmatrix}=0 \qquad J=1/2:\begin{vmatrix}(4a/3)-\epsilon & -(2/9)^{1/2}a\\ -(2/9)^{1/2}a & (5a/3)-2270-\epsilon\end{vmatrix}=0$$

and the corresponding linear combinations by

$$J=3/2\quad \Psi_1=0.998\psi_1-0.0614\psi_2, \qquad J=1/2\quad \Psi_1=0.999\psi_1+0.0360\psi_2,$$
$$\Psi_2=0.0614\psi_1+0.998\psi_2, \qquad \Psi_2=-0.0360\psi_1+0.999\psi_2.$$

For the unperturbed multiplet structure of the p^4p configuration we have

^2P: $\Delta H=(1/6)(-2a-b)(1,-2)$, ^4D: $\Delta H=(-a+b)(1,-1/6,-1,-3/2)$,

^4S: $\Delta H=0$, ^4P: $\Delta H=(1/2)(-a+b)(1,-2/3,-5/3)$.

^2D: $\Delta H=(2/3)[-a-(1/2)b](1,-3/2)$,

The secular equations for $J=5/2$ and $J=3/2$ are given by:

$$J=5/2:\begin{vmatrix}(2/3)[-a-(1/2)b]-\epsilon & (7/18)^{1/2}(-a-2b) & (1/6)^{1/2}(-a+2b)\\ (7/18)^{1/2}(-a-2b) & -577.8-(1/6)(-a+b)-\epsilon & (7/12)^{1/2}(a+b)\\ (1/6)^{1/2}(-a+2b) & (7/12)^{1/2}(a+b) & -1726.3+(1/2)(-a+b)-\epsilon\end{vmatrix}=0,$$

$$J=3/2:\begin{vmatrix}-(1/6)(2a+b)+1262.5-\epsilon & -(2/9)^{1/2}(a-2b) & (5/36)^{1/2}(2a-b) & (5/36)^{1/2}(-2b) & (5/36)^{1/2}(a+2b)\\ -(2/9)^{1/2}(a-2b) & 704.9-\epsilon & 0 & 0 & -(10/9)^{1/2}(a+b)\\ (5/36)^{1/2}(2a-b) & 0 & a+(b/2)-\epsilon & -(1/2)(a+2b) & (1/6)(a-2b)\\ (5/36)^{1/2}(a-2b) & 0 & -(1/2)(a+2b) & -577.8+a-b-\epsilon & (-2/3)(a+b)\\ (5/36)^{1/2}(a+2b) & -(10/9)^{1/2}(a+b) & (1/6)(a-2b) & -(2/3)(a+b) & -1726.3+(1/3)(a-b)-\epsilon\end{vmatrix}=0,$$

and the corresponding linear combinations by

$$J=5/2:\ \Psi_1=0.9700\psi_1-0.0237\psi_2-0.0564\psi_3,$$
$$\Psi_2=0.241\psi_1+0.966\psi_2+0.0873\psi_3,$$
$$\Psi_3=0.0338\psi_1-0.0982\psi_2+0.995\psi_3,$$
$$J=3/2:\ \Psi_3=-0.0983\psi_1+0.984\psi_3-0.145\psi_4+0.0160\psi_5,$$
$$\Psi_4=-0.0335\psi_1+0.145\psi_3+0.984\psi_4-0.0970\psi_5,$$
$$\Psi_5=-0.0211\psi_1+0.0731\psi_2-0.0161\psi_3+0.0978\psi_4+0.992\psi_5.$$

(These latter wave functions Ψ_3, Ψ_4, and Ψ_5 correspond to the perturbed ^2D, ^4D, and ^4P states, respectively.)

The non-diagonal elements of $W=\sum_i w_i$ for the p^4s configuration are given by

$$J=3/2:\ (1\,|\,W\,|\,2)=(1/5)^{1/2}[(-8/9)h_{3s}+(13/15)h_{2p}]\mu\mu_0,$$
$$J=1/2:\ (1\,|\,W\,|\,2)=(2/81)^{1/2}[(-8/3)h_{3s}-h_{2p}]\mu\mu_0,$$

where the numbers 1 and 2 refer to the states with wave functions ψ_1 and ψ_2, respectively, all taken with the maximum M_I.

For the p^4p configuration:

$$J=5/2:\ (1\,|\,W\,|\,2)=(17/30)(2/7)^{1/2}[h_{2p}+2h_{3p}]\mu\mu_0,$$
$$(1\,|\,W\,|\,3)=(3/50)^{1/2}[h_{2p}-2h_{3p}]\mu\mu_0,$$
$$(2\,|\,W\,|\,3)=-(12/7)^{1/2}h_{2p}\mu\mu_0,$$

TABLE II. *Multiplet and hyperfine structure of the $2p^4(^3P)3s$ and $2p^4(^3P)3p$ states of fluorine.*

Config.	State	J	ν (cm^{-1}) (exp)	$\Delta\nu$ (exp)	$\Delta\nu$ (theor.) Unp.	Pert.	$\Delta\nu$ hfs (exp)	$1840\mu/\mu_0$ Unp.	Pert.
$2p^4(^3P)3p$	^2P	1/2	119088.2						
		3/2	118943.2						
	^4S	3/2	118434.0				small		
	^2S	1/2	118411.0				small		
	^2D	3/2	117879.0	249.9	283	253	.11	2.6	2.8
		5/2	117629.1				.18	2.6	2.9
	^4D	1/2	117398.1				.03	(1.1)	
		3/2	117314.7	83.4			.04	(1.8)	(1.8)
		5/2	117170.2	144.5	141	152	.13	3.5	3.5
		7/2	116993.6	176.6	197	182	.25	3.5	3.5
	^4P	1/2	116149.8				small		
		3/2	116047.1	122.9	141	130	.14	4.8	3.8
		5/2	115924.2				.12	4.9	3.6
$2p^4(^3P)3s$	^2P	1/2	105062.9	325.3	339	334	small		
		3/2	104737.6				.14	1.9	1.9
	^4P	1/2	102846.7	160.0	169	174	.02	(1.4)	(1.4)
		3/2	102686.7	274.7	282	275	.05	(13)	(10)
		5/2	102412.0				.27	3.2	3.2

$J=3/2$: $(1|W|2)=0$, $(2|W|4)=(8/5)(1/10)^{1/2}[h_{2p}-h_{3p}]\mu\mu_0$,

$(1|W|3)=(2/5)(1/5)^{1/2}[h_{2p}-h_{3p}]\mu\mu_0$, $(2|W|5)=(8/5)^{1/2}[h_{2p}-h_{3p}]\mu\mu_0$,

$(1|W|4)=-(9/10)(1/5)^{1/2}[h_{2p}-2h_{3p}]\mu\mu_0$, $(3|W|4)=(7/50)[h_{2p}+2h_{3p}]\mu\mu_0$,

$(1|W|5)=(13/6)(1/5)^{1/2}[h_{2p}+2h_{3p}]\mu\mu_0$, $(3|W|5)=(3/50)[h_{2p}-2h_{3p}]\mu\mu_0$,

$(2|W|3)=-(2/5)(1/10)^{1/2}[h_{2p}+2h_{3p}]\mu\mu_0$, $(4|W|5)=(12/25)[h_{2p}-h_{3p}]\mu\mu_0$.

The hyperfine separation formulae, taking into account these perturbations, are then as follows:

p^4s

$^2P_{1/2}$: $\Delta W=[0.0453\,h_{3s}+0.432\,h_{2p}][1,\,-3]\mu\mu_0$,

$^2P_{3/2}$: $\Delta W=[-0.171\,h_{3s}+2.211\,h_{2p}][1,\,(-5/3)]\mu\mu_0$,

$^4P_{1/2}$: $\Delta W=[0.400\,h_{3s}-0.432\,h_{2p}][1,\,-3]\mu\mu_0$,

$^4P_{3/2}$: $\Delta W=[0.438\,h_{3s}-0.0502\,h_{2p}][1,\,(-5/3)]\mu\mu_0$,

p^4p

$^2D_{3/2}$: $\Delta W=[1.134\,h_{2p}+1.490\,h_{3p}][1,\,(-5/3)]\mu\mu_0$,

$^2D_{5/2}$: $\Delta W=[2.003\,h_{2p}+1.894\,h_{3p}][1,\,(-7/5)]\mu\mu_0$,

$^4D_{3/2}$: $\Delta W=[0.632\,h_{2p}+1.692\,h_{3p}][1,\,(-5/3)]\mu\mu_0$,

$^4D_{5/2}$: $\Delta W=[1.213\,h_{2p}+2.191\,h_{3p}][1,\,(-7/5)]\mu\mu_0$,

$^4P_{3/2}$: $\Delta W=[1.094\,h_{2p}-0.399\,h_{3p}][1,\,(-5/3)]\mu\mu_0$,

$^4P_{5/2}$: $\Delta W=[1.075\,h_{2p}+1.171\,h_{3p}][1,\,(-7/5)]\mu\mu_0$.

The results of the calculations are given in Table II. The multiplet structure and the nuclear magnetic moments are given for the calculations with and without perturbations. In most cases, consideration of the perturbation improves the results. Those results considered not reliable because of the smallness of the hfs are enclosed in brackets.

VI. Conclusion

For the calculations for which the data are considered to be fairly accurate there is a fair consistency in the results, the magnetic moment having values ranging from 1.9 to 3.8. (Even considering all results, the only one which varies radically from the mean is the one for $p^4s^4P_{3/2}$. The experimental hfs for this level is obtained from measurements of separations which are not entirely resolved, hence may have considerable error. Also, the calculated splitting of this level is more affected by the value of $G_{3s}{}^2(0)$ than splittings for the other levels would be. This value, of course, cannot be checked from the multiplet structure, as can the other functions.) The nuclear moment of fluorine is, therefore, about 3 nuclear magnetons.

Perhaps the most important theoretical reasons for the still existing inconsistencies are (1) the non-inclusion of additional perturbation terms, (2) the inaccuracy of the radial wave functions, (3) the neglect of relativity corrections (except that approximate Dirac theory is here used for an s-electron), and (4) the incorrectness of the form of the interaction Hamiltonian of Breit and Doermann.

In calculations of this sort one cannot be sure of accuracy unless it is possible at least to estimate the effects due to all perturbing terms. This necessitates rather complete experimental information as to the positions of the energy levels of "neighboring" configurations. For fluorine, the information is far from complete, but, for reasons already stated, it seems probable that the most important perturbing terms have been included. However, a more complete analysis of the F I spectrum is desirable.

In obtaining the Hartree functions, one neglects "exchange" terms, and assumes that all states of a configuration have the same radial functions. More accurate calculations including these terms can be made, but they involve considerable labor. For the p^4p configuration, the effect of the $3p$ wave function is small compared with that of the $2p$ function, so that refinements of the above type are perhaps more important in determining the absolute magnitude of the magnetic moment than in obtaining consistent results. However, it is doubtful if they would be of much influence here, since the $2p$ and $3p$ radial functions have been checked by calculating the multiplet splittings.

Certain relativity corrections can be made, but these are usually small for light elements.

The interaction Hamiltonian, in the form used, has no very great theoretical justification. Apart from the fact that higher order magnetic moments of the nucleus are neglected, it may be that an adequate quantum electrodynamics will entail revision of this Hamiltonian from its present simple form.

It is not easy to say, therefore, which of the above four causes is responsible for the inconsistencies still left, except that the relativity corrections are probably least important.

Finally, we wish to thank Mr. C. G. Dunn for checking part of the calculations.

Vibrations of Tetrahedral Pentatomic Molecules. Part I. Potential Energy. Part II. Kinetic Energy and Normal Frequencies of Vibration

JENNY E. ROSENTHAL, *Physics Department, New York University, University Heights*

(Received November 24, 1933)

Part I. It is shown that the most general potential energy function consistent with tetrahedral symmetry involves five force constants, also that with a suitable choice of variables this expression may be written in a quite simple form convenient for the discussion of different types of vibration. Special cases of potential energy such as the "valence" force and the central force cases involving less than five force constants are considered and their connection with the general case discussed.

Part II. Expressions for the vibration frequencies of molecules of the type YX_3X^* and $YX_2X_2^*$ (X^* being an isotope of X) are derived in terms of constants in the potential energy function and the masses of the various atoms. These expressions are valid for any value of $\Delta m/m$ where m is the mass of X and $m+\Delta m$ the mass of X^*. Hence the results are applicable to the isotopes of hydrogen. While YX_4 has one single, one double and two triple frequencies, the slight asymmetry introduced by X^* in YX_3X^* partially removes the degeneracy giving three single and three double frequencies. For $YX_2X_2^*$ the degeneracy is completely removed and the molecule has nine single frequencies.

THE methods used[1] to derive vibration frequencies of molecules of the type YXX^* and YX_2X^* may be extended to symmetrical tetrahedral pentatomic molecules YX_3X^* and $YX_2X_2^*$. We begin by setting up expressions for the potential energy V and the kinetic energy T. The normal frequencies of vibration ω are then given by the roots of the determinantal equation $|\lambda T - V| = 0$ where $\lambda = 4\pi^2\omega^2$.

PART I

Consider a symmetrical molecule YX_4. At equilibrium the X atoms form the corners of a regular tetrahedron with the Y atom at the center. We study this system when it vibrates with a very small amplitude around its position of equilibrium. Following Dennison[2] we assume that the potential energy function V has the same symmetry as the geometrical configuration of the system; this will be the *only* assumption used in the derivation of an expression for V.

Let the positions of the four X atoms be given by the points A_1, A_2, A_3, A_4 and let A_5 be the position of the Y atom. We denote by the superscript 0 the equilibrium positions of the various atoms. Let:

$$A_iA_j = q_{ij} = q^0 + \delta q_{ij}; \quad A_5A_i = r_i = r^0 + \delta r_i \quad \text{and} \quad \angle A_iA_5A_j = 2\Omega_{ij} = 2(\Omega + \delta\Omega_{ij})$$
$$(i, j = 1, \cdots 4,\ i \neq j,\ q_{ij} = q_{ji}). \quad (1)$$

$r^0 = \frac{1}{2}\sqrt{\frac{3}{2}}q^0$ (since the equilibrium configuration is that of a regular tetrahedron) and the various δq_{ij} and δr_i are taken to be small quantities of the first order.

Since the system has only nine degrees of internal freedom only nine of the ten quantities defined by Eq. (1) are linearly independent. It is, however, convenient to use ten variables in writing V with the same symmetry as the geometrical configuration; one of the variables is then eliminated by the relation which gives the linear dependence.

We have the potential energy then as a function of the mutual displacements of the particles:

$$V = V(\delta q_{12}, \delta q_{13} \cdots \delta q_{34}, \delta r_1, \cdots \delta r_4)$$

[1] E. O. Salant and J. E. Rosenthal, Phys. Rev. **42**, 812 (1932).

[2] D. M. Dennison, Rev. Mod. Phys. **3**, 303 (1931).

and, with force constants K_1, $K_2 \cdots K_7$, it is written in the most general symmetrical form in the δq_{ij} and the δr_i

$$V=\tfrac{1}{2}[K_1\sum_{i,j}\tfrac{1}{2}\delta q_{ij}^2+K_2\sum_{i,j,n}\tfrac{1}{2}\delta q_{ij}\delta q_{jn}+K_3\sum_{i\neq j\neq n\neq 1}\tfrac{1}{2}\delta q_{1j}\delta q_{in}+K_4\sum_i \delta r_i^2+K_5\sum_{i,j}\tfrac{1}{2}\delta r_i\delta r_j$$
$$+K_6\sum_{i,j}\delta r_i\delta q_{ij}+K_7\sum_{i,j,n}\tfrac{1}{2}\delta r_i\delta q_{jn}]. \quad (2)$$

We use $i\neq j\neq n$ and unless otherwise indicated all summations extend from 1 to 4. V may also be written

$$V=\tfrac{1}{2}[(K_1-\tfrac{1}{2}K_2)\sum_{i,j}\tfrac{1}{2}\delta q_{ij}^2+\tfrac{1}{2}K_2(\sum_{i,j}\tfrac{1}{2}\delta q_{ij})^2+(K_3-K_2)\sum_{i\neq j\neq n\neq 1}\tfrac{1}{2}\delta q_{1i}\delta q_{jn}+(K_4-\tfrac{1}{2}K_5)\sum_i \delta r_i^2$$
$$+\tfrac{1}{2}K_5(\sum_i \delta r_i)^2+K_6(\sum_i \delta r_i)(\sum_{j,n}\tfrac{1}{2}\delta q_{jn})+(K_7-K_6)\sum_{i,j,n}\tfrac{1}{2}\delta r_i\delta q_{jn}]. \quad (3)$$

This expression for the potential energy is, however, not convenient for the study of vibrations of the system YX_4 and therefore new variables in which to express V are introduced. As will be seen below, these new variables are the components of vectors giving the displacements of one particle with respect to the center of gravity of others.

We start by defining a cartesian coordinate system x, y, z with its origin at the center of gravity of the tetrahedron; the xy plane is parallel to the $A_1A_2A_3$ plane and the x axis is parallel to A_2A_3, the positive direction being from $A_2\rightarrow A_3$. We let (x_j, y_j, z_j) represent the point $A_j(x_j=x_j^0+\delta x_j$, etc.). We then define new variables ξ, η, ζ, x, y, z, u, v, s by the relations:

$$\xi=x_5-\tfrac{1}{4}\sum_i x_i, \quad \eta=y_5-\tfrac{1}{4}\sum_i y_i, \quad \zeta=z_5-\tfrac{1}{4}\sum_i z_i, \qquad x=x_4-\tfrac{1}{3}(x_3+x_2+x_1), \quad y=y_4-\tfrac{1}{3}(y_3+y_2+y_1),$$
$$q^0\sqrt{\tfrac{2}{3}}+z=z_4-\tfrac{1}{3}(z_3+z_2+z_1), \qquad u=x_1-\tfrac{1}{2}(x_2+x_3), \quad v+\tfrac{1}{2}q^0\sqrt{3}=y_1-\tfrac{1}{2}(y_2+y_3),$$
$$z_1-\tfrac{1}{2}(z_2+z_3)=0, \qquad q^0+s=x_3-x_2, \quad y_3-y_2=0, \quad z_3-z_2=0. \quad (4)$$

Our problem then is to find $V(\xi, \eta, \zeta, x, y, z, u, v, s)=V(\delta q_{12}\cdots\delta q_{34}, \delta r_1\cdots\delta r_4)$. The old variables are, or course, expressed in terms of x_j, y_j, z_j by:

$$q_{ij}^2=(q^0+\delta q_{ij})^2=(x_i-x_j)^2+(y_i-y_j)^2+(z_i-z_j)^2 \qquad (i, j=1\cdots 4, i\neq j),$$
$$r_i^2=(r^0+\delta r_i)^2=(x_5-x_i)^2+(y_5-y_i)^2+(z_5-z_i)^2. \quad (5)$$

Eliminating the various x_j, y_j, z_j between Eqs. (4) and (5) we obtain the following relations:

$$r_1^2+r_2^2+r_3^2+r_4^2=4(\xi^2+\eta^2+\zeta^2)+\tfrac{3}{4}[x^2+y^2+(q^0\sqrt{\tfrac{2}{3}}+z)^2]+\tfrac{2}{3}[u^2+(\tfrac{1}{2}q^0\sqrt{3}+v)^2]+\tfrac{1}{2}(q^0+s)^2,$$
$$\tfrac{1}{3}(r_1^2+r_2^2+r_3^2)-r_4^2=2[\xi x+\eta y+\zeta(z+q^0\sqrt{\tfrac{2}{3}})]-\tfrac{1}{2}[x^2+(z+q^0\sqrt{\tfrac{2}{3}})^2+y^2]$$
$$+2[u^2+(v+\tfrac{1}{2}q^0\sqrt{3})^2]/9+\tfrac{1}{6}(q^0+s)^2,$$
$$\tfrac{1}{2}(r_2^2+r_3^2)-r_1^2=2[\xi u+(v+\tfrac{1}{2}q^0\sqrt{3})\eta]+\tfrac{1}{2}[ux+(v+\tfrac{1}{2}q^0\sqrt{3})y]-\tfrac{1}{3}[u^2+(v+\tfrac{1}{2}q^0\sqrt{3})^2]+\tfrac{1}{4}(q^0+s)^2,$$
$$r_2^2-r_3^2=2(q^0+s)(\xi+\tfrac{1}{4}x+\tfrac{1}{3}u). \quad (6)$$
$$q_{14}^2+q_{24}^2+q_{34}^2=3[x^2+y^2+(z+q^0\sqrt{\tfrac{2}{3}})^2]+\tfrac{2}{3}[u^2+(v+\tfrac{1}{2}q^0\sqrt{3})^2]+\tfrac{1}{2}(q^0+s)^2,$$
$$\tfrac{1}{2}(q_{24}^2+q_{34}^2)-q_{14}^2=2[ux+(v+\tfrac{1}{2}q^0\sqrt{3})y]-\tfrac{1}{3}[u^2+(v+\tfrac{1}{2}q^0\sqrt{3})^2]+\tfrac{1}{4}(q^0+s)^2,$$
$$q_{24}^2-q_{34}^2=2(q^0+s)(x+\tfrac{1}{3}u),$$
$$q_{12}^2+q_{13}^2+q_{23}^2=2[u^2+(v+\tfrac{1}{2}q^0\sqrt{3})^2]+3(q^0+s)^2/2,$$
$$\tfrac{1}{2}(q_{12}^2+q_{13}^2)-q_{23}^2=u^2+(v+\tfrac{1}{2}q^0\sqrt{3})^2-\tfrac{3}{4}(q^0+s)^2,$$
$$q_{12}^2-q_{13}^2=2(q^0+s)u.$$

Expanding and neglecting all small quantities of the second order we obtain

$$\begin{aligned}
\delta r_1+\delta r_2+\delta r_3+\delta r_4 &= z+\tfrac{2}{3}v\sqrt{2}+s\sqrt{\tfrac{2}{3}},\\
\tfrac{1}{3}(\delta r_1+\delta r_2+\delta r_3)-\delta r_4 &= 4\zeta/3-\tfrac{2}{3}z+2v\sqrt{2}/9+\tfrac{1}{3}s\sqrt{\tfrac{2}{3}},\\
\tfrac{1}{2}(\delta r_3+\delta r_2)-\delta r_1 &= \eta\sqrt{2}+y/\sqrt{2}-\tfrac{1}{3}v\sqrt{2}+\tfrac{1}{2}s\sqrt{\tfrac{2}{3}},\\
\delta r_2-\delta r_3 &= 2\sqrt{\tfrac{2}{3}}(\xi+\tfrac{1}{4}x+\tfrac{1}{3}u),\\
\delta q_{14}+\delta q_{24}+\delta q_{34} &= z\sqrt{6}+v/\sqrt{3}+\tfrac{1}{2}s,\\
\tfrac{1}{2}(\delta q_{34}+\delta q_{24})-\delta q_{14} &= \tfrac{1}{2}y\sqrt{3}+\tfrac{1}{2}(-v+\tfrac{1}{2}s\sqrt{3})/\sqrt{3},\\
\delta q_{24}-\delta q_{34} &= x+u/3,\\
\delta q_{12}+\delta q_{13}+\delta q_{23} &= (v+\tfrac{1}{2}s\sqrt{3})\sqrt{3},\\
\tfrac{1}{2}(\delta q_{12}+\delta q_{13})-\delta q_{23} &= -\tfrac{1}{2}(-v+\tfrac{1}{2}s\sqrt{3})\sqrt{3},\\
\delta q_{12}-\delta q_{13} &= u.
\end{aligned} \tag{7}$$

It follows from Eq. (7) that

$$(\delta r_1+\delta r_2+\delta r_3+\delta r_4)\sqrt{6}=(\delta q_{12}+\delta q_{13}+\delta q_{14}+\delta q_{23}+\delta q_{24}+\delta q_{34}), \tag{8}$$

which is the equation of linear dependence,[3] and by using it we may rewrite Eq. (3) as:

$$V=\tfrac{1}{2}[k_1\sum_{i,\,j}\tfrac{1}{2}\delta q_{ij}^2+k_2\sum_{i,\,j,\,n\neq 1}\tfrac{1}{2}\delta q_{1i}\delta q_{jn}+k_3\sum_i\delta r_i^2+k_4(\sum_i\delta r_i)^2+k_5\sum_{i,\,j,\,n}\tfrac{1}{2}\delta r_i\,\delta q_{jn}], \tag{9}$$

making use of *only five* independent force constants. The k's are related to the K's by

$$\begin{aligned}
k_1&=K_1-\tfrac{1}{2}K_2, \qquad k_2=K_3-K_2, \qquad k_3=K_4-\tfrac{1}{2}K_5,\\
k_4&=\tfrac{1}{2}K_5+3K_2+K_6\sqrt{6}, \qquad k_5=K_7-K_6.
\end{aligned} \tag{10}$$

The form of Eqs. (7) suggests that a further simplification may be obtained by introducing new coordinates defined by:

$$\begin{aligned}
\alpha&=x+4u/3, \qquad \beta=y-4v/3+2s/\sqrt{3}, \qquad \gamma=-2z+(\tfrac{2}{3}v+s/\sqrt{3})\sqrt{2},\\
\rho&=x-2u/3, \qquad \sigma=y+2v/3-s/\sqrt{3}, \qquad \tau=2z+(4v/3+2s/\sqrt{3})\sqrt{2}.
\end{aligned} \tag{11}$$

We then substitute[4] in Eq. (9) the expressions for the various δq_{ij} and δr_i in terms of the new variables and we obtain:

$$\begin{aligned}
V&=\tfrac{1}{2}[A(\xi^2+\eta^2+\zeta^2)+B(\alpha^2+\beta^2+\gamma^2)+C(\rho^2+\sigma^2)+2D(\xi\alpha+\eta\beta+\zeta\gamma)+E\tau^2]\\
&=\tfrac{1}{2}[(A\xi^2+B\alpha^2+2D\xi\alpha)+(A\eta^2+B\beta^2+2D\eta\beta)+(A\zeta^2+B\gamma^2+2D\zeta\gamma)+C\rho^2+C\sigma^2+E\tau^2]\\
&=V_1(\xi,\,\alpha)+V_1(\eta,\,\beta)+V_1(\zeta,\,\gamma)+V_2(\rho)+V_2(\sigma)+V_3(\tau).
\end{aligned} \tag{13}$$

---

[3] The exact expression which will be used later is:

$$\sum_{i,\,j}\tfrac{1}{2}\delta q_{ij}-\sqrt{6}\sum_i\delta r_i=2[\sum_i\delta r_i^2-4(\xi^2+\eta^2+\zeta^2)-\tfrac{1}{4}\sum_{i,\,j}\tfrac{1}{2}\delta q_{ij}^2]/q^0. \tag{8'}$$

[4] This substitution is greatly simplified by making use of the identities

$$\begin{aligned}
a_1^2+a_2^2+a_3^2&\equiv\tfrac{1}{3}(a_1+a_2+a_3)^2+\tfrac{2}{3}[\tfrac{1}{2}(a_2+a_3)-a_1]^2+\tfrac{1}{2}(a_3-a_2)^2,\\
a_1b_1+a_2b_2+a_3b_3&\equiv\tfrac{1}{3}(a_1+a_2+a_3)(b_1+b_2+b_3)+\tfrac{2}{3}[\tfrac{1}{2}(a_2+a_3)-a_1][\tfrac{1}{2}(b_2+b_3)-b_1]+\tfrac{1}{2}(a_3-a_2)(b_3-b_2),\\
a_1^2+a_2^2+a_3^2+a_4^2&\equiv\tfrac{1}{4}(a_1+a_2+a_3+a_4)^2+\tfrac{3}{4}[\tfrac{1}{3}(a_1+a_2+a_3)-a_4]^2+\tfrac{2}{3}[\tfrac{1}{2}(a_2+a_3)-a_1]^2+\tfrac{1}{2}(a_2-a_3)^2.
\end{aligned} \tag{12}$$

This form of the potential energy function is very convenient[5] for the study of the vibrations of the molecule YX_4. The constants in Eq. (13) are related to the k's by:

$$A=4k_3/3; \quad B=\tfrac{1}{4}k_1-\tfrac{1}{8}k_2+k_3/12-\tfrac{1}{2}k_5/\sqrt{6}; \quad C=\tfrac{1}{4}(k_1+\tfrac{1}{2}k_2);$$
$$D=\tfrac{1}{3}k_3-k_5/\sqrt{6}; \quad E=\tfrac{1}{4}[k_1+\tfrac{1}{2}k_2+\tfrac{1}{4}k_3+k_4+k_5(3/2)^{\frac{1}{2}}]. \tag{14}$$

This general expression for the potential energy has the disadvantage of involving five independent force constants while (in the absence of isotopic shifts) the spectrum of the symmetrical tetrahedral molecule consists of only four fundamental frequencies. It is possible, however, to reduce the number of these constants by means of suitable physical assumptions. These assumptions and the special potential energy functions they give rise to having been discussed by Urey and Bradley,[6] we shall consider here only the connection between the general expression and some special cases. The potential energy expression which includes central forces and the forces perpendicular to the lines of bonds is:[6a]

$$V'=(\partial V'/\partial q)^0(\sum_{i,j}\tfrac{1}{2}\delta q_{ij}-6^{\frac{1}{2}}\sum_i \delta r_i)+\tfrac{1}{2}(\partial^2 V'/\partial r^2)^0\sum_i \delta r_i^2+\tfrac{1}{2}(\partial^2 V'/\partial q^2)^0\sum_{i,j}\tfrac{1}{2}\delta q_{ij}^2$$
$$+\tfrac{1}{2}f_2'\sum_{i,j}\tfrac{1}{2}(r^0\delta\Omega_{ij})^2. \tag{15}$$

The prime is used to distinguish this function from the general V. Henceforth all quantities referring to V' (the potential energy with four force constants) will be marked by a prime. Similarly we shall indicate by a double prime the central force case and by a triple prime the valence force case.

To compare Eqs. (2) and (15) we have to express the last term in Eq. (15) in terms of the δr_i and the δq_{ij}.[7]

$$r^0\delta\Omega_{ij}=\tfrac{1}{2}[\delta q_{ij}-\sin\Omega(\delta r_i+\delta r_j)]/\cos\Omega=\tfrac{1}{2}\delta q_{ij}\sqrt{3}-(\delta r_i+\delta r_j)/\sqrt{2}. \tag{16}$$

Let

$$(\partial^2 V'/\partial r^2)^0=f_1', \qquad (\partial^2 V'/\partial q^2)^0=f_3', \qquad (\partial V'/\partial q)^0/q^0=f_4'. \tag{17}$$

With the use of Eqs. (17), (16) and (8′) we may write:

$$V'=\tfrac{1}{2}[(\tfrac{3}{4}f_2'+f_3'-f_4')\sum_{i,j}\tfrac{1}{2}\delta q_{ij}^2+(f_1'+(3/2)f_2'+4f_4')\sum_i \delta r_i^2+f_2'\sum_{i,j}\tfrac{1}{2}\delta r_i\delta r_j$$
$$-(3/2)^{\frac{1}{2}}f_2'\sum_{i,j}\delta r_i\delta q_{ij}-16f_4'(\xi^2+\eta^2+\zeta^2)], \tag{18}$$

---

[5] In some cases, however, it is better to define

$$\eta'=(\eta\sqrt{2}+\xi)/\sqrt{3}, \quad \beta'=(\beta\sqrt{2}+\gamma)/\sqrt{3}, \quad \zeta'=(\eta-\zeta\sqrt{2})/\sqrt{3}, \quad \gamma'=(\beta-\gamma\sqrt{2})/\sqrt{3}, \tag{11′}$$

and write

$$V=V_1(\xi,\alpha)+V_1(\eta',\beta')+V_1(\zeta',\gamma')+V_2(\rho)+V_2(\sigma)+V_3(\tau). \tag{13′}$$

This change of variables is equivalent to a rotation of the y and z axes such that the y axis becomes parallel to the direction $A_1^0A_4^0$. Hence η', ζ', β', γ' are suitable variables in any case in which there is a preferred direction $A_1^0A_4^0$ in the molecule.

[6] H. C. Urey and C. A. Bradley, Phys. Rev. **38**, 1969 (1931).

[6a] The last term in this expression—a sum of six terms depending on the square of the change in angle between two bond lines—is not equivalent to the sum of four terms depending on the square of the displacement of the bond line from its equilibrium position (the term in k_2 in Eq. (1) of reference 6). Hence our potential energy function differs to that extent from the expression (1) in reference 6. The only result of this difference, however, is that our frequency $\omega_{(\rho)(\sigma)}$ given by Eqs. (19) and (31) depends in a different way on the "valence" force constant than the corresponding frequency ν_2 in the above reference.

[7] Eq. (16) is obtained by differentiating $2r_ir_j\cos 2\Omega_{ij}=r_i^2+r_j^2-q_{ij}^2$ and retaining only the linear terms in the δr_i and δq_{ij}.

comparing the coefficients in Eq. (18) with those in Eq. (2)[8] we obtain as the connection between the f' and the constants in Eq. (13)

$$A'=4(f_1'+f_2'-8f_4')/3; \qquad B'=(f_1'+\tfrac{1}{4}f_2'+3f_3'+f_4')/12; \qquad C'=\tfrac{1}{4}(\tfrac{3}{4}f_2'+f_3'-f_4');$$
$$D'=\tfrac{1}{3}(f_1'-\tfrac{1}{2}f_2'+4f_4'); \qquad E'=(f_1'+4f_3')/16. \quad (19)$$

Of these five quantities only four are linearly independent. The equation of linear dependence may easily be found to be

$$D'=10B'-2C'-8E'. \quad (20)$$

Eq. (19) may then be solved uniquely for the various f's giving

$$f_1'=\tfrac{1}{4}A'+20B'-4C'-16E'; \qquad f_2'=12B'+4C'-16E';$$
$$f_3'=-\tfrac{1}{16}A'-5B'+C'+8E'; \qquad f_4'=-\tfrac{1}{16}A'+4B'-4E'. \quad (21)$$

Additional equations of linear dependence are obtained for the central force case where $f_2''=0$ and the valence force case where $f_3'''=f_4'''=0$.

PART II

To obtain the kinetic energy expression we begin by referring the positions of the particles to a fixed coordinate system XYZ, which may be made to coincide with the moving system xyz by means of a small rotation in space. The kinetic energy T is expressed in terms of the displacements δX, δY, δZ of the various particles from their positions of equilibrium. For the jth particle:

$$\delta X_j=\delta x_j+\psi y_j^0+\theta z_j^0; \qquad \delta Y_j=-\psi x_j^0+\delta y_j+\varphi z_j^0; \qquad \delta Z_j=-\theta x_j^0-\varphi y_j^0+\delta z_j, \quad (22)$$

combining Eq. (4) with Eq. (22) we obtain the direct connection between the various δX, δY, δZ and our nine variables ξ, η, ζ, x, y, z, u, v, s. We have also three relations of the type:

$$\sum_1^5 m_j\delta\dot{X}_j=0; \qquad \sum_1^5 m_j\delta\dot{Y}_j=0; \qquad \sum_1^5 m_j\delta\dot{Z}_j=0, \quad (23)$$

expressing the conservation of linear momentum. (m_j denotes the mass of the jth particle and may have different values for the two molecules YX_3X^* and $YX_2X_2^*$.) The kinetic energy is, of course:

$$T=\tfrac{1}{2}\sum_{j=1}^{5}\sum_{XYZ} m_j\delta\dot{X}_j^2. \quad (24)$$

Consider first molecule YX_3X^*. Let $m_5=M$, $m_4=m+\Delta m$, $m_3=m_2=m_1=m$. We may now substitute in Eq. (24) for the various $\delta\dot{X}$, $\delta\dot{Y}$, $\delta\dot{Z}$ their values in terms of $\dot{\xi}$, $\dot{\eta}$, $\dot{\zeta}$, $\dot{x}$, $\dot{y}$, $\dot{z}$, $\dot{u}$, $\dot{v}$, $\dot{s}$. (Calculations are greatly simplified by the symmetrical way in which the variables are defined.)

We obtain then:

$$T=\tfrac{1}{2}m\{(1-\epsilon\mu)^{-1}[4\mu(\dot{\xi}^2+\dot{\eta}^2+\dot{\zeta}^2)+\tfrac{3}{4}(1+3\epsilon-\epsilon\mu)((\dot{x}+q^0\dot{\theta}\sqrt{\tfrac{2}{3}})^2+(\dot{y}+q^0\dot{\varphi}\sqrt{\tfrac{2}{3}})^2+\dot{z}^2)$$
$$-6\mu\epsilon(\xi(\dot{x}+\dot{q}^0\dot{\theta}\sqrt{\tfrac{2}{3}})+\dot{\eta}(\dot{y}+q^0\dot{\varphi}\sqrt{\tfrac{2}{3}})+\zeta\dot{z})]+\tfrac{2}{3}[(\dot{u}+\tfrac{1}{2}q^0\dot{\psi}\sqrt{3})^2+\dot{v}^2+\tfrac{3}{4}\dot{s}^2+\tfrac{3}{4}(\dot{\theta}^2+\dot{\varphi}^2+\dot{\psi}^2)q^{02}]\}, \quad (25)$$

where $\epsilon=\Delta m/(4m+\Delta m)$ and $\mu=M/(4m+M)$. We eliminate $q^0\dot{\theta}$, $q^0\dot{\psi}$ and $q^0\dot{\varphi}$ by means of the equations of conservation of angular momentum ($\partial T/\partial\dot{\theta}=0$; $\partial T/\partial\dot{\varphi}=0$; $\partial T/\partial\dot{\psi}=0$) and transform to the new set of variables α, β, γ, ρ, σ, τ. We then have T in the form:

$$T=T^{(1)}(\dot{\xi},\dot{\alpha},\dot{\rho})+T^{(1)}(\dot{\eta},\dot{\beta},\dot{\sigma})+T^{(2)}(\dot{\zeta},\dot{\gamma},\dot{\tau}), \quad (26)$$

where

[8] Attention must be paid to the presence of a term in $(\xi^2+\eta^2+\zeta^2)$.

$$T^{(1)}(\dot\xi,\dot\alpha,\dot\rho)=\tfrac12 m(1+3\epsilon/2-\epsilon\mu)^{-1}[4\mu(1+3\epsilon/2)\dot\xi^2+\tfrac18(1+2\epsilon-\epsilon\mu)\dot\alpha^2+\tfrac14(1+5\epsilon/2-\epsilon\mu)\dot\rho^2$$
$$+\tfrac14\epsilon\dot\alpha\dot\rho-\mu\epsilon\dot\xi(\dot\alpha+2\dot\rho)].$$
$$T^{(2)}(\dot\zeta,\dot\gamma,\dot\tau)=\tfrac12 m(1-\epsilon\mu)^{-1}[4\mu\dot\zeta^2+\tfrac18(1+2\epsilon-\epsilon\mu)\dot\gamma^2+\tfrac{1}{16}(1+\epsilon-\epsilon\mu)\dot\tau^2-\tfrac14\epsilon\dot\gamma\dot\tau+\epsilon\mu\dot\zeta(2\dot\gamma-\dot\tau)]. \tag{27}$$

On account of Eq. (26) we may break up the nine rowed determinant into two three rowed ones, one of which is squared:

$$\{|\lambda T^{(1)}-V^{(1)}|\}^2=0,\qquad |\lambda T^{(2)}-V^{(2)}|=0.^9 \tag{28}$$

Expanding Eq. (28) we get the equations for the frequencies. Instead of numbering the frequencies we shall merely indicate by a series of subscripts as to what variables, hence to what types of motion, they correspond. Double frequencies will be indicated by two sets of subscripts each in a separate parenthesis.

Letting $\frac14\Delta m/(m+\Delta m)=\kappa$

$$[m^3\lambda^3_{(\xi\alpha\rho),\,(\eta\beta\sigma)}-P_1m^2\lambda^2+P_2m\lambda-P_3]^2=0,\qquad m^3\lambda^3_{(\zeta\gamma\tau)}-R_1m^2\lambda^2+R_2m\lambda-R_3=0,$$
$$P_1=\tfrac14A(1-\mu\kappa)/\mu+8B(1-\tfrac12\kappa)+2\kappa D+4C(1-\kappa),$$
$$P_2=AC(1-\kappa-\mu\kappa)/\mu+32BC(1-3\kappa/2)+8\kappa DC+2(AB-D^2)(1-\tfrac12\kappa-\mu\kappa)/\mu,$$
$$P_3=8C(AB-D^2)(1-3\kappa/2-\mu\kappa)/\mu, \tag{29}$$
$$R_1=\tfrac14A(1-\mu\kappa)/\mu+8B(1-2\kappa)-4\kappa D+16E(1-\kappa),$$
$$R_2=4AE(1-\kappa-\mu\kappa)/\mu+128BE(1-3\kappa)-64\kappa DE+2(AB-D^2)(1-2\kappa-\kappa\mu)/\mu,$$
$$R_3=32E(AB-D^2)(1-3\kappa-\kappa\mu)/\mu.$$

It may be pointed out that whereas the results in Part I were approximate these expressions are *exact* and hence valid for any value of κ. In particular Eq. (29) may be used to compute isotope shifts due to the presence of the heavy isotope of hydrogen.

If $\kappa^2\ll1$ Eqs. (29) take the somewhat simpler form

$$[m\lambda_{(\rho),\,(\sigma)}-4C(1-\kappa)]^2\{m^2\lambda^2_{(\xi\alpha),\,(\eta\beta)}-m\lambda[\tfrac14A(1-\mu\kappa)/\mu+8B(1-\tfrac12\kappa)+2\kappa D]$$
$$+2(AB-D^2)(1-\tfrac12\kappa-\mu\kappa)/\mu\}^2=0,$$
$$[m\lambda_{(\tau)}-16E(1-\kappa)]\{m^2\lambda^2_{(\zeta\gamma)}-m\lambda[\tfrac14A(1-\mu\kappa)/\mu+8B(1-2\kappa)-4\kappa D] \tag{30}$$
$$+2(AB-D^2)(1-2\kappa-\kappa\mu)/\mu\}=0.$$

For molecule $YX_2X_2^*$, $m_5=M$; $m_4=m_1=m$; $m_3=m_2=m+\Delta m$. We obtain then instead of Eqs. (25) to (30), Eqs. (25′) to (30′) given below.

$$T=\tfrac12 m(1-2\epsilon'\mu)^{-1}\{4\mu(\dot\xi^2+\dot\eta^2+\dot\zeta^2)+\tfrac14(1+2\epsilon'-2\mu\epsilon')[(\dot x+q^0\dot\theta\sqrt{\tfrac23}+4\dot u/3+2q^0\dot\psi/\sqrt3)^2$$
$$+(\dot y+q^0\dot\varphi\sqrt{\tfrac23}+4\dot v/3)^2+(\dot z-2q^0\dot\varphi/\sqrt3)^2]+4\epsilon'\mu[\dot\xi(\dot x+q^0\dot\theta\sqrt{\tfrac23}+4\dot u/3+2q^0\dot\psi/\sqrt3)$$
$$+\eta(\dot y+q^0\dot\varphi\sqrt{\tfrac23}+4\dot v/3)+\dot\zeta(\dot z-2q^0\dot\varphi/\sqrt3)]\}+\tfrac12 m\{\tfrac12[(\dot x+q^0\dot\theta\sqrt{\tfrac23}-\tfrac23\dot u-q^0\dot\psi/\sqrt3)^2$$
$$+(\dot y+q^0\dot\varphi\sqrt{\tfrac23}-\tfrac23\dot v)^2+(\dot z+q^0\dot\varphi/\sqrt3)^2]+\tfrac12(1+2\epsilon')(1-2\epsilon')^{-1}(\dot s^2+q^{02}\dot\psi^2+q^{02}\dot\theta^2)\}, \tag{25′}$$

where $\epsilon'=\epsilon/(1+\epsilon)$, $\xi,\eta',\zeta',\alpha,\beta',\gamma',\rho,\sigma,\tau$ are suitable variables for this case in which there obviously is a preferred direction $A_1^0A_4^0$ in the molecule. It is also convenient to define $\theta'=\theta\sqrt{\frac23}+2\psi/\sqrt3$, $\psi'=\theta\sqrt{\frac23}-\psi/\sqrt3$ and use $\partial T/\partial\dot\theta'=\partial T/\partial\dot\psi'=\partial T/\partial\dot\varphi=0$. Then we obtain T as:

$$T=T_1'(\dot\xi,\dot\alpha)+T_1''(\dot\zeta',\dot\gamma')+T_2(\dot\rho)+T^*(\dot\eta',\dot\beta',\dot\sigma,\dot\tau), \tag{26′}$$

---

[9] $V^{(1)}(\xi,\alpha,\rho)=V_1(\xi,\alpha)+V_2(\rho)$, $V^{(2)}(\zeta,\gamma,\tau)=V_1(\zeta,\gamma)+V_3(\tau)$.

where

$$T_1'(\dot\xi,\dot\alpha)=\tfrac12 m(1+2\epsilon')(1-2\mu\epsilon'+\epsilon'-2\epsilon'^2)^{-1}[4\mu(1-\epsilon')\dot\xi^2+\tfrac18(1+2\epsilon'-2\mu\epsilon')\dot\alpha^2+2\epsilon'\mu\dot\xi\dot\alpha],$$
$$T_1''(\dot\zeta',\dot\gamma')=\tfrac12 m(1-2\mu\epsilon'+\epsilon')^{-1}[4\mu(1+\epsilon')\dot\zeta'^2+\tfrac18(1+2\epsilon-2\mu\epsilon')\dot\gamma'^2-2\epsilon'\mu\dot\zeta'\dot\gamma'],$$
$$T_2(\dot\rho)=\tfrac12 m[\tfrac14(1+2\epsilon')\dot\rho^2],$$
$$T^*(\dot\eta',\dot\beta',\dot\sigma,\dot\tau)=\tfrac12 m(1-2\mu\epsilon')^{-1}(1-2\epsilon')^{-1}[4\mu(1-2\epsilon')\dot\eta'^2+\tfrac18(1-2\mu\epsilon')\dot\beta'^2$$
$$+\tfrac14(1-2\mu\epsilon'-8\epsilon'^2/3+8\mu\epsilon'^2/3)\dot\sigma^2+\tfrac{1}{16}(1-2\mu\epsilon'-4\epsilon'^2/3+4\mu\epsilon'^2/3)\dot\tau^2-\tfrac13\epsilon'^2(1-\mu)\dot\sigma\dot\tau\sqrt2$$
$$-\epsilon'(1-2\mu\epsilon')\dot\sigma\dot\beta'/\sqrt6+\tfrac12\epsilon'(1-2\mu\epsilon')\dot\tau\dot\beta'/\sqrt3+4\mu\epsilon'(1-2\epsilon')\dot\eta'\dot\sigma\sqrt{\tfrac23}+2\mu\epsilon'(1-2\epsilon')\dot\eta'\dot\tau/\sqrt3]. \quad (27')$$

The determinantal equations are:[10]

$$|\lambda T_1'-V_1|=0,\qquad |\lambda T_1''-V_1|=0,\qquad |\lambda T_2-V_2|=0,\qquad |\lambda T^*-V^*|=0, \quad (28')$$

which on expansion give:

$$m^2\lambda^2_{(\xi\alpha)}-[\tfrac14 A(1-2\mu\kappa)/\mu+8B(1-3\kappa)-4\kappa D]m\lambda+2(AB-D^2)(1-3\kappa-2\mu\kappa+4\mu\kappa^2)/\mu=0,$$
$$m^2\lambda^2_{(\zeta'\gamma')}-[\tfrac14 A(1-2\mu\kappa)/\mu+8B(1-\kappa)+4\kappa D]m\lambda+2(AB-D^2)(1-\kappa-2\mu\kappa)/\mu=0,$$
$$m\lambda_{(\rho)}-4C(1-2\kappa)=0,$$
$$m^4\lambda^4_{(\eta'\beta'\sigma\tau)}-Q_1m^3\lambda^3+Q_2m^2\lambda^2-Q_3m\lambda+Q_4=0, \quad (29')$$
$$Q_1=\tfrac14 A(1-2\mu\kappa)/\mu+(8B+4C+16E)(1-2\kappa),$$
$$Q_2=64CE(1-2\kappa)^2+2(AB-D^2)(1-2\kappa)(1-2\kappa\mu)/\mu$$
$$+4C[\tfrac14 A(1-2\kappa-2\mu\kappa+\tfrac{1}{3}4\mu\kappa^2)/\mu+8B(1-4\kappa+\tfrac{1}{3}8\kappa^2)+\tfrac{1}{3}16\kappa^2D]$$
$$+16E[\tfrac14 A(1-2\kappa-2\mu\kappa+\tfrac{1}{3}8\mu\kappa^2)/\mu+8B(1-4\kappa+\tfrac{1}{4}4\kappa^2)-\tfrac{1}{3}16\kappa^2D],$$
$$Q_3=64CE(1-2\kappa)[\tfrac14 A(1-2\kappa-2\mu\kappa)/\mu+8B(1-4\kappa)]+2\mu^{-1}(AB-D^2)[4C(1-4\kappa-2\mu\kappa+\tfrac{1}{3}8\kappa^2$$
$$+\tfrac{1}{3}16\mu\kappa^2)+16E(1-4\kappa-2\mu\kappa+\tfrac{1}{3}4\kappa^2+\tfrac{1}{3}20\mu\kappa^2)],$$
$$Q_4=128CE(AB-D^2)(1-4\kappa)(1-2\kappa-2\mu\kappa)/\mu.$$

If we had assumed for the masses $m_4=m_1=m+\Delta m$ and $m_3=m_2=m$, the expressions for $\lambda_{(\xi\alpha)}$ and $\lambda_{(\zeta'\gamma')}$ would have been interchanged. The assumption actually used has the advantage of simplifying calculations.

For $\kappa^2\ll1$ the fourth power equation becomes

$$m^2\lambda^2_{(\eta'\beta')}-[\tfrac14 A(1-2\mu\kappa)/\mu+8B(1-2\kappa)]m\lambda+2(AB-D^2)(1-2\kappa-2\mu\kappa)/\mu=0,$$
$$[m\lambda_{(\sigma)}-4C(1-2\kappa)][m\lambda_{(\tau)}-16E(1-2\kappa)]=0. \quad (30')$$

Since for YX_4 (i.e., for $\kappa=0$), the frequencies are given by

$$[m^2\lambda^2_{(\xi\alpha),\,(\eta\beta),\,(\zeta\gamma)}-(\tfrac14 A/\mu+8B)m\lambda+2(AB-D^2)/\mu]^3=0,$$
$$[m\lambda_{(\rho),\,(\sigma)}-4C]^2=0,\qquad m\lambda_{(\tau)}-16E=0, \quad (31)$$

we see that the substitution of X^* for X in YX_4 partially removes the degeneracy of the motion and gives rise to six frequencies. For $YX_2X_2^*$ the degeneracy is completely removed even though two of the frequencies differ only by terms of the order of magnitude of κ^2.

The application of the above results to experimental data together with a discussion of the intensities is postponed until a later paper.

In conclusion I wish to thank Professor E. O. Salant for his interest and advice in this work.

[10] $V^*(\eta',\beta',\sigma,\tau)=V_1(\eta',\beta')+V_2(\sigma)+V_3(\tau)$.

Term Structure of the Non-Collinear Triatomic Molecule of Type X_2Y

A. V. BUSHKOVITCH, *Department of Physics, University of Pennsylvania*

(Received December 26, 1933)

Group theory methods are applied to the molecule of type X_2Y (e.g., H_2O, SO_2) in which the equilibrium configuration of the nuclei is assumed to be that of an isosceles triangle. Electronic motion, vibration of the nuclei and rotation are successively taken into account, and symmetry with respect to interchange of the two equal nuclei, and with respect to inversion at the origin, is considered. Tables are given which allow one to determine, when the electronic, vibrational and rotational symmetries are known, the symmetry of a given term with respect to interchange of nuclei and inversion. Selection rules for all of the types of symmetry except rotational, are given; the selection rules of the asymmetrical rotator are then obtained from these, with the aid of the tables.

INTRODUCTION

THE fact that even the simplest types of polyatomic molecules are not amenable to exact quantum-mechanical treatment, while even approximate methods are not easily applicable, makes it of interest to consider what information about the term structure of polyatomic molecules may be obtained by the methods of group theory. The applicability of such methods to the problem has already been recognized by several investigators. Thus, Wigner[1] and Tisza[2] have given a thorough treatment of the vibrational motion of polyatomic molecules, while Mulliken[3] has discussed the electronic terms. It is now of interest to investigate also the effect of rotation, and here one will naturally attempt to follow as a program the corresponding treatment of the diatomic molecule by Wigner and Witmer.[4] In what follows, we shall attempt to obtain some information regarding the term structure of a simple triatomic molecule of the type X_2Y (e.g., H_2O) whose equilibrium configuration is that of an isosceles triangle, by the group theory method. We shall disregard the effect of spin for the present, reserving it for a later investigation, and shall consider, successively, electronic motion, vibrational motion of the nuclei, and rotation of the molecule as a whole.

THEORY

If, first, the nuclei are considered as fixed in the equilibrium configuration, the field of force admits the following symmetry operations (cf. Fig. 1):

(1) Identity, E
(2) Reflection on XZ plane, $iC_2(y)$
(3) Reflection on YZ (nuclear) plane, $iC_2(x)$
(4) Rotation with angle π about Z-axis, $C_2(z)$.

We have, obviously $iC_2(y)\cdot iC_2(x)=C_2(z)$.

These symmetry elements are isomorphic to the "vierergruppe" and hence possess the fol-

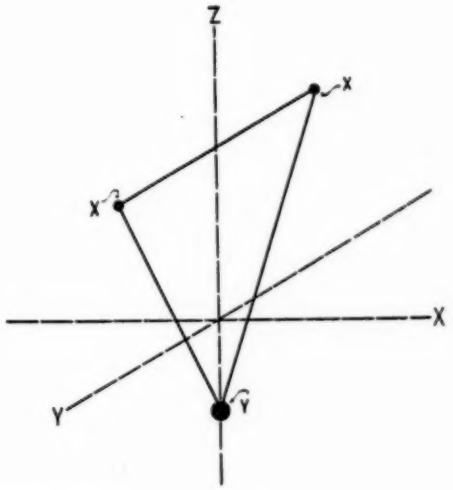

FIG. 1.

[1] E. Wigner, Goettinger Nachr., Math. Phys. Klasse, p. 133 (1930).
[2] L. Tisza, Zeits. f. Physik **82**, 48 (1933).
[3] R. S. Mulliken, Phys. Rev. **43**, 279 (1933).
[4] E. Wigner and E. E. Witmer, Zeits. f. Physik **51**, 859 (1928).

lowing four irreducible representations:

	E	$iC_2(x)$	$iC_2(y)$	$C_2(z)$
A_1	1	1	1	1
A_2	1	−1	−1	1
B_1	1	−1	1	−1
B_2	1	1	−1	−1

There will be, therefore, four types of electronic terms which we may designate as A_1, A_2, B_1, B_2 terms, in accordance with the notation adopted by Tisza and Mulliken.

If vibration is now taken into account, each electronic wave function (the electronic terms are non-degenerate, since their representations are all one-dimensional) must be multiplied by a product of three Hermitean polynomials, functions, respectively, of the three normal coordinates of the problem. The admissible symmetry operations here are the identity and rotation about the axis of symmetry with angle π. Under this last operation the first two polynomials are invariant while the third becomes multiplied by $(-1)^{n_3}$ (since the third normal coordinate is an odd function of y).[5] Hence, the first two polynomials have the representation A_1 for all n_1 and n_2, while the third has the representation A_1 for even n_3 and the representation B_2 for odd n_3. The total vibrational factor, therefore, transforms according to A_1 if n_3 is even, and according to B_2 if n_3 is odd.

Considering now the effect of rotation, the Hamiltonian of our system becomes invariant under the wider group of rotations and inversions at the origin. This allows us to determine the dependence of the wave functions on Euler's angles of the nuclear skeleton (i.e., of the XYZ axes of Fig. 1 which now become moving axes fixed in the body). If q denote the coordinates of the electrons with respect to the XYZ axes fixed in the nuclear frame as in Fig. 1, and ξ the normal coordinates, we have[6]

$$\psi_m{}^{Nln_1n_2n_3}(\alpha, \beta, \gamma, q, \xi) = \sum_\lambda e^{-im\alpha} d_{m\lambda}{}^l(\beta) e^{-i\lambda\gamma} G_\lambda{}^{Nln_1n_2n_3}(q, \xi). \quad (1)$$

Here

$$G_\lambda{}^{Nln_1n_2n_3}(q, \xi) = H_{n_1}(\xi_1) H_{n_2}(\xi_2) H_{n_3}(\xi_3) \varphi^N(q) g_\lambda{}^l,$$

where the g's are constants, and N stands for one of the symbols A_1, A_2, B_1, B_2. $\varphi^N(q)$ is a function of the fixed center problem, $H_n(\xi)$ is a Hermitean polynomial of degree n, and l specifies the total angular momentum of the system. Eq. (1) may be regarded as an expansion of the wave functions of the asymmetrical rotator in terms of the wave functions of the symmetrical rotator. Such expansions are of fundamental importance in the theory of the asymmetrical rotator.[7] The validity of Eq. (1) depends only on the invariance of the system under the rotation-inversion group; it is, therefore, independent of the choice of axes. In the discussions of the asymmetrical rotator it is usual to take the axis of the greatest moment of inertia as the Z-axis. In our case, however, it is necessary to take the axis of symmetry as the Z-axis, and this will be the axis of either the least or middle moment of inertia, depending on the magnitude of the apex angle of the triangle XXY. While the choice of axes is, thus, immaterial for the discussion which follows, it will have to be taken into account when we make use of the results of the theory of the asymmetrical top which is ordinarily based on a different choice of axes.

Eq. (1) would enable us to compute the value of the wave function ψ for any configuration of the molecule obtainable by a rotation or rotation-inversion from some configuration for which ψ is known, were it not for the $2l+1$ constants which appear in the equation. The symmetry of the problem is insufficient to determine all these constants, as was possible in the case of the diatomic molecule; nevertheless, it is possible to obtain all the essential features of the term structure, as we now proceed to show.

It will be convenient to recall, at this point, the classification of the functions of the asymmetrical rotator. It is shown (for instance, in Casimir's monograph), that for any given wave function of the asymmetrical rotator we have in Eq. (1) either only terms with even values of λ or terms with odd values of λ. In the first case,

[5] D. M. Dennison, Revs. Mod. Phys. **3**, 280 (1931).

[6] E. Wigner, *Gruppentheorie*, p. 230, Eq. (10).

[7] S. C. Wang, Phys. Rev. **34**, 243 (1929); Kramers and Ittmann, Zeits. f. Physik **53**, 553 (1929); **58**, 217 (1929); **60**, 663 (1930); H. B. G. Casimir, *Rotation of a Rigid Body in Quantum Mechanics*, Groningen, 1931.

TABLE I. *s = symmetrical; a = antisymmetrical.*

A_1 or A_2				B_1 or B_2			
n_3 even		n_3 odd		n_3 even		n_3 odd	
E	O	E	O	E	O	E	O
s	a	a	s	a	s	s	a

the function (in Casimir's notation) is said to belong to class E, otherwise to class O. Further, we always have either $g_\lambda{}^l = g_{-\lambda}{}^l$ or $g_\lambda{}^l = -g_{-\lambda}{}^l$; the function bears, in the first case, the subscript $+$, otherwise $-$. We thus obtain the four classes E_+, E_-, O_+, O_-. Selection rules hold for transitions between states belonging to the different classes, and we will consider them in greater detail later. It may be remarked here that the class to which a function belongs depends on the choice of axes; the manner in which the wave functions change class when axes are interchanged is given on page 64 of Casimir's book.

We proceed now to determine the connection between the several symmetries of the problem, i.e., of electronic and vibrational symmetry, rotational symmetry class (e.g., E_+, O_-), symmetry with respect to inversion at origin, and symmetry with respect to interchange of the two equal nuclei.

It is natural to require that, for the operations of the electronic symmetry subgroup, ψ^N should transform according to the representation whose index is N. In other words, replacing γ by $\gamma+\pi$ in the functions of Eq. (1), should be equivalent to applying the operation $C_2(z)$ to the function φ and the Hermitean polynomials, and then interchanging the coordinates of the two equal nuclei in ψ. This last operation yields $+1$ for functions symmetrical in the two equal nuclei (para-terms), and -1 for ortho-terms. These requirements will be satisfied if we have, for symmetrical functions:

$$\left.\begin{array}{ll}\text{(a) If } n_3 \text{ is even} & \\ \quad g_\lambda = 0 \quad \text{for } \lambda \text{ odd} & N = A_1 \text{ or } A_2 \\ \quad g_\lambda = 0 \quad \text{for } \lambda \text{ even} & N = B_1 \text{ or } B_2 \\ \text{(b) If } n_3 \text{ is odd} & \\ \quad g_\lambda = 0 \quad \text{for } \lambda \text{ odd} & N = B_1 \text{ or } B_2 \\ \quad g_\lambda = 0 \quad \text{for } \lambda \text{ even} & N = A_1 \text{ or } A_2\end{array}\right\}. \quad (2)$$

Similar relations hold for functions antisymmetrical in the nuclei, with the difference that the words "even" and "odd" are interchanged. These results are summarized in Table I.

We now consider symmetry with respect to inversion at origin. Inversion at origin is equivalent to the following sequence of operations:[8]

(1) $\alpha \to \pi + \alpha$
(2) $\beta \to \pi - \beta$
(3) $\gamma \to \pi - \gamma$
(4) Reflection of the electronic and vibrational functions on YZ (nuclear) plane, $iC_2(x)$.

The last operation gives a factor $+1$ for A_1 and B_2 terms, and a factor -1 for A_2 and B_1 terms.

We also need the formula:[8]

$$d_{\mu\lambda}{}^l(\pi-\beta) = (-1)^{l+\mu} d^l{}_{\mu,\,-\lambda}(\beta). \quad (3)$$

We take first an A_1 term, symmetrical in the nuclei, and with n_3 even. Here λ must be even, and $iC_2(x)$ gives $+1$. Let a dash indicate inversion at origin.

Then

$$\psi_m{}^{A_1 l n} = \sum_\lambda e^{-im\alpha} e^{-im\pi} d_{m\lambda}{}^l(\pi-\beta) e^{i\lambda\gamma} e^{-i\lambda\pi} G_\lambda{}^{A_1 l n}(q, \xi);$$

now $e^{-i\lambda\pi} = 1$ since λ is even; hence

$$\bar{\psi}_m{}^{A_1 l n} = \sum_\lambda e^{-im\pi} e^{-im\alpha} (-1)^{l+m} d^l{}_{m,\,-\lambda}(\beta) e^{i\lambda\gamma} G_\lambda{}^{A_1 l n}(q, \xi)$$

$$= (-1)^{l+m}(-1)^m \sum_\lambda e^{-im\alpha} d^l{}_{m,\,-\lambda}(\beta) e^{i\lambda\gamma} G_\lambda{}^{A_1 l n}(q, \xi)$$

or

$$\bar{\psi}_m{}^{A_1 l n} = (-1)^l \sum_\lambda e^{-im\alpha} d^l{}_{m,\,-\lambda}(\beta) e^{i\lambda\gamma} G_\lambda{}^{A_1 l n}(q, \xi). \quad (4)$$

[8] Cf. Wigner and Witmer, reference 4, p. 865.

But, if w denote the symmetry character, we have

$$\bar{\psi}_m{}^{A_1 l n} = w \cdot \psi_m{}^{A_1 l n}. \tag{5}$$

Combining Eqs. (4) and (5)

$$(-1)^l \sum_\lambda e^{-im\alpha} d^l{}_{m,-\lambda}(\beta) e^{i\lambda\gamma} G_\lambda{}^{A_1 l n}(q, \xi) = w \sum_\lambda e^{-im\alpha} d^l{}_{m\lambda}(\beta) e^{-i\lambda\gamma} G_\lambda{}^{A_1 l n}(q, \xi)$$
$$= w \sum_\lambda e^{-im\alpha} d^l{}_{m,-\lambda}(\beta) e^{i\lambda\gamma} G_{-\lambda}{}^{A_1 l n}(q, \xi).$$

We thus obtain, in the case of symmetrical terms

(a) For A_1 and B_2 terms

$$(-1)^{l+n_3} g_\lambda{}^{Nl} = w g_{-\lambda}{}^{Nl}$$

(b) For A_2 and B_1 terms

$$(-1)^{l+n_3} g_\lambda{}^{Nl} = -w g_{-\lambda}{}^{Nl} \tag{6}$$

For antisymmetrical terms, the minus sign occurs in Eq. (6a) instead of in Eq. (6b). These relations are summarized in Table II.

The Tables I and II may now be used in the following way: suppose we are given an electronic term of type B_2 with n_3 even, l odd, and with rotational symmetry E_+. Table I then shows that it is antisymmetrical, and Table II then gives $w=+1$.

To complete the analysis of the rotational structure, we must make use of the theorem of Kramers and Ittmann[9] that if the $2l+1$ eigenvalues with the same l are ordered according to their magnitude, i.e., $W_l < W_{l-1} < W_{l-2} < W_{l-3} < \cdots$, then, provided that $A_3 > A_2 > A_1$ (the A's are the principal moments of inertia), we have

W_l, W_{l-4}, W_{l-8}, $W_{l-12}\cdots$ are of class E_+
W_{l-1}, W_{l-5}, W_{l-9}, $W_{l-13}\cdots$ " " " O_+
W_{l-2}, W_{l-6}, W_{l-10}, $W_{l-14}\cdots$ " " " E_-
W_{l-3}, W_{l-7}, W_{l-11}, $W_{l-15}\cdots$ " " " O_-.

We are using, however, a different set of axes, and allowance must be made for this. Two cases arise:

(A) The middle moment of inertia is associated with the symmetry axis. We must make the interchange $A_3 \longleftrightarrow A_2$.

(B) The least moment of inertia is associated with the symmetry axis. The proper transformation is here $A_3 \longleftrightarrow A_1$ and $A_2 \longleftrightarrow A_1$.

[9] Cf. Casimir, reference 7, p. 64.

When these interchanges are carried out in accordance with the rules given on page 64 of Casimir's monograph, the theorem of Kramers and Ittmann assumes the form:

	Class			
	Case A		Case B	
	l even	l odd	l even	l odd
W_l, W_{l-4}, $W_{l-8}\cdots$	E_+	O_+	E_+	O_+
W_{l-1}, W_{l-5}, $W_{l-9}\cdots$	O_+	E_+	E_-	O_-
W_{l-2}, W_{l-6}, $W_{l-10}\cdots$	O_-	E_-	O_-	E_-
W_{l-3}, W_{l-7}, $W_{l-11}\cdots$	E_-	O_-	O_+	E_+.

It now remains to consider selection rules. To begin with, the following may be expected to hold rigorously:

(1) Symmetry with respect to inversion must change in any transition.
(2) $\Delta l = \pm 1$ but not $0 \to 0$.
(3) Ortho-terms combine with ortho-terms only; para-terms with para-terms.

The rules governing transitions in which change of electronic type or vibrational quantum numbers takes place, on the other hand, may be expected to be strictly fulfilled only as long as interactions between the several types of motion do not become great.

We consider first the selection rules of the fixed center problem (electronic selection rules). The procedure for obtaining these rules is given in the paper of Mulliken[3] and we merely state the results which one obtains in our particular case:

X	Y	Z
$A_1 \longleftrightarrow B_1$	$A_1 \longleftrightarrow B_2$	$A_1 \longleftrightarrow A_1$
$A_2 \longleftrightarrow B_2$	$A_2 \longleftrightarrow B_1$	$A_2 \longleftrightarrow A_2$
		$B_1 \longleftrightarrow B_1$
		$B_2 \longleftrightarrow B_2$

(7)

But not $A_1 \longleftrightarrow A_2$ or $B_1 \longleftrightarrow B_2$ for any component.

If now vibrational transitions also take place,

TABLE II.

Symmetrical terms								*Antisymmetrical terms*							
A_1 or B_2				A_2 or B_1				A_1 or B_2				A_2 or B_1			
$(l+n_3)$ even		$(l+n_3)$ odd		$(l+n_3)$ even		$(l+n_3)$ odd		$(l+n_3)$ even		$(l+n_3)$ odd		$(l+n_3)$ even		$(l+n_3)$ odd	
+	−	+	−	+	−	+	−	+	−	+	−	+	−	+	−
$w=1$	$w=-1$	$w=-1$	$w=1$	$w=-1$	$w=1$	$w=1$	$w=-1$	$w=-1$	$w=1$	$w=1$	$w=-1$	$w=1$	$w=-1$	$w=-1$	$w=1$

we must distinguish two cases: Δn_3 even and Δn_3 odd. In the first case, the same set of rules is obtained as is given above; in the second case, we obtain a different set, namely:

Δn_3 *odd.*

X	Y	Z
$A_1 \longleftrightarrow A_2$	$A_1 \longleftrightarrow A_1$	$A_1 \longleftrightarrow B_2$
$B_2 \longleftrightarrow B_1$	$A_2 \longleftrightarrow A_2$	$A_2 \longleftrightarrow B_1$
	$B_1 \longleftrightarrow B_1$	
	$B_2 \longleftrightarrow B_2$	

(8)

But not $A_1 \longleftrightarrow B_1$ or $A_2 \longleftrightarrow B_2$ for any component.

Since the rules (7) may be expected to hold fairly rigorously, because of greater energy involved, transitions of the type (8) which involve electronic transitions forbidden by (7) will not occur, or, at most, will give rise to very weak lines.

Since we have now obtained selection rules affecting all possible symmetry changes except rotational, we may, with the aid of Tables I and II, find now the selection rules between the functions of the four classes. They are given in Table III, and may easily be seen to be equivalent to the known selection rules of the asymmetrical top.

TABLE III.

$l \to l$	E_+	E_-	O_+	O_-
K_{iz}	←	—	→	←
		←	→	
K_{iy}	←	—	→	←
		←	—	→
K_{ix}	←	→	←	→

$l \to l-1$	E_+	E_-	O_+	O_-
K_{iz}	←	—	→	←
		←	—	→
K_{iy}	←	—	→	←
		←	→	
K_{ix}	⟷	⟷	⟷	⟷

In conclusion, the author wishes to express his thanks to Professor E. E. Witmer for many stimulating discussions and criticisms.

LETTERS TO THE EDITOR

Prompt publication of brief reports of important discoveries in physics may be secured by addressing them to this department. Closing dates for this department are, for the first issue of the month, the twentieth of the preceding month; for the second issue, the fifth of the month. The Board of Editors does not hold itself responsible for the opinions expressed by the correspondents.

The Nuclear Spin of Deuterium

The relative intensities of 29 lines have been measured in the α-bands of the molecular spectrum of deuterium. They correspond to the transition $3p\pi^3\Pi_u \rightarrow 2p\sigma^3\Sigma_u^+$ and their analysis was kindly given us by Professor G. H. Dieke. The bands lie between 5939 and 6291A and were photographed in the second order of a 21-foot grating by using the usual type of discharge tube with a potential of about 4100 volts and a current of 0.75 ampere. The gas was prepared from heavy water containing more than 90 percent deuterium for which we wish to thank Professor H. C. Urey.

Density marks of known relative intensity were put on each plate by means of a tungsten filament lamp burning with constant current of 0.85 ampere and a set of eight neutral wire screens. By means of a system of slits placed directly in front of the photographic plate we were able to have a separate set of density marks for each band and thus we could correct for the change in sensitivity of the plate with wave-length. The density marks were 0.5 mm wide which corresponded to the slit-width in photographing the molecular spectrum. Under these conditions complete resolution of some of the lines was not obtained and where such was the case these lines were not used in determining the alternation of intensities.

The usual type of photographic density curves were plotted and from these the intensities of the molecular lines were determined. With the equation $\ln I/i = \ln Cg - BJ(J+1)/kT$, we have obtained values for g_s and g_a, the statistical weight due to nuclear spin for the symmetric and antisymmetric levels by a least squares solution for each branch. The measured intensity of the line is I. i is the transition probability and the other quantities have their usual significance.

The results from the Q and R branches of the (0,0), (1,1), (2,2) and (3,3) bands on two different plates gave 1.95 ± 0.06 and 2.02 ± 0.04 for the ratio g_s/g_a. Since the symmetric levels are more intense, the nucleus obeys Bose-Einstein statistics and the nuclear spin of deuterium is 1. A more detailed report will appear shortly.

G. M. MURPHY
HELEN JOHNSTON

Department of Chemistry,
Columbia University,
March 24, 1934.

Transmutation of Lithium by Deutons and Its Bearing on the Mass of the Neutron

It has been recognized for some time that one of the most direct methods of obtaining the mass of the neutron is by a calculation of the mass-energy relations in the reaction

$$Li^7 + H^2 \rightarrow 2\,He^4 + n^1. \qquad (1)$$

Although there is perhaps some justification for assuming that γ-rays are not involved as a product of this reaction, an experimental test has not hitherto been available. Hence, calculations of the mass of the neutron which have been made without certain knowledge as to the presence of γ-rays are to be considered strictly valid only as an upper limit.

Due to the large intensity obtainable with our apparatus, we have been able to make absorption measurements of the radiation (neutrons, plus γ-rays, if present) produced in the above reaction out to large thicknesses of both lead and paraffin, and in that way to analyze the radiation into its components for the purpose of determining whether or not γ-rays are present. It was desirable first to eliminate protons from the ion beam as far as convenient, because protons, in disintegrating lithium produce γ-rays, of the order of one quantum per disintegration, and of hardness about equal to that of the γ-rays from radium after 2 to 3 cm lead filtration.[1] This was accomplished by using rather pure (approximately 90 percent H^2 gas, and for economy it was diluted with an equal amount of helium.* It will be seen later than an effect produced by the relatively small number of protons still present appears, but can readily be identified, in the final results. During all the measurements the tube was run at 900,000 volts, with a total ion current of 5 microamperes, 3 to 4 microamperes of which it is estimated was due to deutons. The intensity of radiation obtained under these conditions was

[1] Lauritsen and Crane, Phys. Rev. **45**, 63 (1934).

* It was first made certain that helium alone produced no measurable effect.

found to correspond to the production of about 2×10^7 neutrons per second.

Curves representing the absorption of the radiation in lead and in paraffin, with both a lead and a paraffin lined ionization chamber, are shown in Fig. 1. The method of analysis is the same as we have used previously in dealing with the neutrons and γ-rays obtained from beryllium and boron bombarded with deutons.[2] The fact that all four absorption curves are nearly straight lines indicates that the radiation is almost entirely of a single kind; and further, the large displacement of the paraffin chamber curves above the lead chamber curves and the large absorption in paraffin indicate that the effect is due to neutrons. A weak component of γ-rays is indicated by the slightly greater absorption by lead for small thicknesses, as recorded by the lead lined chamber (curve IV). The dotted line repre-

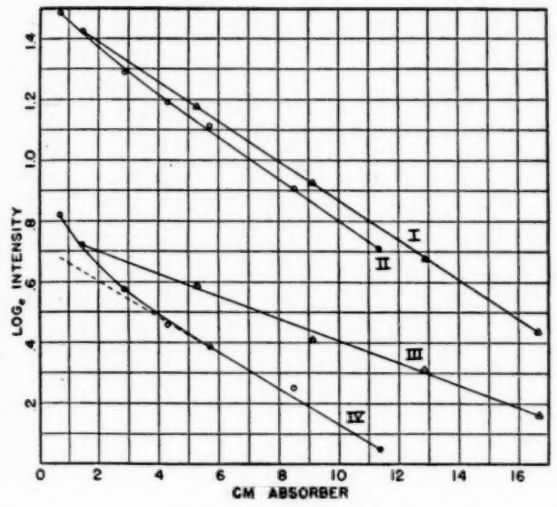

FIG. 1. Absorption of the radiation from lithium. I, paraffin lined chamber, paraffin absorber; II, paraffin lined chamber, lead absorber; III, lead lined chamber, paraffin absorber; IV, lead lined chamber, lead absorber.

sents the intensity due to neutrons alone, obtained by extrapolation, and therefore the difference between curve IV and the dotted line should be just the intensity due to the γ-ray component. The number of γ-ray quanta determined in this way is about 1/10 the number obtained in previous work under the same conditions with a beam of pure H^1, and the absorption coefficient is quite accurately the same. These γ-rays, then, are obviously to be ascribed to the protons present in the beam due to the small amount of H^1 actually contained in the heavy hydrogen used. This leaves only neutrons to be associated with the disintegration of lithium by deutons, and hence the calculations of the mass of the neutron which have been based on this process are correct, subject only to certain assumptions as to the velocity distribution of the neutrons.

If we assume that, as long as momentum is conserved, there are no restrictions on the way in which the available energy may be shared among the three particles[3, 4, 5] the two α-particles and the neutron—then it can be shown that the α-particles which come off with maximum energy would be those corresponding to the case in which the neutron happens to come off parallel to, and with the same velocity as, one of the α-particles. In this circumstance the other α-particle will, from momentum considerations, get 5/9 the total energy of the disintegration. There is no reason to doubt that this case occurs, but, since the neutron must satisfy specifications both as to direction and velocity, the probability of this occurrence must be very small. If, however, we specify simply that the energy carried away by the neutron be zero or nearly zero, then it will not be necessary to make a specification as to direction, and we will have, as the energy of the α-particle in this limiting case, just 1/2 the total energy of the disintegration. Out of a large number of disintegrations, the number which satisfy the second set of specifications will be much greater than the number which satisfy the first set of specifications, and it seems probable that under the conditions of experiment the maximum range observed may in fact correspond to the second mode of disintegration.

Oliphant, Kinsey and Rutherford[3] have made careful measurements of the ranges of the α-particles produced by bombarding lithium with deutons, and have found, as the upper limit of the continuous range, 7.8 cm, corresponding to an energy of 8.3×10^6 e.v. This group they attribute to the disintegration of Li^7, and, superimposed upon that, is a monochromatic group of greater range which is accounted for by the disintegration of Li^6. It seems entirely possible that a small number of particles due to the first mode of disintegration of Li^7 discussed above would be masked completely by the long range group from Li^6.

If we now solve Eq. (1), by using as masses of the atoms Bainbridge's values, $H^2=2.0136$, $Li^7=7.0146$, $He^4=4.0022$, and taking 0.0002 as the mass equivalent of the kinetic energy of the bombarding deutons used by the above investigators, then on the assumption that the α-particle of maximum energy observed corresponds to that mode of disintegration in which it gets half the total energy of the disintegration, we obtain for the mass of the neutron 1.0063. Essentially the same calculation can be performed in a slightly different way,[6] which perhaps involves fewer sources of error than the above, by making use of the known data on the disintegration of lithium by protons.[6, 3] By eliminating between the two equations

$$Li^7+H^2\rightarrow 2\,He^4+n^1+E_1$$

$$Li^7+H^1\rightarrow 2\,He^4+E_2$$

we obtain

$$n^1=H^2-H^1+E_2-E_1$$

in which the only atomic masses involved are those of H^1 and H^2, which are known with considerable precision. The kinetic energy of the bombarding H^1 ions and the H^2 ions

[2] Crane and Lauritsen, Phys. Rev. **45**, 226 (1934); Lauritsen and Crane, Phys. Rev. **45**, 493 (1934).

[3] Oliphant, Kinsey and Rutherford, Proc. Roy. Soc. **A141**, 722 (1933).

[4] R. M. Langer, Phys. Rev. **45**, 137 (1934).

[5] R. Ladenburg, Phys. Rev. **45**, 224 (1934).

[6] Cockroft and Walton, Proc. Roy. Soc. **A137**, 229 (1932).

used by Oliphant, Kinsey and Rutherford was, as far as we know, the same (about 0.2×10^6 e.v.), and hence cancels. The ranges of the α-particles resulting from the two reactions are nearly the same (7.8 and 8.4 cm, respectively) and since only the difference in energy is made use of, any systematic error in the measurements or in the conversion from range to energy tends to cancel out. Using $E_1=16.6\times10^6$ e.v. and $E_2=17.5\times10^6$ e.v., the difference of which is equivalent to 0.0010 mass units, we obtain for the mass of the neutron 1.0068. This we believe to be the best value on the basis of the data here discussed, and it is in agreement with the value found by Chadwick.

It is interesting, and perhaps of some significance, that γ-rays are produced in the disintegration of lithium by protons but not in the disintegration of lithium by deutons. This would lead one to suspect that the γ-ray quantum is not associated with an excitation level in the α-particle, since α-particles with high energy are produced in both instances. A solution which seems very plausible is to associate the γ-ray quantum with excited He^3 in the reaction[3]

$$Li^6+H^1\rightarrow He^4+He^3+\gamma.$$

Oliphant, Kinsey and Rutherford have observed short range particles produced in the disintegration of lithium by protons having ranges 0.65 cm and 1.15 cm. If we assume that the longer of the two ranges corresponds to He^3 and the shorter to He^4, we find that the energies† corresponding to those ranges are 1.6 and 2.1×10^6 e.v., respectively, which are just in the ratio 3 to 4, as would be expected from momentum considerations. Taking into account the γ-ray, and solving the equation for the mass of He^3, we obtain 3.0146, which is in good agreement with that to be expected from the upper branch of Aston's packing fraction curve.

It is a pleasure to acknowledge our gratitude for the support received from the Seeley W. Mudd Fund for carrying out this work.

C. C. Lauritsen
H. R. Crane

Kellogg Radiation Laboratory,
California Institute of Technology,
March 24, 1934.

† The energy of He^3 was obtained from the range-energy curve for α-particles, and corrected for the difference in mass.

The Energy Distribution of the Neutrons from Fluorine

From experiments on the ionization currents in hydrogen produced by neutrons from Be, B and F, Bonner[1] concluded that the neutrons from fluorine must have a considerably smaller average energy than those from beryllium or from boron. Curie and Joliot,[2] on the other hand, concluded that fluorine neutrons must be of high energy since they found them to be weakly absorbed by lead. Accordingly, it was desirable to make, if possible, a direct measurement of the energy of the fluorine neutrons.

It appeared that the methods of energy measurement which have been used for beryllium and boron neutrons were not especially suitable, since the intensity of the fluorine radiation is so small. It seemed entirely impractical to use recoil protons from paraffin, observed with either a counter or a cloud chamber. Indeed it seemed not feasible to observe recoil atoms with any arrangement of an ordinary cloud chamber on account of the excessively large number of photographs which would be necessary to record a reasonable number of tracks. In order to increase this number a special cloud chamber was constructed which allowed the gas pressure to be increased by a factor of more than ten. In this experiment it was used with hydrogen at a pressure of 12.9 atmospheres, so that more than a tenfold increase in sensitivity was attained. The experiment then consisted in measuring by the usual method the range of the recoil protons produced in the gas.

The source of neutrons consisted of a ten millicurie polonium source of α-particles bombarding a piece of fluorite. It was placed near the side wall of the chamber. The tracks were photographed with the usual stereoscopic camera arrangement and were reconstructed by projection.

About 9000 pairs of photographs were taken, on which 205 recoil protons were found. The ranges of these protons were measured and were then converted to air-equivalent by making use of the differential stopping-power data obtained by Gurney.[3] The number of observed recoil protons as a function of the range is shown in the curve of Fig. 1. From the curve it appears that the maximum range

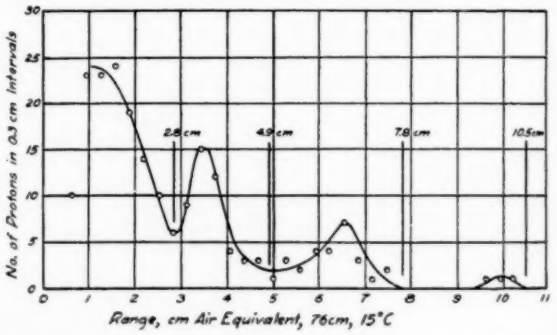

FIG. 1. Range distribution of the recoil protons from fluorine neutrons.

of the recoil protons is about 10.5 cm of air, giving the maximum energy of fluorine neutrons to be 2.5×10^6 e.v. This value is considerably less than the maximum energy of neutrons from beryllium and confirms Bonner's result.

It is seen that the curve shows distinct peaks which we believe definitely means that the neutrons are emitted with

[1] T. W. Bonner (to appear in the May 1st Physical Review).

[2] I. Curie and F. Joliot, J. de Phys. et le Rad. **4**, 278 (1933).

[3] R. W. Gurney, Proc. Roy. Soc. **A107**, 340 (1925).

discrete energies, rather than with a continuous distribution. The values of the maximum range for these groups are given in Table I and are indicated in Fig. 1. The velocity and energy corresponding to these ranges are given in succeeding columns of this table.

TABLE I.

Proton Emission from Fluorine (Chadwick and Constable)				*Neutron Emission from Fluorine*				
Rp (cm)	$Ep/10^6$ e.v.	ΔEp	$R\alpha$ (cm)	Rn (cm)	$Vn/10^9$ cm/sec.	$En/10^6$ e.v.	ΔEn	$R\alpha$ (cm)
56	6.55	0.42	3.9	10.5	2.20	2.54	0.43	3.9 (assumed)
47	6.13	0.55	3.9	7.8	2.01	2.11	0.52	3.9 (assumed)
40	5.58	0.51	2.7	4.9	1.74	1.59	0.49	2.7 (assumed)
33.5	5.07	0.30	2.2	2.8	1.45	1.10		2.3
30.5	4.77	0.51	2.7	—	—	—	—	—
25	4.26		2.2	—	—	—	—	—

Rp = Range of disintegration protons
Ep = Energy of protons.
ΔEp = Energy difference between proton groups.
$R\alpha$ = Range of α-particles producing disintegration.
Rn = Maximum range of recoil protons.
Vn = Neutron velocity.
En = Neutron energy.
ΔEn = Energy difference between neutron groups.

Since the α-particles producing the disintegrations have a continuous range of energy from their maximum to zero (because a thick target was used) it seems probable that the discrete energy groups in the neutron emission are produced by the penetration of the α-particle into the nucleus through resonance levels. Such a resonance phenomenon has been observed in the other type of disintegration of fluorine where a proton is emitted. The latest work on this subject is that of Chadwick and Constable.[4] Since both types of disintegration depend on the entrance of the α-particle into the fluorine nucleus, it was expected that the resonance levels should be the same in both cases. Accordingly, we have looked for a correlation between the proton groups and the neutron groups. It cannot be expected that the actual energies of the groups shall be the same in both cases since the disintegration reactions are entirely different. However, the energy differences between successive groups should be the same if the same resonance levels are involved. The energy differences for both cases are given in Table I. The corresponding differences for the two cases are seen to agree as well as could be expected. It will be noted that the two groups of lowest energy for the neutron disintegration are missing. It is probable that they exist but have not been found because of poor resolving power at the shorter ranges. Further evidence that the same resonance levels are effective comes from the fact that the emission of neutrons from fluorine begins when the α-particle has a range of 2.3 cm.[5] This value agrees with the range of 2.2 cm corresponding to the lowest resonance level which Chadwick and Constable observed in the proton disintegration.

T. W. BONNER
L. M. MOTT-SMITH

The Rice Institute,
Houston, Texas,
March 30, 1934.

[4] J. Chadwick and J. E. R. Constable, Proc. Roy. Soc. **A135**, 48 (1932).
[5] T. W. Bonner, Phys. Rev. **45**, 425 (1934).

Disintegration of Li^6 by Protons and Deutons

In a recent letter to *Nature*, Oliphant, Shire and Crowther[1] reported the results of the disintegration of the separate isotopes of lithium by protons and deutons. The results for Li^7 are well understood, the nuclear reactions being:

$$Li_3^7 + H_1^1 \rightarrow 2\ He_2^4 \quad (1)$$

$$Li_3^7 + H_1^2 \rightarrow 2\ He_2^4 + n_0^1 \quad (2)$$

as shown by Cockroft, Walton,[2] Oliphant, Kinsey and Rutherford.[3] In case (1) the α-particles have a sharp range of 8.4 cm, in case (2) all ranges up to 8 cm are observed.

On bombarding ordinary Li with protons two other groups of α-particles in addition to the 8.4 cm group were observed,[3] having ranges of 6.5 mm and 11.5 mm. The experiments of Oliphant, Shire and Crowther show that the 11.5 mm group is due to Li_3^6. The group of 6.5 mm could not be observed because the screen had a stopping power of about 6 mm. Perhaps it may also be ascribed to Li_3^6. If this is the case one can try to explain these two groups by assuming the reaction:

$$Li_3^6 + H_1^1 \rightarrow He_2^4 + He_2^3 \quad (3)$$

as already suggested by Oliphant, Kinsey and Rutherford.[3] We must assume then further that the 11.5 mm group is really He_2^3. Neglecting the impulse of the proton, the velocity of He_2^4 would then be three-fourths the velocity of He_2^3. Taking tentatively[4] the range of two equally charged particles as proportional to mv^3 one obtains for the range of He_2^4 $(\frac{3}{4})^2 \times 11.5 = 6.47$ mm, in agreement with the observed value. The kinetic energy of an α-particle of 6.5 mm range is 1.6×10^6 e.v. and hence the kinetic energy of the He_2^3 would be 2.1×10^6 e.v. If we use for the values of the nuclear masses $Li_3^6 = 6.0129$, $H_1^1 = 1.0072$, $He_2^4 = 4.0011$ and take for the kinetic energy of the protons 0.0002 M.U., the mass of He_2^3 comes out to be 3.0152. With the value 1.0065 for the mass of the neutron the binding energy of He_2^3 would be 0.0057 or about 5×10^6 e.v. This is a quite

[1] Oliphant, Shire and Crowther, Nature **133**, 377 (1934).
[2] Cockroft and Walton, Proc. Roy. Soc. **A137**, 229 (1932).
[3] Oliphant, Kinsey and Rutherford, Proc. Roy. Soc. **A141**, 722 (1933).
[4] Comp. Blackett, Proc. Roy. Soc. **A135**, 132 (1932); Duncanson, Proc. Camb. Phil. Soc. **30**, 102 (1934).

reasonable value. Assuming with Heisenberg that the main interaction is between protons and neutrons, one must expect that the mass defect of He_2^3 lies between 2×10^6 e.v. (=twice the mass defect of H_1^2) and 12×10^6 e.v. (=one-half the mass defect of He_2^4). Considering also the interaction in triples[5] one gets as a next approximation:

$$[He_2^4]=2[He_2^3]+2[H_1^3]-4[H_1^2], \qquad (4)$$

when the brackets denote the mass defect. This is always still with only proton-neutron interaction. Then also $[He_2^3]\leqq[H_1^3]$ and we get for the mass defect of He_2^3 and H_1^3 about 7×10^6 e.v. Finally one can try to estimate the mass defect of He_2^3 more precisely by assuming with Wigner and Chadwick[6] for the interaction between proton and neutron a very narrow and deep potential hole (width $\leqq10^{-13}$ cm, depth $\leqq90\times10^6$ e.v.). As these authors have shown, one can then understand the large mass defect of He_2^4, and the experimental results on the scattering of neutrons by protons. With this model one obtains for the mass defect of He_2^3 again values between 3×10^6 e.v. and 7×10^6 e.v.[7]

On bombarding Li_3^6 with deutons, α-particles of 13.2 cm range are observed and in addition protons of 30 cm range. The former are explained by the reaction:[8]

$$Li_3^6+H_1^2\rightarrow 2\,He_2^4. \qquad (5)$$

The protons can be explained by assuming:

$$Li_3^6+H_1^2\rightarrow Li_3^7+H_1^1. \qquad (6)$$

Taking for the kinetic energy of the deutons again 0.0002 and substituting for the masses of $Li_3^7=7.0130$, $H_1^2=2.0131$, the kinetic energy of the Li_3^7 and H_1^1 comes out to be 0.0060 M.U. or 5.63×10^6 e.v. Because of the conservation of momentum 7/8 of this or 4.92×10^6 e.v. is taken up by the proton[9]. This corresponds to a velocity of 3.04×10^9 cm/sec., and a range[4] of about 31 cm, in good agreement with the observed value. The reaction (6) is analogous to the capture process of deutons by carbon as proposed recently by Lauritsen and Crane.[9]

TA-YOU WU
GEORGE E. UHLENBECK

Department of Physics,
University of Michigan,
March 30, 1934.

[5] Comp. a forthcoming paper in the Phys. Rev. by Goudsmit and Bacher.

[6] Wigner, Phys. Rev. **43**, 252 (1933); Chadwick, Proc. Roy. Soc. **A142**, 1 (1933).

[7] During the writing of this Letter, the March 17 issue of Nature arrived here, in which Oliphant, Harteck and Rutherford communicate the results of their experiments on the transformation effects observed with heavy hydrogen. In here they also mention that (3) would lead to the mass 3.0165 for He_2^3, which is the same as our value plus two electrons. They further make very probable the existence of H_1^3, for which mass they obtain the value 3.0151. This gives a mass defect of 0.0056 M.U. (mass units) or again about 5×10^6 e.v.! The equality of the mass defects of H_1^3 and He_2^3 seems to us a very strong argument in favor of the Heisenberg hypothesis that the main interaction is between protons and neutrons.

[8] Lewis, Livingstone and Lawrence, Phys. Rev. **44**, 55 (1933). Comp. also reference 3.

[9] Lauritsen and Crane, Phys. Rev. **45**, 345 (1934). With our interpretation of the two short range groups the γ-radiation observed by these authors (Phys. Rev. **45**, 63 (1934)) has become difficult to understand.

The Energy Distribution of Neutrons from Boron

In a previous letter,[1] we have presented energy measurements of the neutrons from a polonium-fluorine source. These measurements were carried out by observing the tracks of the recoil protons produced in a cloud chamber containing hydrogen at high pressure. By means of this method of measurement we were able to show that in the case of this element there were several neutron groups of different energy. In fact this method seemed particularly suitable for detecting neutron groups when they exist. Accordingly, experiments using this same method have been carried out for the neutrons emitted from boron when bombarded by α-particles from polonium.

4000 pairs of photographs have been taken with this source of neutrons. 2000 of these photographs were taken with hydrogen in the chamber at a pressure of 12.9 atmospheres, the remainder with methane (CH_4) at the same pressure. In both cases only tracks of recoil protons were used; those due to the carbon atoms in the methane at this pressure were too short to be measurable or to be confused with the proton tracks. It was convenient to use the two gases because with hydrogen a large number of the faster protons collided with the walls of the chamber and thus could not be measured, while with methane the proton tracks of lower energy were too short to be measured with sufficient accuracy. With hydrogen, 162 tracks were measured; with methane, 210. The observed ranges were converted to their equivalent length in air by using, in the case of hydrogen, the stopping-power data from Gurney,[2] and for methane, the data given by Van der Merwe.[3] The value of the relative stopping-power which was used in this conversion depends somewhat on the range of the proton. The value adopted at our longest range for the stopping-power of hydrogen at one atmosphere relative to air is 0.211. The corresponding stopping-power for methane was taken to be 0.83. The curves of Fig. 1 show the distribution-in-range of the observed recoil protons. As in the case of fluorine, the curves show distinct maxima and minima which we believe cannot be caused entirely by statistical fluctuations but must principally be due to the

[1] T. W. Bonner and L. M. Mott-Smith, Phys. Rev. **45**, 552 (1934).

[2] R. W. Gurney, Proc. Roy. Soc. **A135**, 48 (1925).

[3] C. W. Van der Merwe, Phil. Mag. **45**, 379 (1923).

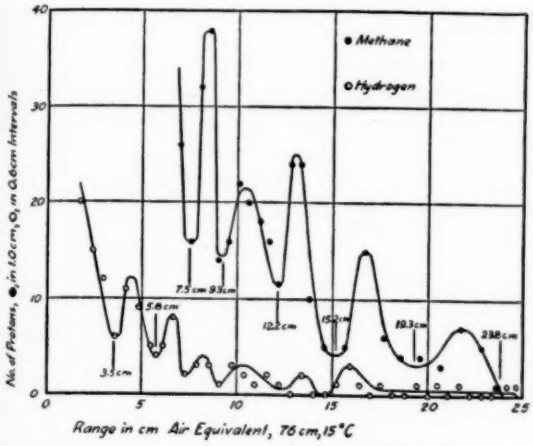

FIG. 1. Range distribution of recoil protons from Po-B neutrons.

existence of groups of neutrons of different energy. From Fig. 1 it is seen that six groups are indicated by the methane curve, while two additional groups are shown by the hydrogen curve below the 7.0 cm range where the methane curve ends. Where the two curves overlap, the hydrogen curve also shows peaks corresponding to the groups of higher energy, and the positions of the minima on this curve correspond approximately with those of the methane curve. The hydrogen curve alone would not be convincing on account of the small number of tracks, but considered in conjunction with that for methane strengthens the evidence for the existence of the groups.

TABLE I.

Maximum range of recoil-proton group (cm)	Velocity of neutron group ($\times 10^9$ cm/sec.)	Energy of neutron group ($\times 10^6$ e.v.)
23.8	2.82	4.16
19.3	2.64	3.65
15.2	2.46	3.17
12.2	2.29	2.75
9.3	2.12	2.35
7.5	1.98	2.05
5.8	1.84	1.77
3.5	1.57	1.29

The maximum ranges corresponding to the eight observed groups are shown in Fig. 1 and are tabulated in Table I. In Table I are also given the velocity and the energy of the neutrons which correspond to the recoil protons of these ranges. The maximum energy of the neutrons from boron is found to be 4.2×10^6 e.v., a value somewhat higher than the value of about 3.3×10^6 e.v. found by previous observers. The new value of the maximum energy lowers the mass of the neutron which is obtained by Chadwick[4] from the reaction $B^{11}+\alpha=N^{14}+n$. Using the value 3.35×10^6 e.v., he finds the mass of the neutron to be 1.0067; introducing our value, we obtain 1.0058. However, we feel that there is considerable doubt as to whether the mass of the neutron can be calculated from this reaction because there is the possibility that the neutrons of maximum energy are due to B^{10}.

Following the same argument which was given in our letter on the neutrons from fluorine, we considered the possibility of correlating the neutron groups with the groups from the proton disintegration of boron. However, with boron this cannot be done at present because of complications caused by the existence of the two isotopes. It is generally believed that only B^{10} disintegrates with the emission of a proton, while the neutron disintegration has been ascribed to both B^{10} and B^{11}. Thus it is possible that the eight neutron groups we have observed are due partly to B^{10} and partly to B^{11}, and in this case we would not be able to assign the various groups to their proper isotope. It is also possible that only B^{11} disintegrates with neutron emission, in which case no correlation is expected. If, on the other hand, only B^{10} undergoes neutron disintegration, a correlation would be expected, but we find that a correlation is impossible because in the proton disintegration of B^{10} only three groups have been observed.[5] This result may be interpreted to mean either that some of the proton groups of B^{10} have not been detected or that B^{10} cannot alone be responsible for the neutron emission.

L. M. MOTT-SMITH
T. W. BONNER

The Rice Institute,
Houston, Texas,
April 2, 1934.

[4] J. Chadwick, Proc. Roy. Soc. **A142**, 1 (1933).
[5] F. Heidenreich, Zeits. f. Physik **86**, 675 (1933).

Evidence for a Resonance Level in the B^{10} Nucleus

Previous studies by Bothe[1] and Heidenreich[2] on the nature of the groups of protons emitted by boron under alpha-particle bombardment lead to somewhat conflicting conclusions. According to Bothe the short-range group extends up to 20 cm, while Heidenreich does not find it to extend beyond 14 cm. This group is of some interest since, if considered to be single, it appears to behave differently from the others when the energy of the alpha-particle or the angle at which the protons emerge is caused to increase. In each case a rapid variation in yield is observed. It has been suggested that these protons may be emitted in a disintegration in which the alpha-particle is not captured.

A preliminary experiment in which a relatively thick layer of powdered boron (more than 2 cm air equivalent) was bombarded by polonium alpha-particles gave a proton absorption curve like that of Bothe, the group extending to approximately 20 cm. The protons were counted by means of an ionization chamber and linear amplifier.

The only considerable difference between the two previous experiments is that Bothe used a thick layer as a target while Heidenreich used a thin film. Thus the pos-

[1] W. Bothe, Zeits. f. Physik **63**, 381 (1930).
[2] F. Heidenreich, Zeits. f. Physik **86**, 675 (1933).

sibility remains that a group of range up to 20 cm is produced by alpha-particles of low energy (near the end of their range in the thick layer). To test this the alpha-particles were retarded by gold foil of 2 cm stopping power and an absorption curve plotted. This is given in Fig. 1.

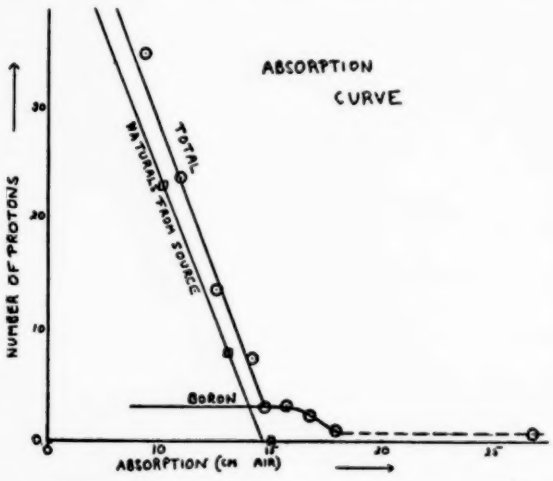

FIG. 1.

The presence of a group of 18.5 cm range can be seen. If the natural protons produced by the source be subtracted, the presence of a single homogeneous group of range 18.5 cm is evident. To trace the origin of these protons the space between the source and the gold foil was evacuated and refilled with oxygen to give any desired range to the impinging alpha-particles. In Fig. 2, the yield is plotted

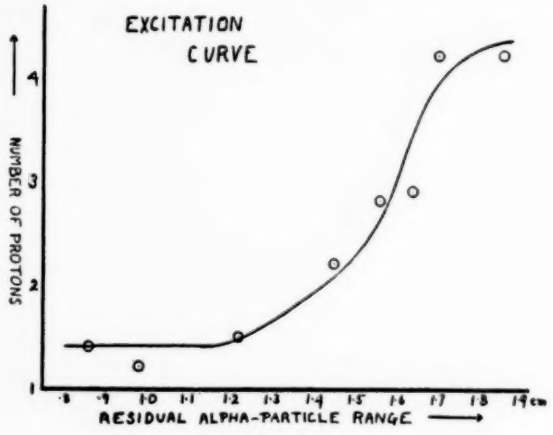

FIG. 2.

against initial alpha-particle range. It will be seen that no protons are emitted until the alpha-particle energy corresponds to a range of 1.20 cm. Beyond this the numbers rise smoothly, flattening off at 1.70 cm. This shows the group to be due to resonance entry of the alpha-particles, and, since there is a rising yield between 1.20 and 1.70 cm, the entry is through a rather wide band, in agreement with the fact that a high probability of penetration through the potential barrier already exists for such energies. The two limits of the band may be set at 3.91×10^{-6} and 5.03×10^{-6} erg, giving a mean of 4.57×10^{-6}. According to Fowler and Wilson the half width of the resonance band divided by the energy ($\Delta E/E$) is of the order of the penetration probability. Thus the results agree with a penetration probability of about 1/7, which is reasonable.

Curves showing evidence of resonance have been given by Curie-Joliot[3] and by Chadwick[4] for excitation of neutrons in boron. These are probably due to excitation of the B^{11} isotope, while the present work applies to B^{10}. Exact agreement would not therefore be expected, yet the curves of Curie-Joliot fit in with resonance between 1.1 cm and 1.45 cm, while Chadwick gives higher values, commencing at 1.4 cm. For a first approximation, this is satisfactory.

The nuclear energy change calculated from the process is $0.21\times10^{-6}\pm0.47\times10^{-6}$ erg or $0.13\pm0.28\times10^{-6}$ electron-volt. [The error is not so great as is apparent since the zero is the important figure.] Chadwick gives the value 0.35×10^{6} electron-volt, calculated from the group of 37.5 cm range due to excitation over the top of the barrier by the unretarded polonium α-particles. The agreement is within the error of the experiment and shows that the new group does not demand any *ad hoc* levels of energy inside the nucleus itself.

The presence of a small yield at larger absorption (beyond 18.5 cm) may mean that the long-range group (82 cm) can also be excited by entry through this resonance level. Assuming the value 4.96×10^{-6} erg for the nuclear energy change as given by Chadwick,[5] this process gives a group of 58 cm range protons numbering about one-third the main group.

The fact that the short range group found by Bothe is complex invalidates any deductions about its behavior. The sharp rise at 14 cm found by Heidenreich may be due to a second excited state which should have associated with it the emission of one or more quanta.

It is a pleasure to acknowledge the help given by Professor A. F. Kovarik in advice and discussion.

ERNEST POLLARD*

Sloane Laboratory,
Yale University,
April 2, 1934.

[3] I. Curie and F. Joliot, C. R. **196**, 398 (1933).
[4] J. Chadwick, Proc. Roy. Soc. **A142**, 1 (1933).
[5] See Duncanson, Proc. Camb. Phil. Soc. **30**, 112 (1934).
* Sterling Fellow.

A Method of Attaching a Fluorite Window to Glass Apparatus

A fluorite window may be attached to a glass tube in such a manner that the apparatus can be evacuated and baked out in the usual way without leakage and without breaking the window upon cooling. The technique is as follows: (1) a glass channel is sealed around the orifice to be covered by the window (Fig. 1). The diameter of the

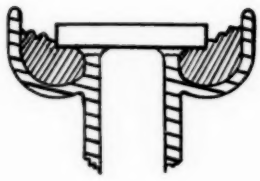

FIG. 1.

orifice should be 3–4 mm less than that of the window so that the latter, when in position, will project over the edge of the orifice to the center of the channel. (2) Before the window is placed in position the channel is filled with crumbs of silver chloride. (3) The apparatus is placed in the furnace and the temperature is raised to 470°C and held there for a minute thus melting the silver chloride. (4) When cool more silver chloride is added and the process is repeated until the outer level of the cold chloride is slightly above the level of the orifice. (5) While the apparatus is cold the fluorite window is laid over the orifice but is supported now at its outer edge by the chloride. (6) The temperature is raised to 450°C and then slowly up while the window is carefully watched. (7) As the chloride melts a thin layer runs in suddenly between the window and the ground surface of the orifice. (8) The heating should be stopped immediately. When cold the joint is vacuum tight and the apparatus may safely be baked out at 430°C.

FREDERIC PALMER, JR.

Haverford College,
Haverford, Pennsylvania,
March 26, 1934.

An Attempt to Find Neutron-Like Particles Accompanying β-Ray Emission

At the suggestion of Professor E. D. Eastman, an attempt was made to determine whether or not particles of the nature of neutrons were emitted simultaneously with β-rays. The apparatus used consisted of an ionization chamber collecting from about 1 cc volume, a linear amplifier and an automatic counter. The zero of the instrument was about 0.5 per minute.

Having placed a sq. cm of paraffin paper over the opening of the ionization chamber, it was exposed to about 100 mc of Ra D and Ra E contained in old Rn tubes. The source was separated from the counter by a lead screen 3 mm thick. If as do Be neutrons, such neutron-like particles from β active bodies produced approximately one proton per 4000 neutrons incident on paraffine, there should have been some 10^5 protons counted per minute. No effect was noticed, the zero count remaining at 0.5 per minute. Negative results were also found for a 300 gram KCl sample and for a 50 gram RbCl sample.

If then, some neutron-like particle is emitted simultaneously with a β-ray, such a particle must have insufficient energy, or have a mass too small to produce recoil protons observable with such apparatus as used here.

G. H. DENISON

Department of Chemistry,
University of California,
Berkeley, California,
March 31, 1934.

Proceedings of the American Physical Society

MINUTES OF THE NEW YORK MEETING, FEBRUARY 23–24, 1934

THE 190th regular meeting of the American Physical Society was held in New York on Friday and Saturday, February 23–24, 1934, as a joint meeting with the Optical Society of America. The presiding officers at the sessions of the Physical Society were Professor Arthur H. Compton, President of the Society, Professor R. W. Wood, Vice-President and Dr. F. L. Mohler. All sessions were held at Columbia University in the Physics Laboratories.

The joint session with the Optical Society of America was held on Friday morning at nine-thirty o'clock. This session was a symposium on *Measuring Spectral Radiation*. The President of the Optical Society, Dr. W. B. Rayton, presided. The invited papers were as follows: *Fundamental Principles* by W. E. Forsythe, General Electric Company; *Methods of Obtaining Spectral Radiation* by Henry Kurtz, Bausch & Lomb Optical Company; *Measuring Energy with Blackened Receivers* by C. G. Abbot, Smithsonian Institution; *Measuring Energy with Photographic Plate* by Brian O'Brien, University of Rochester; *Measuring Energy with Photoelectric Tube* by L. R. Koller, General Electric Company; and *Visual Measurements (Spectroscopy)* by K. S. Gibson, Bureau of Standards. The attendance at this symposium was about three hundred and fifty.

One hundred and thirty-six persons attended the luncheon at the Columbia University Faculty Club on Friday.

On Friday evening the Society joined with the Optical Society for dinner at the Columbia University Faculty Club. This dinner was attended by one hundred and twenty-eight guests. The President of the Physical Society, Professor Arthur H. Compton, presided. The after-dinner speakers were Dr. Karl T. Compton, Dr. Paul D. Foote, Dr. W. B. Rayton and Professor R. W. Wood.

Meeting of the Council. At its meeting on Friday, February 23, 1934, the Council transferred three candidates from membership to fellowship, and elected twenty-three candidates to membership. *Transferred from membership to fellowship:* Reginald L. Jones, Walter C. Michels and R. R. Riesz. *Elected to Membership:* F. R. Abbott, D. E. Ackerman, Lindsay M. Applegate, Otto Beeck, Milton L. Benson, Richard A. Beth, Bernard L. Brinker, Immanuel Estermann, Hampton D. Ewing, Alan M. Glover, William Hurst, Sidney Millman, Herbert Nelson, John P. Nickol, Sidney M. Rubens, Irving J. Saxl, Harold K. Skramstad, George M. L. Sommerman, Reginald J. Stephenson, James H. Sturdivant, Francis J. Sullivan, C. S. Thompson, Alfred L. Vaughan.

The titles and abstracts of papers presented before the Optical Society of America will be found in the Proceedings of that Society, published in the *Journal of the Optical Society*.

The regular scientific program of the American Physical Society consisted of forty-six papers; numbers 8, 16, 23, 28, 29, 31, 32, 33 and 34 were read by title. The abstracts of the contributed papers are given in the following pages. An *Author Index* will be found at the end.

W. L. SEVERINGHAUS, *Secretary*

ABSTRACTS

1. **Fundamental Principles.*** W. E. FORSYTHE, *General Electric Company.*

2. **Methods of Obtaining Spectral Radiation.*** HENRY KURTZ, *Bausch & Lomb Optical Company.*

3. **Measuring Energy with Blackened Receivers.*** C. G. ABBOT, *Smithsonian Institution.*

4. **Measuring Energy with Photographic Plate.*** BRIAN O'BRIEN, *University of Rochester.*

5. **Measuring Energy with Photoelectric Tube.*** L. R. KOLLER, *General Electric Company.*

6. **Visual Measurements (Spectrophotometry).*** K. S. GIBSON, *Bureau of Standards.*

7. **On the Redward Shift of the Spectral Lines of Nebulae.** P. I. WOLD, *Union College, Schenectady, N. Y.*—The redward shift of spectral lines from nebulae has been interpreted, by Doppler's principle, in terms of a recession of the nebulae and an expanding universe. The idea of such a universe has not been wholly pleasing to some and attempts have been made to find other explanations. If one assumes that the velocity of light throughout space is a function of time, and in particular has been slowing down over a long period, then one can account for the redward shift without resorting to recession. This slowing up of velocity is not related in any way to DeBray's suggestion of a few years ago or the recent cyclical variations found in Pasadena, but is of a very much smaller magnitude. Assuming, as a simple case, that the velocity is a linear function of time, given by $c_1=c(1-\alpha t)$, and taking the measurement of shift by Hubble and Humason the coefficient comes out as $\alpha=5.72\times10^{-10}$ with the year as unit of time and $\alpha=1.81\times10^{-17}$ with the second as unit of time. If this rate of decrease were to continue, then the velocity of light would be zero after about 1.7×10^{9} years. It is not likely, however, that the decrease would continue indefinitely but rather that it would be periodic in nature. It is recognized that, for the present at least, the weakness of the speculation here suggested is its high degree of *ad-hocness* but certain experiments suggest themselves which may alter this.

8. **A Relation Between Internuclear Distances and Bond Force Constants.** RICHARD M. BADGER, *Gates Chemical Laboratory, California Institute of Technology.*—It has been found that for diatomic molecules the relation between the internuclear distance r_e and the bond force constant k_0 (calculated from the relation $\omega_e c=(\frac{1}{2}\pi)\sqrt{k_0/\mu}$) is quite accurately given by the expression $k_0(r_e-d_{ij})^3=C$. The constant C is the same for all molecules and the constant d_{ij} depends only on the rows in the periodic table in which the two elements comprising the molecule are located. The expression holds for the normal states and for all excited states, with a few possible exceptions, and is much more reliable than previously proposed expressions relating ω_e and r_e. Uses of the relation are discussed, and values for the constants are given in a paper to appear shortly.

9. **Possible Models of an Electrostatic Neutron.** HENRY MARGENAU, *Yale University.*—Calculations have been made regarding the possibilities of forming a stable structure consisting of a stationary proton and an electron, admitting a deviation of the potential from Coulomb form near the origin. The assumption is that at some distance r_0 from the origin the electron encounters either a potential barrier or a trough of finite height $\Delta\varphi$. We regard as an admissible eigenfunction one which satisfies the usual conditions at $r=0$ and $r=\infty$, and, in addition, behaves properly at r_0. Solutions are found by assuming a value of the binding energy$\sim mc^2$, integrating the wave equation from ∞ inward numerically, and then determining the value of $\Delta\varphi$, for any given r_0, which makes ψ finite at the origin.—Results on basis of Schrödinger's theory are discussed, but are shown to be objectionable. Using Dirac's theory, one can produce stability for any value of r_0 (smaller than the classical electron radius), *provided the binding energy is not larger than 2 mc²*. $\Delta\varphi=0$ is excluded. A particularly interesting model results if we assume the proton to be classically impenetrable (potential wall of great height at r_0). ψ-functions for this case are discussed. The electron is bound essentially by its quasi-electric moment which is drawn into the strong field about r_0. Its average spin is 0, so that the spin of the neutron is that of the proton alone.

10. **Atomic Energy Relations.** R. F. BACHER AND S. GOUDSMIT, *University of Michigan.*—The electrostatic interaction between electrons of many electron atoms is treated in a new way. The method employed by the authors is based on the same principles as Slater's treatment of this problem. It differs from Slater's theory first of all by expressing the interaction in terms of the energy states of the two-electron spectrum instead of expanding it in the usual radial integrals. This modification has several advantages. Its principal advantage is the simplicity with which the method can be extended to include higher approximations. This is done by considering not merely the interaction as revealed by the two-electron ion, but by including also the information obtainable from the three-, four- and more-electron spectra of the same atom. The formal procedure, as usual in such problems, involves simple manipulations with "Pauli tables." The results finally appear in the following form: A particular atomic energy state is expressed in terms of various energy states which occur in the ions of this atom, the degree of approximation depending on the number of ions included. A typical expression of this sort is that for $sp^3\,{}^5S$.

$$(sp^3)^5S=(p^3)^4S^0+3(sp^2)^4P-3(p^2)^3P$$
$$-3(sp)^3P^0+3(p)^2P^0+(s)^2S.$$

* Symposium on *Measuring Spectral Radiation*—Invited papers.

The calculated and observed absolute values for the multiplets of sp^3 in O III are:

	^5S	^3S	^3D	^3P	^1P	^1D
cal. 382399 cm^{-1}	244756	322806	301429	232518	253862	
obs. 382912 cm^{-1}	245720	322768	300420	232348	255757	

These values are obtained directly from the energies of O IV, O V and O VI as observed by Edlén (Zeits. f. Physik **84**, 746 (1933)) without any adjustable constants.

11. Numerical Solution of Eigenvalue Problems in any Number of Dimensions. G. E. KIMBALL AND G. H. SHORTLEY, *National Research Fellows, Massachusetts Institute of Technology.*—A differential equation whose solutions are subject to given conditions on the boundary of a region is approximated to any desired accuracy by a set of difference equations over a lattice covering the region. Two quadratic forms in the function values at the lattice points are found, whose ratio W is a minimum for the lowest state of the difference problem, and approximates the variational integral of the differential problem. A method is developed for calculating rapidly the exact solutions of the difference equations by changing the value of a rough solution at each lattice point in turn in such a way as always to decrease W. For higher states the variation is made subject to orthogonality side-conditions of the usual type. The method is being applied to the solution of Schrödinger's equation for an electron in an arbitrary axially symmetric field such as occurs for diatomic molecules. This problem is conveniently handled in cylindrical coordinates, the singularity of the axis causing no particular difficulty.

12. Indeterminacy Relations in Some Special Problems. F. E. WHITE AND R. B. LINDSAY, *Brown University.*—De Broglie has obtained indeterminacy relations using trains of plane waves. The present paper generalizes these to the case of (a) spherical waves and (b) waves of general type in which the velocity of the point of phase agreement normal to the wave surfaces is constant. The work of Remak is extended by finding higher order indeterminacy products. Thus, e.g., for the harmonic oscillator $(\Delta x)^4(\Delta p_x)^4 = h^4/256\pi^4\cdot(6n^2+6n+3)^2$, while $(\Delta x)^3(\Delta p_x)^3=0$. For the oscillator in a uniform field ($V=\frac{1}{2}kx^2-k\alpha x$) there results $(\Delta x)^2(\Delta p_x)^2=\{(2n+1)h/4\pi\}^2+m_0\nu_0h\alpha^2$. The case of the anharmonic oscillator ($V=\frac{1}{2}kx^2+k\alpha x^3$) is handled by evaluating the eigenfunctions by the perturbation method. It is found that the latter can be expressed in terms of Hermite polynomials of order n, $n+1$, $n-1$, $n+3$, and $n-3$. The indeterminacy relation to terms in α^2 is

$$(\Delta x)^2(\Delta p_x)^2=\{(2n+1)h/4\pi\}^2+\alpha^2h^3(2n+1)(328n^4 +656n^3+650n^2+322n+123)/2304\pi^4m_0\nu_0.$$

In the limit of $\alpha\doteq 0$ these results approach that for the harmonic oscillator.

13. Elastic Wave Analogies of the Motion of Electrons in Force Fields. R. B. LINDSAY, *Brown University.*—In the one dimensional motion of an electron (total energy $W>0$) through a rectangular potential "hollow" of width l and depth V_0, the wave-mechanical probability of transmission is

$$\left[\cos^2\alpha_2 l+\frac{1}{4}\left(\frac{\alpha_1}{\alpha_2}+\frac{\alpha_2}{\alpha_1}\right)^2\sin^2\alpha_2 l\right]^{-1},$$

with $\alpha_1=[(8\pi m_0/h^2)W]^{\frac{1}{2}}$ and $\alpha_2=[(8\pi m_0/h^2)(W+V_0)]^{\frac{1}{2}}$. In the passage of a plane harmonic compressional (acoustic) wave in a fluid through an infinite tube of cross-sectional area S_1 in which there is an abrupt constriction or expansion of length l and cross section S_2, the power transmission ratio is

$$P_r=[\cos^2 kl+\tfrac{1}{4}(S_2/S_1+S_1/S_2)^2\sin^2 kl]^{-1}.$$

The indicated analogy becomes even more striking if the fluid in the expansion or contraction has a different density from that in the rest of the tube. Similarly in the motion of an electron through an infinite one dimensional crystal lattice for which the potential energy variation is represented by a rectangular saw-tooth curve (the potential energy alternating between V_1 and V_2) the criterion for the passage of the electron through the lattice or its complete reflection, in the case where $W>$ both V_1 and V_2, can be shown to be completely analogous to that for transmission or attenuation in an infinite elastic wave filter consisting of a series of alternating layers of two different media (either solid or fluid) with a possible alternation of area of cross section. The analogy breaks down if $W>V_1$ but $W<V_2$.

14. A New Transformation Theory of Linear Canonical Equations. CORNELIUS LANCZOS, *Department of Mathematics, Purdue University.*—The ordinary transformation theory of Hamilton-Jacobi is not adapted to the nature of linear canonical equations, in which case the Hamiltonian function $H(q_k p_k)$ is a quadratic form of the variables $q_k p_k$ and the solution of the partial differential equation of Hamilton-Jacobi involves irrational operations. Instead of that we may ask for linear canonical transformations which bring the quadratic form into a normal form. This normal form turns out to be $\Sigma\lambda_k p_k q_k$ an analogy to the normal form $\Sigma\lambda_k q_k^2$ of the ordinary transformation theory of quadratic forms which use orthogonal instead of canonical transformations. In the normal reference-system the canonical equations are separated and can be integrated immediately. The transformation into the normal form requires no integrations but only algebraic processes. The solution is only approximate since the transformation modifies the Hamiltonian function. A repetition of the procedure is possible, thus approximating the normal form closer and closer. Since any self-adjoint differential equation or sets of such equations can be brought into the canonical form, this theory provides an approximate solution of any self-adjoint system. In the case of a self-adjoint equation of second order the first approximation is identical with well-known approximate solution of Wentzel-Kramers-Brillouin.

15. Calculation of the Total Probability of Excitation by Electron Impact. F. E. NULI, *College of the City of New York.*—Since little is known concerning the combined

probability of excitation by electron impact of all energy levels of the atom, it is interesting to calculate the variation of the total excitation probability with the mean kinetic energy of the exciting electrons. Two simple equations have been applied to the region of electron energy below forty equivalent volts. One equation is the statement of the conservation of energy in a region in which an electron cloud is drifting in an electric field. The other equation equates the ionization produced by electron impact to the product of the number of collisions and the mean probability of ionization per collision as determined by the mean kinetic energy of the electron cloud. The equations give the approximate value of the combined probability of excitation by electron impact of all energy levels. This combined probability plays an important part in the theory of electrical discharges in gases. The equations may be applied to the velocity of drift of an electron avalanche, which is involved in the theories of the mechanism of the spark as given by von Hippel and Franck and by L. B. Loeb.

16. Absorption of Oxygen in the Extreme Ultraviolet. G. B. COLLINS AND W. C. PRICE, *The Johns Hopkins University. (Introduced by R. W. Wood.)*—Absorption bands of oxygen below 1000A, first noticed by Hopfield, were photographed with a 2 m concave grating at grazing incidence. The continuous spectrum was furnished by a Lyman explosive discharge through a glass capillary. It seems certain that the bands are due to normal oxygen. There was always active oxygen in the spectrograph but control experiments indicated that the possibility that the bands are due to O_2^+ or ozone could be excluded. The strongest bands could be arranged into three progressions with the formulae (in cm^{-1})

$$99\,144+1056(v+1/2)$$
$$100\,906+1127(v+1/2)-17(v+1/2)^2$$
$$105\,863+913\ (v+1/2)$$

The numbering of the last progression is uncertain. More than 50 bands were measured at shorter wave-lengths and will be given in a later communication. About 25 bands between 1210 and 1000 were found. They do not form any pronounced sequences and their interpretation is still uncertain.

17. Ultraviolet Absorption of Iodine. DANA T. WARREN, *Yale University.*—Three new lines of evidence show that all the absorption bands of iodine lying between 1765 and 2840A (Jevons *C* and *C'*), discovered by Pringsheim and Rosen, Kimura and Miyanishi, and Sponer and Watson, form a single system. First is the regularity of the development of the bands with temperature and pressure. Second the ease and completeness of overlapping of the regions of different investigators. Thirdly the "long thin bridge" at 2150A is explained as the result of the coincidence of a frequency of 210 cm^{-1} in the ground state and 70 cm^{-1} in the upper state, causing all progressions to coincide. Many new bands have been found, but vibrational assignments are impossible with the present accuracy, which cannot be improved merely by higher dispersion, for the bands become too diffuse for accurate measurement. Even the use of a microphotometer is helpful only where the system is simple. Two new band systems of iodine impurities, one between 1960 and 2223A, the other at high temperatures between 2700 and 3300A, discovered in this investigation are being further studied.

18. Nitrogen Molecular Spectra in the Vacuum Ultraviolet. WILLIAM W. WATSON AND PHILIP G. KOONTZ, *Yale University.*—With a high current discharge in flowing nitrogen gas as the source, spectrograms covering the interval 2300A to 1000A have been taken with a 10-foot vacuum spectrograph; dispersion 5.5A/mm. Quantum assignments have been made for many rotational lines of the (0, 1), (0, 4), (1, 5), (1, 6), (1, 7), and (2, 8) bands of the $a \rightarrow X$ system, (0, 14), (0, 15) and (0, 16) of the $b' \rightarrow X$ system, and (0, 12) of the $c \rightarrow X$ system. For $a\ ^1\Pi_u$, $B_0 = 1.632 \pm 0.002$, while for $X\ ^1\Sigma_g^+$, $B_0 = 1.998 \pm 0.002$. The b' system consists of a progression of singlet Q branches, each $Q(25)$ line displaying an intensity perturbation. The b' state is thus $^1\Pi_u$ with $v=0$, for which $B_0 = 1.147$. Measurement of the strong lines in the $c12$ band indicate a Q branch with $B_0' = 1.159$. Levels with $v>9$ do not occur in $a\ ^1\Pi_u$. If $D = 7.9$ volts for the normal $^1\Sigma_g^+$ state, $v=9$ of $a\ ^1\Pi_u$ coincides with the sensitive $v=13$ level of $B\ ^3\Pi_g$ at the energy of dissociation into $^4S+^2D$ atoms. Also, $v=0$ of the b, b' and c states and $v_{max}=5$ of the $C\ ^3\Pi_u$ state come at the energy for dissociation into $^2D+^2D$ atoms. These facts support the value $D = 7.9$ volts for N_2 (W. W. Lozier, Phys. Rev. **44**, 575 (1933)). Discussion of the various N_2 levels and transitions is included.

19. Intensity Relations in Hyperfine Structure of Optically Excited Mercury Line λ5461. EMILY E. BOGGS AND HAROLD W. WEBB, *Columbia University.*—The relative intensitives of the h.f.s. components of λ5461 in optically excited mercury vapor were computed by using the energy level scheme and intensity distribution given by Schuler and Keyston (Zeits. f. Physik **72**, 423 (1931)), with the assumption that λ2537 is completely absorbed and λ4358 very slightly. Since the excitation is in two steps the ratio of the intensities of the components due to the less abundant isotopes to those due to the more abundant is much less than in the normal low pressure arc, in which excitation of each isotope is proportional to its concentration. These results were checked experimentally by using a Lummer plate. Excitation was by a low pressure quartz arc supplemented by two glass arcs to increase the intensity of λ4358. The quartz and glass arcs gave intensity distributions agreeing well with those of Schuler and Keyston, which indicate small reversal. From the optically excited vapor the relative intensities agreed within experimental error with the values computed as above. For example, the ratio of the intensity of the central component to that of the −0.278 component was found to be six times greater than in the normal arc. Pool and Simmons (Phys. Rev. **44**, 744 (1933)) find this to be less than four. Similar measurements are being made on λ4358 and λ4047.

20. Intensity of the Satellites of the X-Ray Line $L\beta_2$. ANNA W. PEARSALL, *Central Rural School, Hamilton, N. Y.*—The relative intensities of the satellites to that of the parent line have been studied for elements of atomic numbers 40 to 53 inclusive (except 43). The x-ray photographs were made with a Siegbahn vacuum spectrograph by using a calcite crystal. Microphotometer records were made from the plates with a Moll microphotometer. These records were changed to intensity curves in the usual manner and the areas integrated with a planimeter. The results are plotted with relative intensities against atomic number. This curve shows that the ratio of the intensity of satellites to that of the parent line rises from 5 percent at atomic number 40 to a maximum of 53 percent at atomic numbers in the neighborhood of 47, then falls rapidly to zero for atomic number 53. This work was done in the Physics Laboratory of Cornell University.

21. New Satellites of the X-Ray Line $L\beta_2$. S. KAUFMAN AND F. K. RICHTMYER, *Cornell University.*—New faint non-diagram lines on the short wave-length side of the $L\beta_2$ lines for the elements in the atomic number range from 73 Ta to 90 Th have been observed. The energy differences from $L\beta_2$ are greater than those of any other satellites hitherto reported but the regularity of the curves, plotting ν/R differences between the satellites and $L\beta_2$ as a function of the atomic number, suggest that these lines are associated with $L\beta_2$. There are five such new satellites found (here called $L\beta_2''' \cdots L\beta_2^{VII}$). β_2' and β_2'', the strong satellites of $L\beta_2$, have been reported before. The slopes of the respective satellite curves ($L\beta_2' \cdots L\beta_2^{VII}$) increase regularly with respect to the slope of the $L\beta_2$ line, as has been found to be the case with the L-satellites in the lower atomic number range, $40 < Z < 53$.

22. The Relative Intensities of Certain L-series X-Ray Lines of Au(79). F. K. RICHTMYER AND S. W. BARNES, *Cornell University.*—By means of a precision, two-crystal, ionization spectrometer of high resolving power, the relative intensities of the components of certain groups of lines in the L-series of Au(79) have been measured, the lines of each group being sufficiently close together on a wave-length scale so that correction for absorption in the target, tube walls, crystal, etc., is unnecessary. The results (ratio of areas) are as follows:

$$\beta_1 : \beta_3 : \beta_{15} : (\beta_2' + \beta_2'') = 100 : 48.2 : 7.2 : 5.5$$
$$\beta_4 : \beta_6 = 100 : 42.5$$
$$\beta_5 : \beta_9 : \beta_{10} = 100 : 8.8 : 5.0$$
$$\gamma_6 : \gamma_2 : \gamma_3 = 100 : 88 : 3.6$$
$$\gamma_3 : \gamma_4 = 100 : 20$$
$$\alpha_1 : \alpha_2 : (\alpha_1' + \alpha_1'' + \alpha_1''' \cdots) = 100 : 11.2 : 5.0$$

Data will be shown on the widths of these lines (full width at half maximum), which widths vary from 0.6 X.U. for γ_6 to 2.0 X.U. for β_4. Special attention should be called to the data for the satellite groups $\beta_2' + \beta_2''$ and $\alpha_1' + \alpha_1'' + \alpha_1''' \cdots$, the latter group consisting, perhaps, of five satellites, only partially resolved. The lines β_9 and β_{10} are quadrupole lines.

23. Tone Analysis and Physical Characteristics of Violins. II. R. B. ABBOTT AND T. H. STEVENS, *Purdue University.*—This abstract covers the work on *Tone Analysis and Physical Characteristics of Violins* since the June meeting of the Physical Society in Chicago. (See Phys. Rev. **44**, 321 (1933), abstract 33.) Musical terms used by violinists, namely, color, response and carrying power, to express relative values in violins are found to correspond to the physical quantities, quality and efficiency. Quality deals with the distribution and relative power of the partial tones, and efficiency of radiation is found to be closely related to response and carrying power. By using a standard source of sound for calibration purposes and a constant energy input, the authors have measured the relative efficiencies and qualities of violins ranging from poor to very good, by means of a cathode-ray oscillograph. The carrying power was measured by finding the distance in an open field which reduces the sound to the threshold of audibility. The results indicate that the relative values of violins can be determined by physical measurements, and that standard units for such measurements can be established.

24. Further Studies on the Double Refraction of Interfacial Layers of the Normal Aliphatic Acids. ALLEN KING, *Institute of Applied Optics, University of Rochester, Rochester, New York. (Introduced by A. M. Taylor.)*—The fact that the layer of a normal fatty acid just above its melting point exhibits a measurable birefringence has been demonstrated.* The results for lauric and myristic acids indicated a definite positive value of this quantity, whereas that for undecylic acid was weakly negative. Measurements on tridecylic and palmitic acids have now been completed. They verify the previous results.

25. A Graphical Method for Obtaining the Optical Constants of a Medium from the Reflecting Powers at Several Angles of Incidence. RICHARD TOUSEY, *Harvard University.*—For a smooth surface the reflecting power, R, at any angle of incidence, i, is related by a complicated formula to the refractive index, n, and the extinction coefficient, k, for incident light of given polarization. By fitting a curve calculated from this formula to an experimental curve for R *vs.* i, n and k have been determined. A graphical method is here presented by which this fitting may be quickly done. The method can be extended to give the state of polarization of the incident light in addition to n and k. The curves involved have been computed chiefly for reflection conditions likely to occur in the extreme ultraviolet.

26. An X-Ray Study of the Structure of Benzene, Cyclohexane and Their Mixtures. HERBERT K. WARD, *The Pennsylvania State College. (Introduced by Wheeler P. Davey.)*—The x-ray diffraction peaks of carefully purified benzene and cyclohexane and their mixtures were investigated by using Soller type slits and balanced filters. The ionization current was measured directly on a galvanometer (sensitivity 1.3×10^{-8} amperes per division) ampli-

* Taylor and King, J.O.S.A. 23, 308 (1933).

fied by an F.P. 54 tube using a special circuit which gave a sensitivity of 6×10^{-16} amperes per division on the galvanometer. Existing data on the location of the peaks of pure benzene and of pure cyclohexane were confirmed (4.68A and 5.09A, respectively). Mixtures of the two show separate peaks for the benzene and cyclohexane whose positions correspond to those of the pure liquids and whose heights correspond with the proportions used. This is interpreted as indicating an emulsion type of mixture. Since no Tyndal effect was noticeable, the size of the droplets of the emulsion must have been very small. The x-ray data indicate between 10 and 100 molecules per droplet diameter.

27. Crystal Structure of Ammonium Uranyl Acetate. I. FANKUCHEN, *Cornell University.*—Ammonium uranyl acetate is tetragonal, $a=13.79$A, $c=27.60$A. This corresponds to an axial ratio of 1.414 as compared to the reported value 1.4124. The x-ray density is 2.33 as compared to reported value of 2.219. The lattice is body centered. There are 16 molecules to the unit cell. The space group is probably $I4_12$ (D_4^{10}).

28. Stress Analysis by X-Ray Diffraction. C. S. BARRETT AND M. GENSAMER, *Metals Research Laboratory, Carnegie Institute of Technology.*—Precision back reflection x-ray photograms have been used by Sachs and Weerts (Zeits. f. Physik **64**, 344 (1930)) and by Wever and Möller (Archiv. f.d. Eisenhüttenwesen **5**, 215 (1931)) to measure internal stresses in metals. Their calculations give the *sum* of the two principal stresses in the plane of the surface, but not the individual stresses nor their direction. We have developed a mathematical analysis for the case of the incident beam falling perpendicularly upon the metal surface, in which a measurement of the maximum and minimum diameters of a non-circular Debye ring yields the magnitude and direction of each of the two principal stresses in the plane of the surface. Unfortunately, the Debye rings have so little eccentricity that we have been unable to apply this analysis to metals because the width of the diffraction lines has prevented sufficiently accurate measurement of their diameters.

29. X-Ray Determination of the Chemical Composition of Oxide-Coated Cathodes. WILLIAM P. JESSE, *Research Laboratory, General Electric Company, Schenectady, N. Y.*—Satisfactory x-ray powder photographs have been obtained from oxide-coated cathodes enclosed in very thin-walled glass bulbs. Various mixtures of $BaCO_3$ and $SrCO_3$ on pure nickel ribbon ($35\times\frac{1}{2}$ mil) were transformed into the oxides and, after proper vacuum precautions, the containing bulbs were sealed off from the pump. The chemical changes in the coatings were determined from x-ray photographs (copper radiation) after successive heatings of the filament under varying temperature conditions. A summary of the results is as follows: (a) When heated to approximately 800°C, the carbonates of the mixtures are transformed into the individual oxides, BaO and SrO. (b) Further heating at approximately 960°C results in a slow transformation into a solid solution BaO–SrO. At higher temperatures this reaction is more rapid. (c) Calibration photographs from various coatings of known composition show that the BaO–SrO solid solution follows closely Vegard's law. With such a calibration, it becomes possible to determine within two percent the relative proportions of BaO and SrO at any time during the life history of a particular filament. These results are in general agreement with the work of Burgers (Zeits. f. Physik **80**, 322 (1933)).

30. Space Charge Grid Tube with Variable Mu Grid. WALTER DEHLINGER, *Hygrade Sylvania Corporation, Emporium, Pennsylvania.*—Solutions of the generalized equations of the variable Mu triode $\exp(pv)=\int_{-\infty}^{z}(v+z)^k \times F(z)(dx/dz)dz$ and $(v+z_0)^n=\int_{-\infty}^{z_0}(v+z)^k F(z)(dx/dz)dz$ for dx/dz are given by means of the gamma-function. Here z is the reciprocal of the amplification constant, x is the axial distance along the grid, v is the ratio of grid to plate voltage and k is the space charge constant, usually 3/2. The constant n or p determines the shape of the plate current, grid voltage curve desired. The only restrictions for the values of n and k are $n>k>0$, and $\Pi(n-k-1)\neq\infty$. The solution of the integral equation of the space charge grid tube is reduced to that of the triode by a process of summation. Graphical methods are developed by means of which the distribution of grid pitches can be determined from the solution of the integral equation.

31. Laboratory Applications of Kathetrons. PALMER H. CRAIG, *Invex Corporation, New York City.*—The Kathetron (a grid controlled, mercury vapor rectifier) has been previously described (cf.: Electronics, 70–72, March, (1933)). Its use in the laboratory field has been expanded to include rheostatic control of loads from a few milliamperes, by the use of miniature Kathetrons, up to loads of 100 kilowatts with a single 15 ampere tube. The output current through the load is varied from zero to maximum by means of a grid potential, the current associated with which is negligible. Other applications include voltage regulation, time delay, operation from photo-cells, inversion and frequency conversion. Graphs are shown giving the voltage regulation characteristics, and circuit diagrams and oscillograms are presented to explain the theory and operation of the tube and its associated circuits.

32. An Electrical Device for Remote Indicating, Recording and Integrating the Indications of a Float Type Fluid Meter. JOSEPH RAZEK, *University of Pennsylvania.*—The type of fluid meter in which the rate of flow is determined by the rise of a float in a vertical conical tube has recently found wide application, particularly for corrosive fluids. To provide for remote indication and integration an electrical device was developed. This consists of a long induction unit in which a rod of magnetic material, attached to the float can move, thereby inducing a voltage which varies with the float position. A suitable opposing voltage causes the induced voltage to be linearly related to the float position. Indication and recording on ordinary d.c. instruments is made possible by the use of a diode. The time integral of the float position is obtained by impressing

the resultant voltage on the potential coil of an induction type watt-hour meter, whose current coil carries a constant current. The revolutions of the watt-hour meter are counted by a photo-cell and light arrangement actuating a magnetic counter through an amplifier. The whole unit is supplied by a voltage regulating transformer, or stabilizing network. Tests show that the indications of the meters and the speed of the meter disk are nearly proportional to the float position, which in turn, is proportional to the flow. This device should find application for other than fluid meter use.

33. Alpha-Particle Spectra and the Geiger-Nuttall Law. ARTHUR E. RUARK, *University of Pittsburgh.*—Gamow's theory gives the relation $\log \lambda = a(r_0, j) - bE^{-\frac{1}{2}}$; λ is a decay constant, E is disintegration energy, r_0 is "nuclear radius," j is azimuthal quantum number; b depends only on universal constants and atomic number. Thus a and b should vary slowly with Z. Gamow uses λ- and E-values to obtain r_0 and j. Kurie found that plotting $\log \lambda$ against $E^{-\frac{1}{2}}$ yields straight lines. I have made such plots, showing points for all of Rosenblum's alpha-groups. The groups, α_0, α_2, α_4 of Th C lie on the line representing the average trend of the Ac family. The groups α_1, α_3 lie well off the line. This suggests reconsideration of Gamow's assignment of j values. (His computations of relative intensities contain numerical errors.) We must look at such problems from the standpoint of transition probabilities, remembering that the potential barrier alters as the alpha-particle emerges from the nucleus. The constants a, b for the U, Th and Ac families are 70.6, 18.0: 82.3, 21.4: 74.7, 19.9. Gamow's theory yields 53.4, 14.7 if we take $r_0 = 8 \times 10^{-13}$ cm, $Z = 88$; other potential barriers are being studied in the hope of reducing this discrepancy.

34. Alpha-, Beta- and Gamma-Rays of the Actinium Family. ARTHUR E. RUARK, *University of Pittsburgh.*—Rosenblum's work on alpha-particle spectra leads to classifications of actinium family beta-rays. Also we can show that some unclassified lines are due to K-conversion, because if they were converted in any other shell we should expect strong K-conversion lines which are not observed. (1) *Pa.Ac.* Beta-ray 93.9 ekv (electron kilovolts) represents conversion of gamma-ray 94.9 ekv in the N shell. Beta-rays 245 and 257 ekv represent K-conversion of gamma-rays 3.514 and 3.64 ekv. All recorded lines are now explained. (2) *AcX.An and An.AcA.* Rosenblum found levels 115 and 190 ekv for AcX.An, and 270 and 397 ekv for An.AcA. Meitner's beta-spectrum obtained with AcX should contain lines of An.AcA. One might think her gamma-ray 268.8 ekv is due to An.AcA, but the following facts support its assignment to AcX.An: (a) the difference of this ray and the ray 153.0 ekv (certainly due to AcX.An) is 115.8, checking Rosenblum's levels: (b) the beta-ray 175.9 ekv can represent K-conversion of a gamma-ray 268.5 of An.AcA. Beta-rays 104.3 and 180.0 are best interpreted as K- and L-conversion of a ray 196.9 of An.AcA. Beta-rays at 223.0 and 236.9 must be due to K-conversion, but we cannot say in what element.

35. Ionization in Air and the Biological Effects of Gamma-Rays. G. FAILLA, *Memorial Hospital, New York.*—The experiments of Packard have shown that the same number of ions produced in free air by x-rays of different wave-lengths, kills the same percentage of fruit fly eggs, under specified conditions. Since the definition of the roentgen is based on air ionization, he has concluded that the same dose of radiation measured in roentgens produces the same biological effect, irrespective of the wave-length. By extrapolation it has been contended that the same relation would also hold for gamma-rays. A crucial experimental test has not been possible heretofore. We have now developed a method for the measurement of the actual ionization in air under the conditions in which Packard carried out his experiments with gamma-rays. The results show very definitely, that equal ionizations *in air* are not equally effective in killing fruit fly eggs in the case of x-rays and gamma-rays. The difference is much greater than any possible experimental error. This result and others obtained in the course of the work, show that the therapeutic efficacy of very high voltage x-rays and gamma-rays cannot be predicted by the usual biological and physical tests.

36. Cosmic-Ray Ionization in a Heavy Walled Chamber at High Altitudes. A. H. COMPTON AND R. J. STEPHENSON, *University of Chicago.*—A recording cosmic-ray meter whose steel ionization chamber was surrounded by a spherical shell of lead shot, equivalent to 6 cm of solid lead, was carried into the stratosphere by Commander Settle and Major Fordney, up to a barometric pressure of 50.5 mm, as read from a mercury barometer. Previous tests with heavy walled chambers at an altitude of 4300 meters (barometer 447 mm) show that the screen of lead shot was sufficient to eliminate practically all transition effects due to secondary radiations excited in the air. If the cosmic rays are of the γ-ray type, i.e., exponentially absorbed, the ionization should therefore follow either the "Gold integral" curve, which takes account of their isotropic origin, or some curve which is the resultant of several such Gold integrals. The experimental ionization-depth seems to follow more nearly a simple exponential law than that represented by the Gold integral. A curve of such a shape cannot be described by a γ-ray beam of any assumed components, but is closely represented by the ionization by α-rays (i.e., ionizing particles with a definite range) having a Maxwellian distribution of energies.

37. Electrical Latent Image. V. K. ZWORYKIN, *Electronic Research Laboratory, RCA Victor Company, Inc., Camden, N. J.*—The paper deals with an apparatus capable of storing electrically the information from an optical image projected on a sort of photoelectric mosaic, and reproducing it at the desired moment. Several possible embodiments of the same idea are described. The operation, merits and limitations of each are discussed. Although the original device was developed as a pickup camera for television purposes, it can be used in the same or modified form for many other purposes. Its sensitivity in the ultraviolet and infrared part of the spectrum opens new possi-

bilities for investigation in these regions. The device also allows a number of other interesting applications, such as the amplification of the light intensity of the image over its original value, the electrical magnification of the size of the image, and various new combinations with regular optical devices.

38. New Experiments on Bitter's Powder Patterns. K. J. SIXTUS, *Research Laboratory, General Electric Co., Schenectady, N. Y.*—On six single crystals of silicon-iron (3.5 percent Si) the properties of the powder patterns first observed by F. Bitter (Phys. Rev. **38**, 1903 (1931) and **41**, 507 (1932)) have been studied. Three different types of pattern can be distinguished: I, on the straight part of the magnetization curve at low fields, II, from the knee of the magnetization curve nearly up to saturation, III, near to and at saturation. I consists of rather broad lines which lie in the direction of intersects between (100) crystal-planes and the sample surface, II of very distinct lines, multiplying as the field is increased and parallel to intersects between (110) planes with the surface, III of broad bands in general perpendicular to the applied field. The different directions of the patterns can be explained by the present theory of the magnetization process, while for the understanding of other properties, particularly the line spacing (about 10^{-2} cm) and its field dependence, a hypothesis is suggested.

39. The Vapor Pressure of Deuterium. F. G. BRICKWEDDE, R. B. SCOTT, HAROLD C. UREY AND M. H. WAHL. *The Bureau of Standards, Washington, D. C. and Columbia University, New York, N. Y.*—The vapor pressure of a sample of deuterium, Hd_2, of nearly 100 percent purity, was measured with a mercury filled manometer connected to a bulb containing liquid or solid deuterium. The bulb of the manometer was immersed in a liquid or solid hydrogen cryostat connected with a vacuum pump for temperature regulation. Temperatures were determined with a vapor pressure thermometer filled with ordinary hydrogen. The results are as follows:

Temperature	*V.P. of* Hp_2	*V.P. of* Hd_2
14.0°K (Triple pt. of Hp_2)	5.4 cm of Hg	0.5₃ cm of Hg
18.3° (Triple pt. of Hd_2)	45.₄	13.
20.4° (Boiling pt. of Hp_2)	76.0	25.

Preliminary results show that the ratio of the heats of vaporization, sublimation and fusion are: 1.25, 1.46, and 1.6 respectively, the values for deuterium being larger in each case. Also, the difference in vapor pressures is larger than expected from the theory given by Urey, Brickwedde and Murphy (Phys. Rev. **40**, 1 (1932)). Additional measurements are being made with another sample of deuterium prepared from water further electrolyzed beyond that from which the above sample was prepared.

40. Raman Spectrum of Heavy Water. R. W. WOOD, *The Johns Hopkins University.* Raman spectra of 18 and 80 percent heavy water have been obtained by Hg 2536 excitation. H^2OH^2 gives a Raman band of much shorter wave-length than ordinary water. H^2OH^1 gives two bands, one nearly but not quite in coincidence with the bank just mentioned and another nearly in coincidence with the band of ordinary water. Heavy water vapor should show two double lines corresponding to the partially superposed bands.

41. Small Angle Scattering of Potassium Atoms. W. H. MAIS AND I. I. RABI, *Columbia University.*—A narrow beam of neutral potassium atoms was scattered by six different gases. The scattering was investigated by means of a surface-ionization detector. The detecting filament subtended an angle of approximately 4′. From the ratio $I/I_0=e^{-d/\lambda}$ one can calculate by a method analogous to Tait's an effective collision radius for scattering greater than 4′. If we include in I all potassium atoms which are scattered less than 1° we obtain another set of collision radii. These two sets of values are presented in the table together with the σ_{12} obtained by using 3A for the radius of the potassium atom and the kinetic theory radii for the gases. If we are to take account of the quantum theory scattering of hard spheres which gives a tremendous preference to small angle scattering we should multiply the kinetic theory radii by about 1.5. It is then evident that except in the case of hydrogen and helium, the hard sphere picture is not sufficient to account for the scattering at very small angles.

Gas	σ_{12} in A angle = 4′	σ_{12} in A angle = 1°	σ_{12} in A Kinetic Theory
H_2	7.2	5.7	4.18
He	6.9	5.0	3.95
Ne	8.7	6.0	4.20
N_2	12.5	7.3	4.64
A	11.3	8.8	4.49
CO_2	13.3	9.6	4.78

42. Deflection of Cosmic-Ray Secondaries in Magnetized Iron. W. F. G. SWANN AND W. E. DANFORTH, JR., *The Bartol Research Foundation.*—A mathematical analysis by one of us (W.E.D.), taking into account counter sizes and distances, has shown that the results of L. M. Mott-Smith's experiments on deviation of cosmic rays by magnetized iron are not inconsistent with the assumption that magnetic induction is the fundamental vector operative to cause the deflection. The said experiments, however, appear inconclusive for a decision of the point. We have repeated these deflection experiments under conditions which take account of the geometrical considerations involved and of the energy loss of the particles in the iron. In the actual experiments a 7.8 percent decrease of counting rate was observed with a probable error of 1 percent. On the assumption that the magnetic induction B is the vector involved, the results can be explained on the assumption that those rays having energy greater than that necessary to penetrate the iron (4.5×10^8) have an "effective" energy of 1.9×10^9. On the other hand, the assumption that the magnetic intensity H is the vector concerned would point to an energy much less than that necessary to penetrate the iron.

43. Comments on the Analysis of an Intensity Complex with Special Reference to that of Hα. R. C. WILLIAMS AND R. C. GIBBS, *Cornell University.*—Any analysis based solely on a microphotometer curve of a photographic record of a complex is in general quite unreliable, especially when it is necessary to take into account any shift in the spectral position of a maximum caused by overlapping components. Such a procedure will yield results that will vary widely with exposure conditions. Reduction of microphotometer curves to intensity curves by means of suitable intensity marks, preferably on the same plate, is necessary if precise quantitative results are to be obtained. Examples are given to show that the practice often followed of treating the "center of gravity" of even a fairly symmetrical complex and its position of maximum intensity as identical is unsound. The latter, but not the former, depends upon the shape or half-line width. For example, in the low-frequency member of the $H^1\alpha$ "doublet," consisting of three components and often treated as symmetrical, the shift of the theoretical center of gravity from the main component is 0.006 cm^{-1}, whereas for the same component intensities and positions and a half-line-width of 0.180 cm^{-1} which is easily obtainable, the displacement of the maximum intensity from this component is only 0.003 cm^{-1}. Generalized formulae, useful in checking empirical analyses, are given for finding both the center of gravity and the position of a maximum or minimum intensity, relative to any chosen component, of an intensity complex composed of any number of similar and perfectly symmetrical components with given intensities, positions and shape.

44. The Interior Magnetic Field in Iron. LUIS ALVAREZ, *University of Chicago. (Introduced by Arthur H. Compton.)*—Beta-rays of radium C ($H\rho=5900$) were focussed in a field of 1900 gauss, and after passing through 0.36 mm of soft iron, were registered on a photographic film, which was parallel to and 1.53 mm from the iron sheet. Alternate exposures were made with a copper sheet. The image on the film was a line, broadened by scattering. Beta-rays passing though a slit in contact with the film produced a sharp fiducial mark near the broadened line. If the deflecting field in the iron were the induction (17,000), the point of maximum density on an iron photograph should have been displaced 0.15 mm with respect to that on a copper film. Measurements were made on enlargements of microphotometer traces (×5), where the expected shift was 0.92 cm. Three copper and two iron films were photometered, and the mean shift was 0.02 cm in the expected direction. The greatest shift among traces from the same metal was in both cases 0.12 cm. These results indicate that the deflecting field is less than $B/3$, and are in accord with the views that it is equal (1) to the magnetizing field, or (2) to the field in a spherical cavity in the iron.

45. A Cascade Electrolytic Process for Separating the Hydrogen Isotopes. HAROLD C. UREY AND M. H. WAHL, *Columbia University.*—A cascade of five electrolytic cells with KOH electrolyte and internally cooled nickel electrodes has been devised which gives after 72.5 hours of operation, a ratio of concentration ratios between the last cell and a reservoir of approximately 1000. Numbering the cells beginning with the cell next to the low concentration reservoir as one, the process consists in catalytically recombining the gases ($2H_2+O_2$) from cell ($i+1$) and passing the water into the ith cell and at the same time distilling water from the ith cell into the $(i+1)$th cell. Simple considerations show that after a long time the ratio of the concentration ratios between each two consecutive cells should be equal to the fractionation factor α so that the overall enrichment should be α^5 in the limit. Our results give an effective α of approximately 4. The cells contain about 40 cc of electrolyte and carry about 33 amperes. The catalyst is copper oxide with a layer of platinized asbestos at the outlet of the catalyst chambers which are heated to 420°C in a bath of sodium and potassium nitrates. The capacity is approximately 35 cc of the concentrated water per 72 hours run.

46. The Raman Spectrum of Neopentyl Deuteride. D. H. RANK, E. R. BORDNER AND K. D. LARSEN, *Pennsylvania State College.*—Neopentyl deuteride prepared by F. C. Whitmore and G. H. Fleming was used to obtain the Raman spectrum of this compound. The heavy water used in this synthesis had a specific gravity of 1.073. The Raman spectrum has been obtained by using a spectrograph having a dispersion of 14A per mm at λ4500. Plates were obtained with two differed sets of filters. The plates show that the vibrational degeneracy of the neopentane molecule is partially removed by the introduction of a deuterium atom in place of a protium atom. The carbon deuterium vibration makes itself evident by the appearance of a line at 2179 cm^{-1}.

AUTHOR INDEX TO ABSTRACTS OF THE NEW YORK MEETING

Abbot, C. G.—No. 3
Abbott, R. B. and T. H. Stevens—No. 23
Alvarez, Luis—No. 44

Bacher, R. F. and S. Goudsmit—No. 10
Badger, Richard M.—No. 8
Barnes, S. W.—see Richtmyer
Barrett, C. S. and M. Gensamer—No. 28
Boggs, Emily E. and Harold W. Webb—No. 19
Bordner, E. R.—see Rank
Brickwedde, F. G., R. B. Scott, Harold C. Urey and M. H. Wahl—No. 39

Collins, G. B. and W. C. Price—No. 16
Compton, A. H. and R. J. Stephenson—No. 36
Craig, Palmer H.—No. 31

Danforth, W. E., Jr.—see Swann
Dehlinger, Walter—No. 30

Failla, G.—No. 35
Fankuchen, I.—No. 27
Forsythe, W. E.—No. 1

Gensamer, M.—see Barrett
Gibbs, R. C.—see Williams
Gibson, K. S.—No. 6
Goudsmit, S.—see Bacher

Jesse, William P.—No. 29

Kaufman, S. and F. K. Richtmyer—No. 21
Kimball, G. E. and G. H. Shortley—No. 11
King, Allen—No. 24
Koller, L. R.—No. 5
Koontz, Philip G.—see Watson
Kurtz, Henry—No. 2

Lanczos, Cornelius—No. 14
Larsen, K. D.—see Rank
Lindsay, R. B.—No. 13
—— see White

Mais, W. H. and I. I. Rabi—No. 41
Margenau, Henry—No. 9

Nuli, F. E.—No. 15

O'Brien, Brian—No. 4

Pearsall, Anna W.—No. 20
Price, W. C.—see Collins

Rabi, I. I.—see Mais
Rank, D. H., E. R. Bordner and K. D. Larsen—No. 46
Razek, Joseph—No. 32
Richtmyer, F. K. and S. W. Barnes—No. 22
—— see Kaufman
Ruark, Arthur E.—Nos. 33, 34

Scott, R. B.—see Brickwedde
Shortley, G. H.—see Kimball
Sixtus, K. J.—No. 38
Stephenson, R. J.—see Compton
Stevens, T. H.—see Abbott
Swann, W. F. G. and W. E. Danforth, Jr.—No. 42

Tousey, Richard—No. 25

Urey, Harold C.—see Brickwedde
—— **and M. H. Wahl**—No. 45

Wahl, M. H.—see Brickwedde
—— see Urey
Ward, Herbert K.—No. 26
Warren, Dana T.—No. 17
Watson, William W. and Philip G. Koontz—No. 18
Webb, Harold W.—see Boggs
White, F. E. and R. B. Lindsay—No. 12
Williams, R. C. and R. C. Gibbs—No. 43
Wold, P. I.—No. 7
Wood, R. W.—No. 40

Zworykin, V. K.—No. 37